SLAC-PUB-2157
July 1978
(T/E)

THE TRANSITION FROM CONSTITUENT INTERCHANGE TO QCD p_T^{-4} DOMINANCE AT HIGH TRANSVERSE MOMENTUM*

D. Jones
Physics Dept., University of California at Davis
Davis, California 95616

J. F. Gunion†
Stanford Linear Accelerator Center
Stanford University, Stanford, California 94305

and

Physics Dept., University of California at Davis
Davis, California 95616

ABSTRACT

We discuss the relationship, in quantum chromodynamics, between constituent interchange (CIM) processes (e.g. $qM \to qM$) and the most elementary QCD processes, such as $qq \to qq$, as manifested in single particle inclusive production at high transverse momentum, p_T. Based on the "subprocess expansion" the CIM contributions are seen to be the next to leading terms in an asymptotic expansion of the cross section, p_T^{-8} (or p_T^{-12}) behavior vs. p_T^{-4} for the elementary subprocesses. We explore the systematic features of the transition from CIM behavior to p_T^{-4} behavior with increasing p_T. Marked variations with trigger particle type (π, K^-, p or $\bar{p}$) and beam type (pp, π^+p and π^-p) emerge.

(Submitted to Phys. Rev.D)

---

* Work supported in part by the Department of Energy.
† A. P. Sloan Foundation Fellow

INTRODUCTION

High transverse momentum single particle cross sections are recognized as a powerful probe of the short distance properties of the strong interactions. In the context of quantum chromodynamics (QCD) such cross sections should exhibit scaling behavior for asymptotically large transverse momentum,[1] p_T:

$$E\frac{d\sigma}{d^3p}(A+B\to C+X) \overset{90^\circ \text{ c.m.}}{\sim} \frac{1}{p_T^4} F(2\ p_T/\sqrt{s} = x_T)$$

(Corrections due to scale breaking[2,3,4] are potentially capable of altering this form somewhat.) This behavior arises from the most elementary scattering mechanisms at the quark gluon level[3]—e.g. $qq \to qq$. For moderate values of p_T it is clear, however, that other mechanisms with more rapidly damped p_T behavior could become important. The purpose of this paper is to systematically discuss the various terms in an asymptotic series approximation to the inclusive cross section. In addition to the elementary QCD (p_T^{-4}) contributions we find that only the contituent interchange[5] (CIM) contributions (which yield p_T^{-8} behavior for mesons and p_T^{-12} behavior for baryons) are of significant importance.

For power low behaved theories, such as QCD, each term in the expansion series corresponds to a different region of the loop and phase space integration variables of the various Feynman diagrams contributing to production of a given particle and may be associated with a large momentum transfer subprocess as illustrated in Fig. 1.

In this figure low p_T secondary particles a and b, emitted from A and B respectively, scatter at large angles to produce c which fragments to C. By carefully including all subprocesses a+b→c+d and using complete

probability distributions $G_{a/A}(x_a)$, $G_{b/B}(x_b)$, and $D_{C/c}(x_c)$ ($x_a=p_a/p_A$ etc.) we include, in principle, the effects of all Feynman diagrams. Two examples of this process are given in Fig. 2a and 2b for quark production at high p_T.

In Fig. 2a we show for quark production how two regions of phase space for a given diagram correspond to the distinct subprocesses $qq \to qq$, with a radiated gluon at low p_T, and $qg \to qg$ where the radiated gluon is now the high p_T balance of the produced quark and thus part of the subprocess. Phrased differently we can say that one of the interacting quarks in the $qq \to qq$ subprocess can itself have large fluctuations[4] in k_T (its transverse momentum relative to the beam) as a result of the prior emission of a hard gluon; the leading asymptotic limit of this high k_T tail corresponds to the $qg \to qg$ subprocess. Both subprocesses lead to p_T^{-4} behavior in the cross section.

In Fig. 2b the large k_T fluctuations of one of the interacting quarks in a $qq \to qq$ subprocess correspond to the subprocess $gM \to q\bar{q}$[6] which by dimensional counting[7] leads to a term with p_T^{-6} behavior in the asymptotic expansion series for the cross section. This illustrates how the subprocess expansion can be used to systematically obtain contributions to the inclusive cross section which have non-leading behavior and will be important at moderate p_T. This subprocess expansion method has been verified for certain ϕ^3 models;[8] inclusion of all subprocesses gives an excellent representation of the full Feynman amplitude so long as p_T is substantially larger than the (short distance) masses of the particles involved.

Thus to obtain an expression for a single particle cross section which is reliable at moderate as well as high p_T we need to know which subprocesses will yield substantial contributions. The important cases are:

a) p_T^{-4} subprocesses:[3]

$$qq \to qq$$

$$qg \to gq + \text{crossed versions}$$

$$gg \to gg$$

The only reason these do not dominate over most of the p_T range is that the observed hadron C must emerge as a fragment of a quark or gluon. The fragmentation leads to a severe numerical suppression[9] (by a factor of 100-1000). Quark and gluon jet cross sections are not suppressed in this manner.

b) p_T^{-6} subprocesses:[6]

$$gq \to Mq + \text{crossed versions}$$

These are potentially large since an observed meson may be produced directly without fragmentation suppression. However gauge invariance for the external gluon combined with the color singlet nature of M can be shown to lead to a subtle cancellation which makes these subprocesses insignificant.

c) Constituent interchange subprocesses (p_T^{-8} and p_T^{-12}):[10,11]

$$qM \to qM$$

$$qB \to qB + \text{crossed versions}$$

$$q(2q) \to MB$$

These have been discussed in a recent paper[5] (hereafter called I). Their contributions are normalized by determining: a) the hadron vertex couplings

which appear ($\alpha_M \sim 2$ GeV^2 and $\alpha_B \sim 10$ GeV^4 for the $q\bar{q} \to M$ and $q(2q) \to B$ vertices, respectively); and b) the various required distribution functions $G_{M/p}$, $G_{q/p}$, $G_{B/p}$ etc. ... .Again these contributions are significant at moderate p_T because the observed hadrons (mesons or baryons) can be produced directly, without fragmentation suppression and because the α_M and α_B coupling constants are big.

We have not considered carefully the following subprocesses:

i) $gq \to (2q)\bar{q}$: this p_T^{-6} process is suppressed (for meson production) relative to $gq \to Mq$ by final fragmentation; in addition, the coupling constant describing the $qq \to (2q)$ vertex, α_{2q}, is presumably much smaller than α_M. This is because the α's are proportional to the wave function at the origin squared. A $(2q)$ state is presumably unbound or only weakly bound in comparison to a color singlet meson state so that $|\psi_{(2q)}(0)| << |\psi_M(0)|$. On the other hand, the subtle gauge invariance cancellation which occurs for $gq \to Mq$ will be absent.

ii) $q(2q) \to (2q)q$: this p_T^{-8} subprocess is suppressed for the same reasons as (i) and, in addition, does not become enhanced, as p_T increases, relative to the $qM \to qM$ CIM subprocess with the same p_T behavior.

iii) p_T^{-10} subprocesses such as $g(2q) \to B\bar{q}$: We presume that gauge invariance yields cancellations analogous to those found in $gq \to Mq$.

We will ignore asymptotic freedom (ASF) type modifications and discuss computations within an exact scaling framework. It has been claimed in the literature[2,3,4] that scaling violations should be expected since the distribution functions $G_{a/A}$, $G_{b/B}$ and $D_{C/c}$ when defined by deep inelastic type probes do not scale and since the subprocess cross section will have corrections from higher order virtual gluons as incorporated in

the moving coupling constant. This "factorized" method of computing ASF corrections, though apparently correct to first order[12] in α_s, is not obviously the full story. There are virtual gluon corrections of many types to the subprocess, virtual gluon connections between subprocess diagrams and distribution function diagrams and real gluon emission of many types. It is not inconceivable that the net correction could be very small i.e. that the factorized approach breaks down in higher order calculations. In e^+e^- annihilation to a $q\text{-}\bar{q}$ pair virtual gluon corrections (i.e. the gluons do not appear in the final state) lead to a sharp modification of the expected scaling behavior while real gluon final states compensate leading to the well known exact scaling for $\sigma_{e^+e^- \to \text{hadrons}}$. We do not know how to handle the full complexity of the QCD structure yet and thus the approach here is to retain the simplicity of exact scaling and dimensional counting; dimensional counting does yield excellent descriptions of elastic cross sections and form factor behaviors.[13] In general scaling violations alone (i.e. without the k_T fluctuations incorporated in the subprocess expansion) are not capable of explaining the low to moderate p_T inclusive data in any case.

The new features of this paper will include a careful treatment of all QCD (p_T^{-4}) contributions for both π and p beams and a careful discussion of the CIM contributions for π and p beams to exotic channels such as $\bar{p}$ production which turn out to be very interesting. We will present a complete summary for all inclusive particle trigger types and systematically discuss the transition from p_T^{-8} (or p_T^{-12}) CIM behavior to p_T^{-4} QCD behavior. The most significant results are:

a) The CIM naturally describes both the p_T behavior and normalization of all measured single particle cross sections in the moderate p_T range. This was shown for π and p production in I and is extended to $\bar{p}$ and K^- production here. Resort to large arbitrary transverse quark or gluon momentum fluctuation corrections[4] to the p_T^{-4} subprocesses is not required; the CIM and QCD contributions systematically organize and normalize all such effects via the subprocess expansion. In fact the subprocess expansion approach predicts a big difference between p and $\bar{p}$ trigger subasymptotic contributions (behaving as p_T^{-12} in the CIM) compared to those for π or K triggers (with p_T^{-8} behavior). Such a difference appears awkward from the simpler fluctuation point-of-view since to first approximation the fluctuations of the colliding quarks and gluons would not depend on trigger type.[14]

b) At higher p_T the p_T^{-4} contributions do become dominant. The point of crossover where

$$E \frac{d\sigma}{d^3p} \text{ (CIM)} = E \frac{d\sigma}{d^3p} (p_T^{-4})$$

exhibits interesting dependence on beam and trigger type. For instance, for $\bar{p}$ production the p_T^{-4} subprocesses take over by $p_T \sim 4.5$ GeV/c even at FNAL energies at which π production is always CIM dominated.

c) Large ratios within the CIM dominated realm are predicted for

$$E \frac{d\sigma}{d^3p} (\pi p \to \bar{p} X) / E \frac{d\sigma}{d^3p} (pp \to \bar{p} X)$$

Values as high as 30 are typical and would certainly confirm the correctness of the CIM approach; much smaller ratios are predicted for the QCD contributions.

Our calculations will be performed using the analytic techniques of I. These techniques require using simplified forms for distribution functions and are in general accurate to within 50% by the time all approximation inaccuracies are taken into account. In the extended calculations of this paper some additional ingredients are required which should be regarded as having slightly larger errors than this:

i) gluon fragmentation functions, which appear for many p_T^{-4} subprocesses:

$$D_{p/g},\ D_{\bar{p}/g},\ D_{\pi^{\pm}/g},\ \cdots \quad .$$

The shapes are determined by dimensional counting but their normalization should be regarded as uncertain by a factor of 2; and

ii) The distribution function $G_{\bar{B}/p}$ which is prominent in the CIM contributions to $\bar{p}$ production. Again a factor of 2 uncertainty should be assigned; however $G_{\bar{B}/p}$ cancels out in the $(\pi p \to \bar{p})/(pp \to \bar{p})$ ratio referred to earlier, which is thus an especially interesting test of the CIM framework.

In general the reader should take precise numerical values given for cross sections as accurate to within a factor of 2. The emphasis of this paper will be on the overall systematics of the CIM (p_T^{-8}, p_T^{-12})—QCD (p_T^{-4}) crossover and on global features of the two domains which are not critically dependent on exact numerology. These results are reviewed in Ref. 6.

The organization of the paper is as follows:

Section 1, "Ingredients": this section is divided into four parts. The subprocess differential cross sections, distribution functions, and quark/gluon decay functions are discussed in turn. The section ends with a quick review of the analytical calculational methods developed in I.

Section II, "Results": this section is divided into three parts. Explicit expressions for all cross sections are given in the first part. The source of the various contributing terms is indicated. Quark/gluon "jet" cross sections are also quoted. In the second part the interesting features of the single particle cross sections are illuminated with emphasis on the features a) - c) mentioned earlier. The third part discusses jet cross sections.

I. INGREDIENTS

Within the subprocess expansion framework a high p_T inclusive cross section is calculated as a sum of contributions of the type illustrated in Fig. 1. Each contribution takes the form

$$E\frac{d\sigma}{d^3p} = \frac{1}{\pi}\int dx_a\, dx_b\, G_{a/A}(x_a)G_{b/B}(x_b)\,\frac{dx_c}{x_c^2}\,D_{C/c}(x_c)$$

$$\hat{s}\,\delta(\hat{s}+\hat{t}+\hat{u})\,\frac{d\sigma}{d\hat{t}}^{ab\to cd}(\hat{s},\hat{t},\hat{u})\Big|_{\substack{\hat{s}=x_a s_b\, s\\ \hat{t}=x_a/x_c\, t\\ \hat{u}=x_{b/x_c}\, u}} \tag{1}$$

To calculate such a contribution we need to know:

a) The scattering subprocess cross section $\frac{d\sigma}{d\hat{t}}^{ab\to cd}$ — both normalization and angular dependence;

b) The distribution functions $G_{a/A}$ ($G_{b/B}$) describing the probability of finding secondary a(b) in primary A(B) with light-cone momentum fraction $x_a(x_b)$; and

c) The decay probability function $D_{C/c}$ describing the emission of C from c as a function of the light-cone momentum fraction of C relative to c. If C participates in the subprocess, i.e. is produced "promptly", this last, "fragmentation" stage, is omitted.

A. Subprocess Cross Sections

We begin by tabulating all the required subprocess differential cross sections yielding p_T^{-4}, p_T^{-8} and p_T^{-12} behavior for $E\frac{d\sigma}{d^3p}$. Subprocesses yielding intermediate powers, such as gq→Mq (p_T^{-6}), are known to be small contributors as mentioned in the introduction.[6] The expressions, appearing in Table 1, were calculated[3,5] for a spin 1/2 quark, spin 1 gluon model.

The many crossed versions of the tabulated cross sections are easily obtained. All cross sections are averaged over initial color configurations. Diquarks entering a hadron vertex are necessarily in a color triplet; thus we will later determine the color triplet portion of diquark distributions. We will be concentrating on production at 90° in the center of mass. Equation (1) can be shown to imply at 90° that $\frac{\hat{s}}{2} \sim |\hat{t}| \sim |\hat{u}|$ as $x_T = \frac{2p_T}{\sqrt{s}} \to 1$ and also for a substantial range of x_T away from zero. Thus we may simplify the cross sections as in Table 2 where we now specify a variety of crossings. The ab ... labelings will be useful later. The relative sizes of the various subprocesses within a class are made more apparent in this manner. We parameterize the subprocess forms of Table 2 as

$$\frac{d\sigma}{d\hat{t}}^{90^\circ}(ab \to cd) = \pi \frac{\mathscr{D}}{\hat{s}^N}^{90^\circ} \tag{2}$$

The cross section magnitudes are determined by the hadron vertex couplings α_B and α_M which describe, respectively, the coupling of $p \to d(uu)$ and $\pi^+ \to u\bar{d}$ per color of the quarks. They were determined in I in three independent ways: from elastic scattering normalizations, from form factor normalizations and from momentum sum rule constraints. All three determinations yielded consistent values for both α_B and α_M:

$$\begin{aligned} \alpha_B &\sim 10 \text{ GeV}^4 \\ \alpha_M &\sim 2 \text{ GeV}^4 \end{aligned} \tag{3a}$$

As in I we also adopt the diquark mass value $M^2_{eff} \sim 1 \text{ GeV}^2$ (which appears in the $q\ 2q \to BM$ subprocesses). Note that in $q\ 2q \to BM$ etc. the 2q must be in a color triplet state. The quoted cross section is per color of

the color triplet 2q. We will ultimately find that the standard quark gluon coupling at large momentum transfers is of order

$$\alpha_s = \frac{g_s^2}{4\pi} = .15 \tag{3b}$$

At this point we also mention a subtlety which will be incorporated in our later calculations. It arises only for p_T^{-12} contributions (Class I). Due to the indistinguishability of identical quarks coherence factors arise. For example consider up → up versus dp → dp via the ut topology illustrated under Class I in Table 1. The amplitude for up → up contains an extra coherence factor $N_{coh}=2$ relative to dp → dp. (Either of the u quarks in the proton can attach to the external u's.) As a consequence

$$\frac{d\sigma}{dt}(up \to up) = N_{coh}^2 \frac{d\sigma}{dt}(dp \to dp) = 4 \frac{d\sigma}{dt}(dp \to dp)$$

As another example, for ut topologies

$$\frac{d\sigma}{dt}(d\Delta^{++} \to up) = 3 \frac{d\sigma}{dt}(dp \to dp)$$

in the SU(6) symmetry limit.

B. Distribution Functions

Next we turn to the distribution functions, G. Many of these have already been discussed in I but we shall also require a number of new ones. Each G is assumed to have a simplified form

$$x_a G_{a/A}(x_a) = \begin{cases} f_{a/A} N_{a/A}(1+g_{a/A})(1-x_a)^{g_{a/A}} & x_a > \hat{x}_a \\ f_{a/A} N_{a/A}(1+g_{a/A})(1-\hat{x}_a)^{g_{a/A}} & x_a < \hat{x}_a \end{cases} \tag{4}$$

$$N_{a/A} = \left[(1-\hat{x}_a)^{g_{a/A}}(1+g_{a/A}\hat{x}_a)\right]^{-1}$$

Here $f_{a/A}$ is the fraction of A's momentum carried by a, $g_{a/A}$ is the dimensional counting determined power damping as $x_a \to 1$, and $N_{a/A}$ is a shape factor which accounts for the fact that, typically, $x_a G_{a/A}$ does not rise monotonically to its $x_a \to 0$ limit, but rather flattens out (perhaps even falling) in the small x_a region. This behavior is related to the presence of contributions to a given $G_{a/A}$ from non-minimal Fock components of A; for example $G_{u/p}$ receives contributions from 3, 5, ... (qqq, qqq($q\bar{q}$), ...) quark components of the p. The approximation Eq. (4) which includes all such components is a simple way of incorporating this effect. Our goal is to obtain inclusive cross section normalizations to within a factor of two, for which this procedure is entirely adequate. A tabular summary of the cases of interest appears in Table 3 for both pion and proton primaries. For secondary quarks or gluons with non zero color we quote the "per color" distribution function. For instance the full momentum carried by u quarks in the proton is

$$\sum_{\text{colors}} f_{u/p} = .3$$

For secondary 2q ($2\bar{q}$)'s we quote the distribution for a 2q ($2\bar{q}$) to be in a color triplet state of given color. For secondary hadrons the momentum fractions are those carried by a secondary of one specific type; overlapping ways of obtaining the secondary at the minimal Fock state level are not included. For instance, in the case of $f_{M/p}$ we could consider $M=\pi^+$. Such a secondary meson must come from (at least) a 5 quark uud $d\bar{d}$ Fock state of the proton. In this state <u>one</u> of the $u\bar{d}$ pairings carries this Fock state's contribution to $f_{\pi^+/p}$; the other $u\bar{d}$ pairing is not included in defining the $f_{\pi^+/p}$ normalization parameter. In the case of G_{B/π^+} we can consider B=p. A minimal Fock state is $u\bar{d}$ $u\bar{u}$ $d\bar{d}$. There

is only one way to obtain the p state at this minimal level. At the level of higher Fock states the overlap problem becomes more complicated; we will use the minimal Fock state prescriptions.

These considerations become important in high p_T reactions where we must, in general, include all possible ways of obtaining a secondary (carrying a given momentum fraction) from the primary beam—each extraction represents a distinct subprocess contribution. Thus in π^+ production in proton-proton collisions the CIM subprocesses $\pi^+q \to \pi^+q$ require that we include all ways of obtaining the initial π^+ from a proton beam. Thus we sum separately over the two pairings of the $\bar{d}$ (in the $uudd\bar{d}$ state) with a u quark ($uud\,s\bar{s}$ and $uud\,u\bar{u}$ pair states make no contribution to π^+ emission). The $d\bar{d}$ combinations are also two in number. Each of the four meson-like states is characterized by the "non-overlap" momentum fraction of Table 3, $f_{M/p} = .1$, yielding an effective contribution from mesons containing a $\bar{d}$ of 4 times this "non-overlap" value. For more discussion see I.

Many of the entries of the Table have appeared in Reference 1. We concentrate on those not previously considered. These are

$$G_{g/p}\ G_{g/M}\ G_{\bar{B}/p}\ G_{\tilde{B}} \text{ or } B/\pi\ G_{2\bar{q}/p}\ G_{2q} \text{ or } 2\bar{q}/\pi \quad .$$

In all cases we use the dimensional counting constraint[15]

$$G_{a/A}(x) \overset{x \to 1}{\sim} (1-x)^{2n_s^h + n_s^{p.\ell.f.} - 1} \tag{5}$$

where n_s^h is the number of quark spectators to the emission of a which were part of the original A Fock state and $n_s^{p.\ell.f.}$ is the number of fermions

produced through point-like couplings during the emission of secondary a —gluon spectators are not counted. As an example consider the case of g emission for which there are two possibilities:

a) the gluon is part of the original Fock state of p or π, (see Fig. 3a),

$$n_s^h = \begin{cases} 2 & \pi \\ 3 & p \end{cases}$$

and

$$n_s^{p.\ell.f.} = 0 \quad .$$

b) the gluon is emitted in point-like fashion from one of the quarks (see Fig. 3b),

$$n_s^h = \begin{cases} 1 & \pi \\ 2 & p \end{cases}$$

and

$$n_s^{p.\ell.f.} = 1 \quad .$$

We adopt prescription b) so that

$$\begin{aligned} G_{g/p} &\sim (1-x)^4 \\ G_{g/\pi} &\sim (1-x)^2 \end{aligned} \tag{6}$$

Prescription a) yields substantially different inclusive spectra, for sub-processes involving gluons, only near the phase space boundary $x_T \to 1$ (at 90^o c.m.) where $qq \to qq$ scattering is generally more important anyway. We assume that there is no shape factor, $\hat{x}_g=0$, and normalize the total gluon momentum fraction to 50%

$$\sum_{\text{colors}} f_{g/p \text{ or } n} = .5 \tag{7}$$

In the quark-gluon basis the total proton momentum is then

$$\sum_{\substack{q=uds\ \bar{u}\bar{d}\bar{s} \\ \text{colors}}} f_{q/p} + \sum_{\text{colors}} f_{g/p} = 1.12 \tag{8}$$

versus the theoretical constraint of 1. Because of the nature of the shape factor approximations etc. we regard this as acceptable.

The $\bar{B}$ and $2\bar{q}/p$ distributions are determined by a combination of constraints.

a) Pomeron theorem; $B=\bar{B}$ at $x=0$ and $2q=2\bar{q}$ at $x=0$;

b) Dimensional counting which implies

$$g_{\bar{B}/p} = 11 \quad g_{2\bar{q}/p} = 9 \tag{9}$$

c) Reasonable shape factor choices; the value of x_a is chosen to be somewhat below the value of $\hat{x}_a$ at the quasi elastic or weak binding limit peak

$$\hat{x}_{\text{quasi-elastic}} = \frac{n_a}{n(\bar{a}A) + n_a}$$

in the minimal Fock state. Here $n(\bar{a}A)$ is the minimum number of quarks in an $\bar{a}A$ overlap state and n_a the number in a itself. Further discussion appears in I.

As an example, we use our earlier determination of $G_{B/p}$ from momentum sum rule constraints etc. (see I) and $g_{\bar{B}/p} = 11$ to determine $f_{\bar{B}/p}$ from the $x=0$ constraint equation based on a) above,

$$\begin{aligned}(1 + g_{B/p})\ f_{B/p}\ N_{B/p}\ (1-\hat{x}_{B/p})^{g_{B/p}} \\ = (1 + g_{\bar{B}/p})\ f_{\bar{B}/p}\ N_{\bar{B}/p}\ (1-\hat{x}_{\bar{B}/p})^{g_{\bar{B}/p}}\end{aligned} \tag{10}$$

which implies

$$\frac{f_{\bar{B}/p}}{(1 + 11\ \hat{x}_{\bar{B}/p})} = .02 \tag{11}$$

The naive value for $\hat{x}_{\bar{B}/p}$ is $3/9 = \frac{1}{3}$ and we choose $\hat{x}_{\bar{B}/p} = .2$ which yields $N_{\bar{B}/p} = 3.6$ and $f_{\bar{B}/p} = .06$. Clearly one is sensitive to the $\hat{x}_{\bar{B}/p}$ choice because of the large $g_{\bar{B}/p}$ value. In particular for the region $x > \hat{x}_{\bar{B}/p}$ (probed at high p_T)

$$G_{\bar{B}/p}(x) = (1 + g_{\bar{B}/p})\, f_{\bar{B}/p}\, N_{\bar{B}/p}\, \frac{(1-x)^{g_{\bar{B}/p}}}{x} = \frac{.24}{(1-\hat{x}_{\bar{B}/p})^{11}}\, \frac{(1-x)^{11}}{x} \tag{12}$$

indicating that one should regard $G_{\bar{B}/p}$ as uncertain to a factor of 2 or 3 in this region. $G_{2\bar{q}/p}$ is determined from the $G_{2q/p}$ parameters of I and Table 3 in a similar way. We again emphasize that the 2q ($2\bar{q}$) from the p is presumed to be in a color triplet state (as is necessary for the 2q in the valence Fock state); the distribution is per color of the triplet state. Note also that a color singlet "exotic" meson (K^- is an important example) will have the same distribution parameters as for the triplet $2\bar{q}$ of given color; the same minimal Fock state is required and the color factors work out to be the same.[16]

$G_{B,\bar{B}/\pi}$ is determined by noting that in the proton case

$$\lim_{x \to 0} x\, G_{M/p}(x) = \lim_{x \to 0} x\, G_{B/p}(x) = .24 \tag{13}$$

which physically means that sufficiently slow moving particles of these basic types may be extracted with equal ease (despite the difference in the number of quarks contained) from the infinite "sea" of slow or "wee" $q\bar{q}$ pairs. Since we have already, in I, given a rough estimate for $G_{M/\pi}$ we retain it and use the constraint

$$.18 = \lim_{x \to 0} xG_{M/\pi}(x) = \lim_{x \to 0} xG_{B \text{ or } \bar{B}/\pi}(x) \quad , \tag{14}$$

combined with dimensional counting and a reasonable shape factor (or $\hat{x}_{B/\pi}$) choice, to determine the $G_{B \text{ or } \bar{B}/\pi}$ normalization. Note that

$$\lim_{x \to 0} xG_{M \text{ or } B/\pi}(x) < \lim_{x \to 0} xG_{M \text{ or } B/p}(x)$$

as for quarks. $\left(\frac{2}{3}G_{(u+d)/p} \approx G_{(q+\bar{q})/\pi} \text{ at } x=0\right.$ as anticipated from quark counting total cross section relationships.) Of course one might choose to enforce quark counting relations more rigorously by requiring

$$\lim_{x \to 0} xG_{M/\pi} = \frac{2}{3} \lim_{x \to 0} xG_{B/\pi} = \frac{2}{3} \lim_{x \to 0} xG_{M/p} = \frac{4}{9} \lim_{x \to 0} xG_{B/p} \tag{15}$$

(Recall that the $x \to 0$ limit of $G_{a/A}$ is determined by a certain integral over the off shell $\bar{a}A$ cross section.) If we did this and retained the $\hat{x}$ value of Table 3 a 30% increase in the value of $f_{B/p}$ would be required. Of course one could additionally choose a smaller $\hat{x}_{B/p}$ value so as to leave the $x>\hat{x}$ behavior of $G_{B/p}$ unchanged from that given by the parameters of Table 3. This illustrates the typical uncertainties which one should associate with these distribution functions.

Finally $G_{2q \text{ or } 2\bar{q}/\pi}$ is determined by the same principles: dimensional counting, reasonable $\hat{x}_{2q/p}$ choice and the $x \to 0$ constraint

$$\lim_{x \to 0} xG_{2q/\pi}(x) = \lim_{x \to 0} xG_{M \text{ or } B/\pi}(x) \tag{16}$$

Alternatively it is clear that the same pion Fock states which contain a secondary meson also contain a 2q and $2\bar{q}$ pair and that one, therefore, expects

$$G_{2q/\pi}(x) = G_{M/\pi}(x) \tag{17}$$

for a given 2q and M choice provided both the 2q and the M have one quark or antiquark in common with the valance π state. The above naive arguments appear to neglect color. However to good approximation the probability of finding a color singlet secondary meson is the same as that for finding a diquark or anti-diquark in a color triplet state of given color. (Recall again that only color $3(\bar{3})$, $2q(2\bar{q})$ combinations enter into CIM subprocesses.)

Finally we note that fragmentation functions do not appear to satisfy some of the theoretical constraints. For example, the quark distributions u/p and $\bar{u}/p$ appear to lead to a divergent expression for the charge constraint

$$\sum_{\text{color}} \int_0^1 \left(G_{u/p}(x) - G_{\bar{u}/p}(x)\right)\, dx = 1 , \tag{18}$$

since they violate the Pomeron constraint

$$\lim_{x \to 0} xG_{u/p}(x) = \lim_{x \to 0} xG_{\bar{u}/p}(x) \tag{19}$$

However it is clear that $xG_{u/p}(x)$ has a large quasi-elastic peak and, as a consequence, falls as $x \to 0$. As discussed in Appendix A, it is very easy to incorporate this fall off at very small x in such a way as to satisfy both the above constraints without altering the large x ($x > \hat{x}$) behaviors of $G_{u/p}$ and $G_{\bar{u}/p}$ which determine the high p_T results for $x_T = \frac{2p_T}{\sqrt{s}} > \hat{x}$ and which, in turn, are determined by the experimentally well known momentum fractions $f_{u/p}$ and $f_{\bar{u}/p}$.

C. Quark and Gluon Decay Functions

Next we turn to a discussion of the fragmentation functions $D_{C/c}(z)$. We adopt a simple parameterization

$$D_{C/c}(z) = d_{C/c} \frac{(1-z)^{g_{C/c}}}{z} \tag{20}$$

As always $g_{C/c}$ is determined by dimensional counting which controls the $z \to 1$ behavior. The d's will be determined from experiment where possible and otherwise by theoretical constraints. Each D is per color of c. D includes all ways of obtaining C from c including decay via all intermediate unstable particle resonances etc. This is the reason why no flattening of $z\, D_{C/c}$ as $z \to 0$ is incorporated—the resonance etc. contributions fill in the small z region. We are mainly interested in the large z behavior, in any case, as the trigger bias effect implies that the trigger particle C at high p_T takes most of the momentum of c. However the small z behavior will be useful in relating quark decay functions to those for gluons.

The quark decay functions are easily determined from experiment.[17] Within the framework of the form Eq. (20) we will assume that $d_{\pi^+/u} = d_{\pi^+/\bar{d}} = d_{\pi^-/\bar{u}} = \ldots$ corresponding to equal numbers of soft pions of any type in any quark. (This is the decay analogue of the Pomeron theorem for distribution functions.) We employ dimensional counting $g_{\pi^+/u} = 1$, $g_{\pi^-/u} = 5$, $g_{\pi^+/\bar{d}} = 5$ etc.. The $g_{\pi^-/u} = 5$ value neglects possible resonance background, $u \to \rho \to \pi^-$, which could yield $g_{\pi^-/u} = 2$ as the leading term. Our high p_T results are not sensitive to this as for any meson trigger there is always a leading g=1 contribution—for example a d quark for π^- production. Higher g values are dramatically

suppressed by the trigger bias effect. (Only in a case like $\pi^+ + \pi^+ \to \pi^- X$ would these background terms be important—there being no valence d quark to fragment to the π^-.) With these ingredients we find

$$d_{\text{any given charged } \pi/\text{any } q \text{ or } \bar{q}} = .5 \quad g = \begin{cases} 1 \text{ valence } q \\ 5 \text{ non-valence } q \end{cases} \tag{21}$$

per color of the q or $\bar{q}$, (π^0 is taken as $\frac{1}{2}(\pi^+ + \pi^-)$). The resulting fit to experimental data is shown in Fig. 4a, neglecting charmed particle decays into pions. While not perfect in the middle z range, it is good as either $z \to 0$ or $z \to 1$. The middle z range (to which we are not sensitive) is easily fixed up by including the $u \to \rho \to \pi^-$ type contributions with $(1-z)^2$ behavior, just discussed. Kaons are incorporated by assuming SU(3) symmetry (which may overestimate their contributions somewhat)—e.g. $d_{K^+/u} = d_{\pi^+/u} \cdots$.

The baryon d's are based on the experimental $e^+e^- \to \bar{p}$ annihilation data.[17] In order to account for the $z \to 1$ valence ratios and dimensional counting powers we take

$$d_{p/u} = d_{\bar{p}/\bar{u}} = 1 \quad d_{p/d} = d_{\bar{p}/\bar{d}} = .5 \quad g = 3 \tag{22}$$

for the leading $z \to 1$ terms. However the $z \to 0$ limit requires a background term in $D_{p/d}$ and $D_{\bar{p}/\bar{d}}$ characterized by

$$d'_{p/d} = d'_{\bar{p}/\bar{d}} = .5 \quad g = 7 \tag{23}$$

(the 7 corresponding to the 3q $q\bar{q}$ type baryon state's dimensional counting leading power) so that

$$\lim_{z \to 0} D_{p/d}(z) = \lim_{z \to 0} D_{p/u}(z) \tag{24}$$

Thus

$$D_{p/u} = 1\,\frac{(1-z)^3}{z} \qquad D_{p/d} = .5\,\frac{(1-z)^3}{z} + .5\,\frac{(1-z)^7}{z} \tag{25}$$

and so on. Similarly for non valence quarks we assume all things are equally likely as $z \to 0$ so that

$$D_{p/\bar{u}} = D_{\bar{p}/u} = \ldots = \frac{(1-z)^7}{z} \tag{26}$$

The fit to $\bar{p}$ production in e^+e^- annihilation (which determines the overall normalization incorporated in Eqs. (25) and (26)) is shown in Fig. 4b and is surprisingly good.

At this point we may determine the total momentum carried by "stable" hadrons which are decay products of a given quark. (For the purpose of our high p_T phenomenlogy we wish to let the quark decay to its "stable" content.) The momentum fraction is given by

$$f_{C/c} = \frac{d_{C/c}}{1 + g_{C/c}} \tag{27}$$

so that (assuming that $\pi^o = \frac{1}{2}(\pi^+ + \pi^-)$ and that K_s feeds the π channels)

$$\begin{aligned}\sum_H f_{H/u} = {} & \frac{d_{p/u}}{4} + \frac{d_{n/u}}{4} + \frac{d'_{n/u}}{8} + \frac{3}{2}\left(\frac{d_{\pi^+/u}}{2} + \frac{d_{\pi^-/u}}{6}\right) + \frac{d_{K^+/u}}{2} \\ & + \frac{d_{K^-/u}}{6} + \frac{\frac{1}{2}d_{K_o/u}}{2} + \frac{\frac{1}{2}d_{\bar{K}_o/u}}{6} + \frac{d_{\bar{p}/u}}{6} + \frac{d_{\bar{n}/u}}{8}\end{aligned} \tag{28}$$

$$= \frac{1}{4} + \frac{1}{8} + \frac{1}{16} + \frac{3}{2}\left(\frac{1}{4} + \frac{1}{12}\right) + \frac{3}{2}\left(\frac{1}{4} + \frac{1}{12}\right) + \frac{1}{16} \times 2$$

$$= 1.56$$

Theoretically the number should be 1. Clearly the kaon's are overestimated and perhaps also the antibaryons. Given the approximate nature of our parametrization the result is again remarkably good. The high p_T predictions will of course be sensitive only to the valence type distributions at large z which are in quite good agreement with data as we have seen.

Turning now to the gluons we are, of course, faced with a distinct lack of data. Our determination of the decay distributions will be theoretical. There are two major ingredients.

First is the color separation model of Ref. 18 which states that the logarithmic coefficient for the charged multiplicity of a gluon jet should be 9/4 that of a quark jet. This will be used to determine the $z \to 0$ behavior of $D_{M/g}$ and $D_{B/g}$. The coefficient of $\frac{1}{z}$ in $D_{A/g}(D_{A/q})$ gives the coefficient of the logarithm in $\langle n \rangle_A$ for a gluon (quark) jet.

Second we employ dimensional counting and a point-like gluon coupling in our calculations. We begin by reminding the reader that the distribution for a gluon to turn into a q or $\bar{q}$ by the point-like QCD virtual pair diagram is[19]

$$D_{q/g}(z) \overset{z \to 1}{\underset{\alpha}{\sim}} 1 + (1-z)^2; \tag{29}$$

the first term is related to the quark helicity non flip transition for the crossed reaction $q \to q + g$ while the second term corresponds to the quark helicity flip possibility. In our point-like emission picture this type of distribution underlies the emission of a hadron from a gluon—first a $q\bar{q}$ pair is created and then the q or $\bar{q}$ picks up additional quarks from the vacuum to form the observed hadron. These additional quarks (1 for a meson—2 for a baryon) give rise to an equal number of hadronic spectators; in addition we have the 1 unused point-like fermion q or $\bar{q}$

spectator which was part of the initial pair. Thus we incorporate dimensional counting and the two distinct $z \to 1$ behaviors (and their relative coefficient) through the forms[20]

$$D_{M/g} = d_{M/g}\left[\frac{(1-z)^2}{z} + \frac{(1-z)^4}{z}\right] \qquad n_s^h = 1 \; n_s^{p.\ell.f.} = 1$$
$$D_{B/g} = d_{B/g}\left[\frac{(1-z)^4}{z} + \frac{(1-z)^6}{z}\right] \qquad n_s^h = 2 \; n_s^{p.\ell.f.} = 2 \tag{30}$$

with the $z \to 0$ limits

$$\lim_{z \to 0} z\, D_{M(B)/g} = 2d_{M(B)/g} \tag{31}$$

Our <u>charged</u> multiplicity constraints are (separating baryons from mesons and using a u quark jet)

$$\frac{9}{4}\left[\langle n\rangle_{\pi^+/u} + \langle n\rangle_{\pi^-/u} + \langle n\rangle_{K^+/u} + \langle n\rangle_{K^-/u}\right]$$
$$= \langle n\rangle_{\pi^+/g} + \langle n\rangle_{\pi^-/g} + \langle n\rangle_{K^+/g} + \langle n\rangle_{K^-/g} \tag{32}$$

and

$$\frac{9}{4}\left[\langle n\rangle_{p/u} + \langle n\rangle_{\bar{p}/u}\right]$$
$$= \langle n\rangle_{p/g} + \langle n\rangle_{\bar{p}/g} \tag{33}$$

The notation $\langle n\rangle$ actually refers to the coefficient of the logarithm in $\langle n\rangle$. They become

$$\frac{9}{4}\left[d_{\pi^+/u} + d_{\pi^-/u} + d_{K^+/u} + d_{K^-/u}\right]$$
$$= 2\left[d_{\pi^+/g} + d_{\pi^-/g} + d_{K^+/g} + d_{K^-/g}\right] \tag{34}$$

and

$$\frac{9}{4}\left[d_{p/u} + d_{\bar{p}/u}\right] = 2\left[d_{p/g} + d_{\bar{p}/g}\right] \tag{35}$$

Noting that, of course, $d_{\pi^+/g} = d_{\pi^-/g}$ and $d_{p/g} = d_{\bar{p}/g}$ and assuming SU(3) symmetry $d_{K^+/g} = d_{K^-/g} = d_{\pi^+/g}$ we obtain

$$d_{\pi^+/g} = \frac{9}{16} \tag{36}$$

and

$$d_{p/g} = \frac{18}{16} \tag{37}$$

We adopt the crude values of .5 and .9 respectively—both d's are almost certainly overestimated above as we see below.

We may check the stable hadron momentum content of the gluon

$$\sum_H f_{H/g} = \left(d_{p/g} + d_{n/g} + d_{\bar{p}/g} + d_{\bar{n}/g}\right)\left(\frac{1}{5} + \frac{1}{7}\right) \tag{38}$$

$$+ \left(d_{\pi^+/g} + d_{\pi^-/g} + d_{K^+/g} + d_{K^-/g} + d_{\pi^o/g} + \frac{1}{2} d_{(K^o + \bar{K}^o)/g}\right)\left(\frac{1}{3} + \frac{1}{5}\right)$$

(The two numbers in parenthesis are from the helicity non-flip and flip terms respectively). Using .5 for all meson d's and .9 for all baryon d's yields

$$\sum_H f_{H/g} = \underset{1.2}{\text{Baryons}} + \underset{1.6}{\text{Mesons}} \tag{39}$$

indicating that our naive determinations yield too much momentum per hadron. Since we are not certain where to apply a correction we retain the naive values $d_{M/g} = .5$ and $d_{B/g} = .9$ in future calculations. However the reader should keep in mind that the gluon decay contributions may be too large by roughly a factor of two. Of course high p_T experiment probes only the $(1-z)^2$ and $(1-z)^4$ terms for $g \to M$ and $g \to B$ respectively which could still

be correct. (For instance by discarding the nonleading terms only, $(1-z)^4$ and $(1-z)^6$ for $g \to M$ and $g \to B$, the momentum sum becomes 1.7 and the theoretical constraint is considerably closer to being satisfied.) Also one should keep in mind that both the quark and gluon momentum contents are somewhat too large; reduction of both can be counteracted by an increase in the value of α_s which is a yet to be determined parameter of the p_T^{-4} reactions yielding quark and gluon jets. The general systematics which we hope to reveal are not, in any case, sensitive to factors of 2.

Thus our effective results for high p_T calculations, keeping only leading $z \to 1$ terms, because of severe trigger bias suppression of non-leading terms, are given in Table 4. Results not listed are to be obtained by SU(3), SU(2), or charge conjugation, e.g. $D_{+/u} = D_{-/\bar{u}} = D_{-/d} = \ldots$.

D. Calculational Techniques

In I a simple analytic result for $E\frac{d\sigma}{d^3p}$, as given by Equation (1) was derived. Using the distribution, subprocess and decay function forms previously discussed we may summarize the results for 90° c.m. as follows:

a) First consider production of c at 90° c.m. We find that the contribution of a given subprocess is given by (for $x_T \gtrsim \hat{x}_a, \hat{x}_b$)

$$E\frac{d\sigma}{d^3p}(AB \to cX) = I_{c/AB}\frac{(1-x_T)^F}{(p_T^2)^N} \tag{40}$$

where N is that of the $ab \to cd$ subprocess, Eq. (2), $F=1 + g_{a/A} + g_{b/B}$ and

$$I_{c/AB} = \mathcal{D}90^\circ\, f_{a/A}\, f_{b/B}\, \frac{\Gamma(2+g_{a/A})\Gamma(2+g_{b/B})}{\Gamma(2+g_{a/A}+g_{b/B})}\, 2^{2+g_{a/A}+g_{b/B}-2N} \tag{41}$$

Typical values of x_a and x_b in the convolution, Eq. (1), are also found to be of order x_T, i.e. we are sensitive to the middle ranges of x_a and x_b.

b) If there is a final quark or gluon fragmentation $c \to C$ then we compute $E \frac{d\sigma}{d^3p}$ $(AB \to CX)$ starting from the form Eq. (41) and obtain

$$E \frac{d\sigma}{d^3p} \overset{ab \to cd}{(AB \to CX)} = I_{c/AB} \frac{\left(1-x_T\right)^{1+g_{C/c}+F}}{\left(p_T^2\right)^N} \tag{42}$$

$$\frac{\Gamma(1+g_{C/c})\Gamma(F+1)}{\Gamma(2+F+g_{C/c})} \hat{J}(x_T)$$

where

$$\hat{J}(x_T) = \left(\frac{1}{1 - \frac{g_{C/c}}{F+g_{C/c}} (1-x_T)} \right)^{3+F-2N} . \tag{43}$$

Typical values of x_C in Eq. (1) (i.e. z of Eq. (20)) are of order $\frac{F}{F+g_{C/c}} + \frac{g_{C/c}}{F+g_{C/c}} x_T$ i.e. very near 1 for $F >> g_{C/c}$. This shows why the exact $z \to 1$ behavior of $D_{C/c}(z)$ is so critical.

As $x_T \to 1$ $\hat{J}(x_T) \to 1$, and we see that the result is especially simple for our two typical meson choices $g_{C/c}$=1 and 2. The trigger bias suppression factor coming from the Γ functions is

$$\begin{array}{ll} \frac{1}{(F+2)(F+1)} & g_{C/c} = 1 \quad \text{(quark)} \\ & C = \text{meson} \\ \frac{2}{(F+3)(F+2)(F+1)} & g_{C/c} = 2 \quad \text{(gluon)} \end{array} \tag{44}$$

.

For baryons the standard values are $g_{C/c}$=3 and 4 for which the Γ function factor is

$$\frac{6}{(F+4)(F+3)(F+2)(F+1)} \qquad g_{C/c} = 3 \quad \text{(quark)}$$

$$C = \text{baryon} \qquad (45)$$

$$\frac{24}{(F+5)(F+4)(F+3)(F+2)(F+1)} \qquad g_{C/c} = 4 \quad \text{(gluon)}$$

It is clear that these are progressively smaller numbers.

c) If C can be produced by a given subprocess without fragmentation (i.e. promptly), as for CIM contributions, and can also be produced as a decay product of a resonance which can be produced promptly by the same subprocess then we include a total/prompt ratio, T/P. It accounts for this resonance feed through relative to the prompt production cross section for the trigger particle. We will see that for mesons T/P is of order 2 while for baryons T/P $\sim$1.2. Such ratios represent the result of a large number of contributing resonances (decaying to a given meson or baryon trigger) each suppressed by the type of fragmentation trigger bias effect discussed under b). Further discussion appears in I. It should be noted that we use the same T/P for direct processes as for indirect processes. Direct processes are slightly more restrictive as to what resonances may be produced so that in a finer comparison one might wish to decrease T/P for the direct processes.

II. RESULTS

A. Numerology

We will not present any specific calculations. Examples appear in I although the complexities of coherence factors were not elaborated on there. We will summarize all cross section contributions including those already presented in I. We begin by concentrating on single particle cross sections. We use the notation $\varepsilon = 1-x_T$. Only contributions which are of significant size are retained. All expressions are valid only for $x_T \geq .15$ where x_a and x_b (of order x_T) are typically larger than $\hat{x}_{a/A}$ and $\hat{x}_{b/B}$ as required for use of the simple analytic approximations. Thus $\sqrt{s}$ = 63 GeV plots presented later are only completely reliable for p_T's > 4.5 GeV/c. The trends shown below this p_T value are, however, quite representative of more precise calculations (this is discussed more fully in the first Appendix of I). The results are presented as a series of equations. In order to indicate what subprocess underlies each contribution a label appears above each term. This label refers to the subprocess labelling of Table 2. For example, a label ${}_{q}{}^{M}\mathrm{II}_{c}$ refers to the ut topology for qM → qM, while ${}_{\bar{q}}{}^{M}\mathrm{II}_{c}$ refers to the ut topology for $\bar{q}$ M → $\bar{q}$ M. For proton proton scattering there is, of course, no point in labelling the sources of the q and M as they are both protons. In a term like ${}_{q}{}^{M}\mathrm{II}_{c}$ the symmetric term, ${}_{M}{}^{q}\mathrm{II}_{c}$, is automatically included. For A=$\pi^{\pm}$ and B=p these left side labels <u>will</u> indicate the source. For instance ${}_{M}{}^{q}\mathrm{II}_{c}$ refers to qM → qM (ut topology) initiated by a q from the π^+ or π^- and an M from the p. For gluon/quark scattering followed by fragmentation a label appears to the right which indicates which final state particle fragments. For example, III^{q}_{c1} indicates that gq scattering occurred

followed by q fragmentation to the observed final state particle. We do not indicate where the initial q and g come from (A or B) even in the $\pi^{\pm}$ p scattering case. The two contributions $\pi^{\pm} \to g\ p \to q$ and $\pi^{\pm} \to q\ p \to g$ followed by qg scattering have the same ϵ power (if the q is a valence q for both π and p) and are lumped together. This particular case is, in fact, the only case in which the reader cannot use the ϵ power to determine where the initial particles (assuming they are not the same, i.e. for $q\bar{q} \to q\bar{q}$ $gq \to gq$ $g\bar{q} \to g\bar{q}$ and $q\bar{q} \to gg$) came from in $\pi^{\pm}$ p scattering. As an example consider $\pi^{\pm}\ p \to \pi^{+}$. A glance at the expression for this reaction indicates a $g\bar{q} \to g\bar{q}$ $\left(III^{g}_{c2}\right)$ contribution with ϵ power ϵ^{9}. It is clear that the $\bar{q}$ came from the π ($g_{\bar{q}/\pi} = 1$) and the g from the p ($g_{g/p} = 4$) so that with gluon fragmentation ($g_{\pi^{+}/g} = 2$) the total ϵ power is

$$2 + g_{\bar{q}/\pi} + g_{g/p} + g_{\pi^{+}/g} = 2+1+4+2 = 9 \quad .$$

Had the $\bar{q}$ come from the p and the g from the π the ϵ power would have been 13. In the process III cases we do not indicate the precise fractional breakup when more than one subprocess contributes to a given term.

Another subtlety which might confuse the reader is the presence of contributions with different ϵ power but with the same subprocess label. For instance in $pp \to \pi^{\pm}$ there are two CIM terms with the label II_{c} but with ϵ powers of 9 and 13 respectively. The higher ϵ power as indicated comes from $\bar{q}M \to \bar{q}M$ (instead of $qM \to qM$) which has the same ut topology but the $\bar{q}$ is a member of the proton sea and is characterized by $g_{\bar{q}/p} = 7$ versus $g_{q/p} = 3$. Another case appears in $pp \to \binom{K^{+}}{K^{-}}$; there are two III^{q}_{a1} and two III^{q}_{c1} terms. Here the difference is again whether or not a valence proton quark has initiated the reaction—the higher ϵ power terms arise from $\bar{s}(s)$ quarks which can yield substantial contributions to K^{+} (K^{-}) production.

The coupling constant dependence of the different subprocesses appears in Table 2. We have already incorporated the canonical values of Eq. (3a) and (3b) in the numbers we present. Finally "direct" contributions are indicated by a "dir." for whichever of the incoming particles is the direct participant.

$$E\frac{d\sigma}{d^3p}\left(pp \to \begin{matrix}\pi^+\\ \pi^-\end{matrix} X\right) = \frac{T}{P}\frac{\varepsilon^9}{p_T^8}\left\{\begin{matrix}.95^{M}_{q}II_c + .05^{M}_{q}II_b \\ \binom{4.6}{3.1}\end{matrix} + \begin{matrix}\frac{q}{q}II_a \\ \binom{.42}{.33}\end{matrix}\varepsilon^2 + \right.$$

$$\left. + \begin{matrix}.95\frac{M}{q}II_c + .05\frac{M}{q}II_b \\ \binom{1.0}{.58}\end{matrix}\varepsilon^4\right\} + 10^{-4}\frac{\varepsilon^9}{p_T^4}\left\{\frac{III^{q}_{a1}}{\binom{2.4}{1.7}/(1-.13\varepsilon)^6} + \frac{III^{q}_{c1}}{\binom{6.4}{4.3}/(1-.11\varepsilon)^7}\varepsilon + \frac{III^{g}_{c1}}{\binom{1.94}{1.94}/(1-.2\varepsilon)^7}\varepsilon^2\right.$$

$$\left. + \frac{III^{g}_{f}}{\binom{3.3}{3.3}/(1-.18\varepsilon)^8}\varepsilon^3 + \frac{III^{q+\bar{q}}_{b}}{\binom{1.3}{1.1}/(1-.08\varepsilon)^{10}}\varepsilon^4\right\}$$

$$E\frac{d\sigma}{d^3p}\left(pp \to \begin{matrix}K^+\\ K^-\end{matrix} X\right) = \frac{T}{P}\frac{\varepsilon^9}{p_T^8}\left\{\begin{matrix}.95^{M}_{q}II_c + .05^{M}_{q}II_b \\ \binom{4.6}{0}\end{matrix} + \begin{matrix}\frac{q}{\bar{q}}II_a \\ \binom{.42}{.15}\end{matrix}\varepsilon^2 + \begin{matrix}.95\frac{M}{q}II_c + .05\frac{M}{q}II_b \\ \binom{1.0}{.72}\end{matrix}\varepsilon^4\right\}$$

$$+ 10^{-4}\,\frac{\varepsilon^9}{p_T^4}\left\{\begin{matrix} III_{a1}^{q} & III_{c1}^{q} & III_{c1}^{g} & III_{f}^{g} \\ \frac{\binom{2.4}{0}}{(1-.13\varepsilon)^6} + \frac{\binom{6.4}{0}}{(1-.11\varepsilon)^7}\,\varepsilon + \frac{\binom{1.94}{1.94}}{(1-.2\varepsilon)^7}\,\varepsilon^2 & + \frac{\binom{3.3}{3.3}}{(1-.18\ )^8}\,\varepsilon^3 + \end{matrix}\right.$$

$$\left.\begin{matrix} III_{b}^{q+\bar{q}} + III_{a1}^{q} & III_{c2}^{\bar{q}} + III_{c1}^{q} & III_{c2}^{g} \\ + \frac{\binom{1.3}{.8}}{(1-.08\varepsilon)^{10}}\,\varepsilon^4 + \frac{\binom{.6}{1.2}}{(1-.077\varepsilon)^{11}}\,\varepsilon^5 + \frac{\binom{.3}{.3}}{(1-.14\varepsilon)^{11}}\,\varepsilon^6 \end{matrix}\right\}$$

$$E\,\frac{d\sigma}{d^3p}\,(pp \to p\,X) = \frac{T}{P}\,\frac{\varepsilon^3}{p_T^{12}}\left\{\begin{matrix} {}^{dir}_{q}I_c & & {}^{2q}_{q}I_d \\ 342(1-\varepsilon)^2\,[1 + .25(1+\varepsilon)^2] + & 3.9\,\varepsilon^2 & \end{matrix}\right.$$

$$\left.\begin{matrix} .2^{2q}_{M}I_e + .8^{B}_{q}I_c & {}^{dir}_{\bar{q}}I_b & .12^{B}_{q}I_b + .88^{q}_{q}I_a \\ + \left(426.3 + 15(1-\varepsilon)^6\,(1+\varepsilon)^{-2}\left[1 + \frac{(1-\varepsilon)^2}{(1+\varepsilon)^2}\right]\right)\varepsilon^4 + & 16.8\,\varepsilon^8 & \end{matrix}\right\}$$

$$+ 10^{-5}\,\frac{\varepsilon^{11}}{p_T^4}\left\{\begin{matrix} III_{a1}^{q} & III_{c1}^{q} & III_{c1}^{g} & III_{f}^{g} \\ \frac{3.5}{(1-.3\varepsilon)^6} + \frac{7.8}{(1-.27\varepsilon)^7}\varepsilon + \frac{2.8}{(1-.33\varepsilon)^7}\varepsilon^2 + \frac{4.1}{(1-.31\varepsilon)^8}\,\varepsilon^3 & & & \end{matrix}\right.$$

$$\left.\begin{matrix} III_{a1}^{q} + III_{b}^{q} \\ + \frac{.71\varepsilon^4}{(1-.21\varepsilon)^{10}} \end{matrix}\right\}$$

$$E\frac{d\sigma}{d^3p}(pp \to \bar{p}X) = \frac{T}{P}\frac{\varepsilon^{11}}{p_T^{12}}\left\{\begin{matrix} {}^{q}_{\bar{q}}I_a & .5{}^{\bar{B}}_{q}I_b + .5{}^{M}_{2\bar{q}}I_e & {}^{\bar{B}}_{\bar{q}}I_c \\ 11 + & 92\ \varepsilon^4 & + 52\ \varepsilon^8 \end{matrix}\right\}$$

$$+ 10^{-5}\frac{\varepsilon^{13}}{p_T^4}\left\{\begin{matrix} III^{g}_{c1} & III^{g}_{f} & III^{\bar{q}}_{b} & III^{\bar{q}}_{c2} \\ \frac{2.8}{(1-.33\varepsilon)^7} + & \frac{4.1}{(1-.31\varepsilon)^8}\varepsilon + & \frac{.35}{(1-.21\varepsilon)^{10}}\varepsilon^2 + & \frac{.44}{(1-.2\varepsilon)^{11}}\varepsilon^3 \end{matrix}\right\}$$

The cross sections for pion beams appear next.

$$E\frac{d\sigma}{d^3p}\begin{pmatrix}\pi^+\\ \pi^-\end{pmatrix} p \to \pi^+ X) = \frac{T}{P}\frac{\varepsilon^3}{p_T^8}\left\{\begin{matrix} {}^{q}_{q}II^{dir}_{c} & {}^{q}_{q}II^{dir}_{b} & {}^{\bar{q}}_{q}II_a \\ \left(2.91(1-\varepsilon) + \begin{matrix}0\\ .11\end{matrix}(1-\varepsilon)^5\right) & + & \begin{pmatrix}.28\\ .11\end{pmatrix}\varepsilon^2 \end{matrix}\right.$$

$$\begin{pmatrix}.72\\ 0\end{pmatrix}{}^{q,\bar{q}}_{M}II_c + \begin{pmatrix}.24\\ .74\end{pmatrix}{}^{M}_{q}II_c + \begin{pmatrix}.02\\ .2\end{pmatrix}{}^{q,\bar{q}}_{M}II_b + \begin{pmatrix}.02\\ .06\end{pmatrix}{}^{M}_{q}II_b$$

$$+ \begin{pmatrix}9.17\\ .75\end{pmatrix}\varepsilon^4 \quad + \quad +$$

$$\left.\begin{matrix} {}^{\bar{q}}_{q}II^{dir}_{b} & {}^{\bar{q}}_{q}II^{dir}_{c} & {}^{q}_{\bar{q}}II_a & \begin{pmatrix}0\\ .76\end{pmatrix}{}^{q,\bar{q}}_{M}II_c + \begin{pmatrix}.96\\ .24\end{pmatrix}{}^{M}_{\bar{q}}II_c + \begin{pmatrix}.04\\ 0\end{pmatrix}{}^{M}_{\bar{q}}II_b \\ \left(.47\frac{(1-\varepsilon)^5}{(1+\varepsilon)^4} + \begin{matrix}0\\ 7.7\end{matrix}\frac{(1-\varepsilon)}{(1+\varepsilon)^4}\right)\varepsilon^4 + & \begin{pmatrix}.08\\ .11\end{pmatrix}\varepsilon^6 + & \begin{pmatrix}.67\\ .69\end{pmatrix}\varepsilon^8 \end{matrix}\right\}$$

$$+ 10^{-4}\,\frac{\varepsilon^7}{p_T^4}\left\{\frac{III^q_{a1}+III^q_b}{\binom{4.8}{2.2}(1-.17\varepsilon)^4} + \frac{III^q_{c1}}{\binom{12.6}{3.6}(1-.14\varepsilon)^5}\,\varepsilon + \frac{III^g_{c1}+III^g_{c2}}{\binom{3.33}{3.33}(1-.25\varepsilon)^5}\,\varepsilon^2\right.$$

$$\left. + \frac{III^g_f}{\binom{5.4}{5.4}(1-.22\varepsilon)^6}\,\varepsilon^3 + \frac{III^q_{a1}+III^{\bar q}_{a2}+III^{q+\bar q}_b}{\binom{2.9}{1.1}(1-.1\varepsilon)^8}\,\varepsilon^4 + \frac{III^q_c+III^{\bar q}_{c2}}{\binom{.67}{1.1}(1-.09\varepsilon)^9}\,\varepsilon^5\right\}$$

$$E\,\frac{d\sigma}{d^3p}\binom{\pi^+}{\pi^-} p \to \pi^- X = \frac{T}{P}\,\frac{\varepsilon^3}{p_T^8}\left\{\binom{q^{dir}{}_{II_c}}{0} + \binom{q^{dir}{}_{II_b}}{1.97\,(1-\varepsilon)+.19(1-\varepsilon)^5} + \binom{\bar q_{II_a}}{.08}\varepsilon^2\right.$$

$$+ \binom{0}{.73}{}^{q,\bar q}{}_{M}II_c + \binom{.8}{.23}{}^{M}_{q}II_c + \binom{.16}{.03}{}^{q,\bar q}{}_{M}II_b + \binom{.04}{.01}{}^{M}_{q}II_b$$

$$+ \binom{.5}{6.61}\varepsilon^4 +$$

$$+ \left(.47\,\frac{(1-\varepsilon)^5}{(1+\varepsilon)^4} + 7.7\,\frac{(1-\varepsilon)}{(1+\varepsilon)^4}\right)\varepsilon^4 + \binom{.11}{.083}\varepsilon^6 +$$

$$\left. \binom{.7}{0}{}^{q,\bar q}{}_{M}II_c + \binom{.3}{.94}{}^{M}_{\bar q}II_c + \binom{0}{.06}{}^{M}_{\bar q}II_b + \binom{.55}{.67}\varepsilon^8\right\}$$

$$+\frac{10^{-4}\varepsilon^7}{p_T^4}\left\{\frac{\binom{1.45}{4.39}}{(1-.17\varepsilon)^4}+\frac{\binom{2.42}{11.4}}{(1-.14\varepsilon)^5}\varepsilon+\frac{\binom{3.3}{3.3}}{(1-.25\varepsilon)^5}\varepsilon^2+\frac{\binom{5.4}{5.4}}{(1-.22\varepsilon)^6}\varepsilon^3+\right.$$

$$\left.+\frac{\binom{1.1}{2.8}}{(1-.1\varepsilon)^8}\varepsilon^4+\frac{\binom{1.14}{.67}}{(1-.09\varepsilon)^9}\varepsilon^5\right\}$$

The p_T^{-4} genealogy for the above equation is as for π^+ production.

$$E\frac{d\sigma}{d^3p}\binom{\pi^+}{\pi^-}p\to K^+X=\frac{T}{P}\frac{\varepsilon^3}{p_T^8}\left\{\begin{matrix}q^{dir}{}_{II_b} & \bar{q}_{II_a}\\ \binom{.12\ (1-\varepsilon)^5}{0} & +\binom{.11}{.11}\varepsilon^2\end{matrix}\right.$$

$$\binom{.05}{.2}_{q,\bar{q}}{}_{M}{}_{II_b}+\binom{.03}{.05}_{q}{}^{M}{}_{II_b}+\binom{.75}{0}_{M}{}^{q}{}_{II_c}+\binom{.17}{.75}_{q}{}^{M}{}_{II_c}$$

$$+\binom{3.2}{.75}\varepsilon^4+$$

$$\bar{q}^{dir}{}_{II_c}\qquad {}^{q}_{q}II_a\qquad \binom{.35}{.7}_{q,\bar{q}}{}^{M}{}_{II_c}+\binom{.65}{.3}_{q,\bar{q}}{}_{M}{}_{II_c}\Bigg\}$$

$$\binom{7.7\ \frac{(1-\varepsilon)}{(1+\varepsilon)^4}}{0}\varepsilon^4+\binom{.34}{.11}\varepsilon^6+\binom{.97}{.69}\varepsilon^8\Bigg\}$$

$$+\frac{10^{-4}\varepsilon^7}{p_T^4}\left\{\frac{\binom{3.2}{2.2}}{(1-.17\varepsilon)^4}+\frac{\binom{8.1}{3.6}}{(1-.14\varepsilon)^5}\varepsilon+\frac{\binom{3.3}{3.3}}{(1-.25\varepsilon)^5}\varepsilon^2+\frac{\binom{5.4}{5.4}}{(1-.22\varepsilon)^6}\varepsilon^3+\right.$$

$$\left.+\frac{\binom{2.1}{1.1}}{(1-.1\varepsilon)^8}\varepsilon^4+\frac{\binom{.9}{1.1}}{(1-.09\varepsilon)^9}\varepsilon^5\right\}$$

The p_T^{-4} genealogy for the above equation is as for π^+ production.

$$E\frac{d\sigma}{d^3p}\begin{pmatrix}\pi^+\\ \pi^-\end{pmatrix} p \to K^- X\Big) = \frac{T}{P}\frac{\varepsilon^5}{p_T^8}\Bigg\{ \begin{matrix}\bar{q}_{II_a} & \begin{pmatrix}.87\\.16\end{pmatrix}^{q,\bar{q}}_{M^{II}_b} + \begin{pmatrix}.13\\.02\end{pmatrix}^{M}_{q^{II}_b} + \begin{pmatrix}0\\.82\end{pmatrix}^{\bar{q}}_{M^{II}_c}\\ \begin{pmatrix}0\\.18\end{pmatrix} + & \begin{pmatrix}.086\\.72\end{pmatrix}\varepsilon^2\end{matrix}$$

$$+\left(\begin{matrix}\bar{q}^{dir}{}_{II_b} & \bar{q}^{dir}{}_{II_c}\\ 0 & \frac{q}{q}_{II_a}\\ .47\frac{(1-\varepsilon)^5}{(1+\varepsilon)^4}+7.7\frac{(1-\varepsilon)}{(1+\varepsilon)^4} & \begin{pmatrix}.4\\.2\end{pmatrix}_{q,\bar{q}}{}^{M}_{II_c} + \begin{pmatrix}.6\\.8\end{pmatrix}^{q,\bar{q}}_{M^{II}_c}\end{matrix}\right)\varepsilon^2 + \begin{pmatrix}.19\\.19\end{pmatrix}\varepsilon^4 + \begin{matrix}\\ \begin{pmatrix}.58\\1.03\end{pmatrix}\varepsilon^6\end{matrix}\Bigg\}$$

$$+10^{-4}\frac{\varepsilon^7}{p_T^4}\Bigg\{\frac{\begin{pmatrix}.13\\1.86\end{pmatrix}}{(1-.17\varepsilon)^4}+\frac{\begin{pmatrix}0\\4.5\end{pmatrix}}{(1-.14\varepsilon)^5}\varepsilon+\frac{\begin{pmatrix}3.3\\3.3\end{pmatrix}}{(1-.25\varepsilon)^5}\varepsilon^2+\frac{\begin{pmatrix}5.4\\5.4\end{pmatrix}}{(1-.22\varepsilon)^6}\varepsilon^3+$$

$$+\frac{\begin{pmatrix}1.4\\2.2\end{pmatrix}}{(1-.1\varepsilon)^8}\varepsilon^4+\frac{\begin{pmatrix}1.8\\1.6\end{pmatrix}}{(1-.09\varepsilon)^9}\varepsilon^5\Bigg\}$$

The p_T^{-4} genealogy for the above equation is as for π^+ production.

$$E\frac{d\sigma}{d^3p}\begin{pmatrix}\pi^+\\ \pi^-\end{pmatrix} p \to pX\Big) = \frac{T}{P}\frac{\varepsilon}{p_T^{12}}\Bigg\{ \begin{matrix}2q^{dir}{}_{I_e} & \bar{q}^{}_{dir}{}_{I_b}\\ (1-\varepsilon)(1+\varepsilon)^4\begin{pmatrix}1.2\\.6\end{pmatrix} + & \left[(1-\varepsilon)^8(1+\varepsilon)^2 + \right.\end{matrix}$$

$$\left. + (1-\varepsilon)^6(1+\varepsilon)^4\right]\begin{pmatrix}.05\\.21\end{pmatrix} + (1-\varepsilon)^2\left[(1+\varepsilon)^2 + .25(1+\varepsilon)^4\right]\begin{pmatrix}13.7\\3.4\end{pmatrix} + \begin{matrix}{}^{q}_{dir}{}_{I_c} & {}^{}_{2q}{}^{q}_{}{}_{I_d}\\ \begin{pmatrix}.37\\.37\end{pmatrix}\varepsilon^2\end{matrix}$$

$$.04\frac{\bar{q}}{q}_{I_a} + .01\frac{\bar{q}}{B}_{I_b} + .14\ {}^{M}_{2q}{}_{I_e} + .81\ {}^{q}_{B}{}_{I_c}\ \ {}^{2q}_{q}{}_{I_d}$$

$$+\begin{pmatrix}117.3\\42.7\end{pmatrix}\varepsilon^4 \qquad\qquad +\begin{pmatrix}1.8\\1.2\end{pmatrix}\varepsilon^6 +$$

$$.06\frac{q}{q}_{I_a} + .78\ {}^{B}_{q}{}_{I_c} + .16\ {}^{2q}_{M}{}_{I_e}\Bigg\}$$

$$+\begin{pmatrix}172.2\\135.1\end{pmatrix}\varepsilon^8$$

$$+\frac{10^{-5}\varepsilon^9}{p_T^4}\left\{\begin{array}{lll} III_{a1}^q + III_b^q & III_{c1}^q & III_{c1}^g + III_{c2}^g \\ \binom{6.3}{5.6} & \frac{\binom{12.4}{9.4}}{(1-.37\varepsilon)^4} + \frac{}{(1-.33\varepsilon)^5}\varepsilon + & \frac{\binom{6.8}{6.8}}{(1-.4\varepsilon)^5}\varepsilon^2 + \end{array}\right.$$

$$\left.\begin{array}{ll} III_f^g & III_{a1}^q + III_b^q \\ \frac{\binom{9.2}{9.2}}{(1-.36\varepsilon)^5}\varepsilon^3 + & \frac{\binom{1.22}{.84}}{(1-.25\varepsilon)^8}\varepsilon^4 \end{array}\right\}$$

$$E\frac{d\sigma}{d^3p}\binom{\pi^+}{\pi^-} p \to \bar{p}\, X) = \frac{T}{P}\frac{\varepsilon^5}{p_T^{12}}\left\{\begin{array}{lll} \bar{q}I_a & .65^{2\bar{q}}_{M}I_e + .05^{\bar{B}}_{q}I_b + .3^{q}_{\bar{q}}I_a & \\ \binom{4.6}{8.4} + & \binom{19.3}{27.3}\varepsilon^4 & + \end{array}\right.$$

$$\left.\begin{array}{lll} 2\bar{q}^{dir}I_e & .97_{2\bar{q}}^{\bar{q}}I_e + .03^{2\bar{q}}_{\bar{q}}I_e & .94\,\frac{\bar{q}}{\bar{B}}I_c + .04^{q}_{\bar{B}}I_b + .01\left(\frac{\bar{B}}{q}I_c + 2^{M}_{\bar{q}}I_e\right) \\ + \binom{9.2}{9.2}\frac{(1-\varepsilon)}{(1+\varepsilon)^4}\varepsilon^4 + & \binom{12.5}{12.9}\varepsilon^6 + & \binom{2205}{4263}\varepsilon^8 \end{array}\right\}$$

$$+10^{-5}\frac{\varepsilon^9}{p_T^4}\left\{\begin{array}{lll} III_b^{\bar{q}} & III_{c2}^{\bar{q}} & III_{c1}^g + III_{c2}^g \\ \frac{\binom{1.6}{3.1}}{(1-.38\varepsilon)^4} + & \frac{\binom{3.0}{6.0}}{(1-.33\varepsilon)^5}\varepsilon + & \frac{\binom{6.8}{6.8}}{(1-.4\varepsilon)^5}\varepsilon^2 + \end{array}\right.$$

$$\left.\begin{array}{l} III_f^g \\ \frac{\binom{9.2}{9.2}}{(1-.36\varepsilon)^6}\varepsilon^3 \end{array}\right\}$$

The quark/gluon subprocesses also, of course, lead to quark or gluon jet production. The decomposition of these jet cross section contributions appears in Tables 5 and 6. These can easily be used to reconstruct the single particle cross sections of the previous equations. The letters refer to the subprocess III labels (a1, a2 ...).

There is, of course, a great deal of information contained in these equations and tables. The goal of the following section will be to elucidate the important experimental signatures for CIM and p_T^{-4} contributions which these equations predict. The detail kept in the equations should allow the reader to reproduce the individual terms and to alter them should he wish to employ different α_M or α_B values or different distribution function parameters. Also more detailed quantum number correlation questions can be discussed by a close examination of the relative magnitudes of the various contributing terms. This is outside the scope of the present paper.

B. Discussion and Comparison with Data

We begin with a comparison between the analytic expressions of the previous section and data. For this purpose, we take as representative the data from Antreasyen et al.[21] at $\sqrt{s}$ = 27.4 GeV for $\pi^{\pm}$ $K^{\pm}$ p and $\bar{p}$ and the $pp \to \pi^{o}$ data at $\sqrt{s}$ = 62.4 GeV and 52.7 GeV from Eggert et al. and Clark et al.[22] and from the very high p_T preliminary results of the CCOR group at ISR.[23] A comparison with the only existing π beam data (Donaldson[24] et al. for $\pi^{\pm} p \to \pi^{o}$) appeared in Reference I. We remind the reader that for the CIM terms, we employ a uniform total/prompt ratio, T/P, of 2 for meson production and 1.2 for baryon production. Mass corrections have also been included, $p_T^2 \to p_T^2 + \underline{M}^2$. These are unimportant except for p and $\bar{p}$ production where the inverse p_T power is biggest. $\underline{M}^2$ = 1 GeV^2 was chosen. The effects are at most a factor of 2 at $p_T \sim 2$ GeV/c.

In Fig. 5a we compare our predictions to the $\sqrt{s}$ = 27.4 data for $\pi^{\pm}K^{+}$ and p production. The QCD terms are not important for these triggers and this energy, as we emphasize later. It is clear that the π^{+} and π^{-} CIM predictions are in excellent agreement with experiment. The K^{+} prediction has the correct shape but is slightly larger than the data; very probably this is simply a consequence of our ignoring SU(3) symmetry breaking. The prediction for p production reveals a possible discrepancy. From Fig. 5a it is clear that, while agreement with data is excellent for $p_T < 4$ GeV/c, the CIM prediction lies above the data by a factor 2 - 3 for the larger p_T values. An examination of the CIM forms reveals that this excess is entirely due to the "direct" contributions (with lowest ϵ powers) in which one proton is a direct participant in the subprocess $qp \to qp$. These direct contributions are an inherent feature of the

subprocess expansion and continuing failure to observe them in future higher p_T measurements at this moderate energy (so that ε is small and direct terms enhanced) would be surprising.

In Fig. 5b, the $\sqrt{s}$ = 27.4 GeV data for K^- production is compared to our predictions. While the α_s = .15 choice will be more thoroughly motivated shortly (by comparing to $pp \to \pi^o$), it is clear from the graph that the p_T^{-4} QCD terms are an important component of the cross section at the higher p_T values. The case for their presence is, however, far from conclusive here. Indeed the CIM prediction, while lying below the data, has exactly the right shape.

A more convincing case for the presence of p_T^{-4} terms is that based on $\bar{p}$ production at $\sqrt{s}$ = 27.4 GeV, Fig. 5c. Here it is clear that while the CIM terms describe the cross section at low p_T remarkably well (especially given our guess work for $G_{\bar{B}/p}$ which enters into the major CIM contribution), they fall systematically low for $p_T \gtrsim 4.5$ GeV/c. Indeed there would be a factor of $\sim$ 20 discrepancy at $p_T \sim 6$ GeV/c without the QCD - p_T^{-4} contributions. One should note that the α_s = .15 choice which is made for $pp \to \pi^o$ is approximately correct for this situation. Of course, gluon fragmentation to a $\bar{p}$, which is an important ingredient in the p_T^{-4} component, must be regarded as uncertain in normalization. One further interesting observation is possible. The British-French-Scandinavian ISR collaboration has shown[25] that the same side momentum associated with a $\bar{p}$ rises dramatically for $p_T > 4$ GeV/c while other triggers show much smaller effects. In our approach, this is clearly a signal for the onset of p_T^{-4} subprocess dominance; the fragmenting quark/gluon producing the $\bar{p}$ retains a reasonable fraction of its total momentum which appears in same side hadrons.

The most convincing case for the existence of a crossover between CIM contributions and QCD-p_T^{-4} terms is that based on ISR energy $pp \to \pi^o X$, mostly because of the extensiveness of the data. The need for p_T^{-4} terms is most apparent at $\sqrt{s}$ = 62.4 GeV, Fig. 6a. For p_T's below 6 GeV/c, we use the data of Eggert et al.[22] which agree with that of the CCRS group.[23] For $6 < p_T < 13$ GeV/c, we show the data of Clark et al.[22] and the preliminary CCOR data.[23] As was shown in Section I, the CIM terms are in excellent agreement with the data in shape and, especially, normalization for p_T's below 6 GeV/c. Figure 6a shows that the CCOR and Clark et al. higher p_T data at $\sqrt{s}$ = 62.4 GeV, however, deviate very systematically from the CIM terms alone. Inclusion of QCD-p_T^{-4} terms with α_s = .15 restores virtually perfect agreement with the CCOR data. The data of Clark et al. are slightly higher in the $p_T < 8$ GeV/c region and are not in exact agreement with the prediction. At $\sqrt{s}$ = 52.7, we show the Eggert et al.[22] and CCRS[23] data for $p_T < 8$ GeV/c in Fig. 6b and the new Clark et al.[22] and preliminary CCOR[23] data for $p_T > 5$ GeV/c in Fig. 6c. Here it appears, Fig. 6c, that the CCOR data do not require p_T^{-4} terms while the R702 data of Clark et al. do. The p_T^{-4} terms, in π^o production, are relatively insensitive to the poorly determined gluon decay normalization, rather depending primarily on the quark decay functions determined from e^+e^- annihilation data. Hence, it is clear, at least at $\sqrt{s}$ = 62.4, that neither CIM nor p_T^{-4} terms are separately able to describe the data over the entire p_T range. In some respects a meson spectrum is, however, a difficult place to see p_T^{-4} terms; even at p_T = 13 GeV/c, the CIM deviates from CIM + p_T^{-4} by less than a factor of 10. The p_T^{-12} falloff in $\bar{p}$ production, of CIM terms, brings p_T^{-4} contributions into play much more

quickly. A second systematic study of $\bar{p}$ production over an extended p_T range would be very helpful. In any case, several distinct sets of data show signs of p_T^{-4} behavior at p_T values which are consistent with <u>one</u> very reasonable choice for α_s.

In order to emphasize the general features of the crossover between CIM and p_T^{-4} contributions we present a series of graphs of the ratio

$$R = \frac{E\,\frac{d\sigma}{d^3p}\,(\text{CIM}) + E\,\frac{d\sigma}{d^3p}\left(p_T^{-4}\right)}{E\,\frac{d\sigma}{d^3p}\,(\text{CIM})} \quad . \tag{46}$$

When R rises above the value 2 p_T^{-4} terms have become dominant. In Fig. 7a we show R for $pp \to \bar{p}\,p\,K^-$ and π^o at $\sqrt{s} = 27$ GeV. From this graph it is immediately clear that p_T^{-4} terms are never substantial for p and π^o production but that for $\bar{p}$ and K^- production (in general, "exotic" particle production) they play an important role at the higher p_T values. Interesting structure in R is apparent as one approaches the phase space boundary—$R(pp \to K^-)$ remains large while $R(pp \to \bar{p})$ approaches 1. These behaviors reflect the ε powers of the contributing terms. For instance the lowest ε power for $\bar{p}$ production occurs in the CIM terms which thus dominate as $\varepsilon \to 0$ at the boundary. The $\sqrt{s} = 63$ GeV graph of these same R's, Fig. 7b, shows the higher energy systematics. There is a hierarchy of crossovers; p_T^{-4} becomes dominant first for $\bar{p}$ then for p, then K^-, then π^o. (The phase space boundary structure is present but is off the plot.) This hierarchy is easily understood. The p and $\bar{p}$ production CIM terms have p_T^{-12} behavior which decays rapidly, exposing the p_T^{-4} terms. The CIM p_T^{-8} contributions to K^- and π^o production take longer to become negligible. For a given class of hadron (baryon vs. meson) the

"exotic" particle having no valence quarks in common with the beam always has a substantially suppressed normalization for its CIM terms; the p_T^{-4} contributions coming from gluon decay are not suppressed for such an exotic hadron (though the quark decay contributions are). Thus the exotic particles such as $\bar{p}$ and K^- always show p_T^{-4} behavior sooner than their non-exotic counterparts p and π^o, respectively.

In Figs. 8a, 8b, and 8c we illustrate the dependence of R, for production of a given particle type, on the type of incoming beam. Figure 8a does this for π^+ production. It is clear that there is a strong beam dependence. For instance R is biggest at any given energy for $\pi^- p \to \pi^+$, for which the CIM terms are somewhat suppressed in normalization due to the π^+ being "exotic" relative to the π^-. The graphs for π^- production are essentially an isospin flipped version of those for π^+ production. The R's for K^+ production are very similar to those for π^+ production in shape—the magnitude of R for $\pi^+ p \to K^+$ is always somewhat bigger than that for $\pi^+ p \to \pi^+$ which has substantial "direct" CIM contributions.

The R's for K^- production, Fig. 8b, exhibit some interesting peculiarities as $\varepsilon \to 0$ near the phase space boundary. For the proton beam $R(pp \to K^-)$ rises monotonically to large values as $\varepsilon \to 0$. For the π^+ beam $R(\pi^+ p \to K^-)$ rises, falls and then approaches a constant as $\varepsilon \to 0$. For the π^- beam $R(\pi^- p \to K^-)$ always approaches 1 as $\varepsilon \to 0$. As always these behaviors reflect the varying ε powers predicted for the CIM contributions in these cases and constitute an interesting test of the subprocess expansion framework. It is unfortunate that the cross sections are so small in the $\varepsilon \to 0$ limit. In general, as explained previously, $R(K^-)$ is much larger than $R(\pi^+)$ for a given beam type.

Figure 8c compares $R(\pi^- p \to p)$ and $R(\pi^+ p \to p)$; they are substantially the same at all energies. Similarly a comparison of $R(\pi^+ p \to \bar{p})$ to $R(\pi^- p \to \bar{p})$ would reveal results that are virtually identical at every energy but substantially larger than those for p production. As expected, CIM contributions in the $\bar{p}$ case are small except for $\epsilon \to 0$ and at low p_T.

As a general note, it is not clear that the "modified p_T^{-4}" models such as that of Feynman and Field[4,14] would yield such systematic differences between the various types of produced particles and beams. These systematics, if verified, will be strong support for non-leading p_T power terms which depend on the trigger particle as predicted by the CIM.

In summary, it is clear that for most reactions the region of CIM dominance is, in fact, relatively small. By far the bulk of phase space at high energies is p_T^{-4} dominated. Only the experimental limitations of low energy and low to moderate p_T have made the CIM terms play such an important role. Nonetheless their success in describing this region of data is an important test of our basic picture of hadronic bound states in QCD.

Within the p_T^{-4} dominated realm it is interesting, especially with regard to correlations to investigate the relative roles of the various quark/gluon subprocesses. We do this in Figs. 9a-9d, for pp collisions, where the ratios of the various p_T^{-4} subprocesses relative to $gg \to gg$ for π^+, p, K^- and $\bar{p}$ production are presented.

For π^+ and p production, Figs. 9a and 9b, the $qq \to qq \hookrightarrow \pi^+, p$ subprocess dominates at low ϵ, $\epsilon < .4$. The balancing jet to the trigger π^+ or p is a quark. For moderate ϵ values, $.8 > \epsilon > .4$, the subprocess $gq \to gq \hookrightarrow \pi^+, p$

is dominant. The balancing jet is a gluon jet. Gluon jets should exhibit stronger $\frac{dN}{dx}$ fall off as $x \to 1$ than the quark jets of e^+e^- annihilation and should have a higher jet multiplicity. According to the gluon radiation theory of multiplicity[18] $\langle n \rangle_{\text{gluon jet}} = \frac{9}{4} \langle n \rangle_{\text{quark jet}}$. As $\varepsilon \to 1$ the $gg \to gg_{\hookrightarrow \pi^+,p}$ subprocess becomes slightly more important than $gq_{\hookrightarrow \pi^+,p}$ but, again, the balancing jet is gluonic in origin. Note that if the "modified p_T^{-4}" approach which employs only p_T^{-4} type subprocess is correct at lower p_T $\left(2 < p_T < 8 \frac{GeV}{c}\right)$ for FNAL and ISR energies then, since $\varepsilon > .4$, a gluon jet (not a quark jet) should balance the trigger particle. The rough similarity[26] of the opposite side jet for π triggers, as measured at ISR, to the quark jets of e^+e^- annihilation and deep inelastic scattering argues against this model and in favor of the CIM $qM \to qM$ dominant subprocess. (Where CIM terms dominate, quark jets (or possibly resonance jets) balance all trigger types.) However the lack of scaling[26] in the 45° data makes any firm conclusion impossible.

For K^- and $\bar{p}$ production, Figs. 9c and 9d, the subprocess $qg \to qg_{\hookrightarrow \bar{p},K^-}$ dominates for $\varepsilon < .55 - .6$ while $gg \to gg_{\hookrightarrow \bar{p},K^-}$ dominantes for $\varepsilon > .55 - .6$. The typical jet balancing the trigger switches from quark to gluonic origin. Of course the precise ratios are sensitive to the precise normalization of the gluon decay functions.

A similar discussion could be given for π beams. The tabulated results for p_T^{-4} processes may be used by the reader for this purpose.

Another interesting way of revealing the transition from CIM to p_T^{-4} domination is through ratios such as

$$\frac{\pi^- p \to \bar{p}}{pp \to \bar{p}} \quad , \quad \frac{\pi^- p \to \pi^-}{pp \to \pi^-} \quad , \text{ and } \quad \frac{\pi^- p \to p}{pp \to p} \quad .$$

For instance in the CIM dominated regime the ratio $\frac{\pi^- p \to \bar{p}}{pp \to \bar{p}}$ is very large. This is easily demonstrated intuitively by noting that both $\bar{p}$ CIM cross sections are typified by graphs in which a secondary $\bar{B}$ arises from the proton and scatters via ut topology, $\bar{q}\bar{B} \to \bar{q}\bar{p}$, or via st topology, $q\bar{B} \to q\bar{B}$. (The latter is significant only for pp collisions.) Thus a rough approximation is

$$\frac{E\frac{d\sigma}{d^3p}(\pi^- p \to \bar{p})}{E\frac{d\sigma}{d^3p}(pp \to \bar{p})} \sim \frac{\varepsilon^{13}\Sigma(fN)_{\bar{B}/p}(fN)_{\bar{q}/\pi}\, 2^{2+11+1-12}\,\frac{\Gamma(3)\Gamma(13)}{\Gamma(14)}\,\mathcal{D}_{90^\circ}^{I_c}}{2\Sigma(fN)_{\bar{B}/p}\left[(fN)_{\bar{q}/p}\, 2^{2+11+7-12}\,\frac{\Gamma(9)\Gamma(13)}{\Gamma(20)}\,\mathcal{D}_{90^\circ}^{I_c}\,\varepsilon^{19} + (fN)_{q/p}\, 2^{2+11+3-12}\,\frac{\Gamma(5)\Gamma(13)}{\Gamma(16)}\,\mathcal{D}_{90^\circ}^{I_b}\,\varepsilon^{15}\right]} \tag{47}$$

$$\overset{\varepsilon \to 1}{\sim} \frac{.0913\; 2^1\,\Gamma(3)/\Gamma(14)\; 80}{2\left(.01\; 2^7\,\frac{\Gamma(9)}{\Gamma(20)}\,80 + .1\;\; 2^3\,\frac{\Gamma(5)}{\Gamma(16)}\;\; 2\right)} \approx 37 \quad .$$

Note that the somewhat uncertain $(fN)_{\bar{B}/p}$ cancels and the extra 2 in the denominator is from beam target symmetry in the pp case. The big ratio arises primarily because of the factorials which are least detrimental in the highly asymmetric $g_{\bar{q}/\pi} = 1$ $g_{\bar{B}/p} = 11$ case. In comparison much smaller ratios at any given ε are expected in a QCD dominated realm. Figure 10a illustrates this more explicitly. We plot the above ratio for:

i) QCD p_T^{-4} contributions only to both cross sections, labeled QCD;

ii) CIM p_T^{-4} contributions only to both cross sections, labeled CIM;

iii) p_T^{-4} + CIM contributions present in the mixture predicted by our calculations, labeled QCD + CIM.

We see that at low p_T the predicted ratio, QCD + CIM, is near the CIM dominance value. As p_T increases it exhibits a sudden drop to the p_T^{-4} result. This transition is apparent at both energies, $\sqrt{s}$ = 27 GeV and $\sqrt{s}$ = 63 GeV, but is most striking at the latter. The fact that the CIM contribution to $\bar{p}$ production in pion beams is much larger than for proton beams, correlates with the fact that the crossover point for p_T^{-4} contributions will be correspondingly higher. In fact at FNAL energies p_T^{-12} CIM contributions dominate $\pi^{\pm} p \to \bar{p} X$ for all p_T whereas in $pp \to \bar{p} X$ p_T^{-4} contributions are dominant over a substantial range of p_T. The "modified p_T^{-4}" approach of Feynman and Field[4] probably would, in its simplest form, yield a less striking contrast between these two reactions.

Equally striking transitions are predicted for the ratio $\frac{\pi^- p \to p}{pp \to p}$, Fig. 10b. Here QCD + CIM starts out at the CIM value at low p_T deviates toward the QCD value in the middle p_T range (for $\sqrt{s}$ = 63 GeV) and then returns to the CIM value near the phase space boundary where low ε powers cause the CIM contributions to dominate.

Finally $\frac{\pi^- p \to \pi^-}{pp \to \pi^-}$ shows a similar back and forth transition at $\sqrt{s}$= 63 GeV (both are CIM dominated at $\sqrt{s}$ = 27 GeV). Again pure CIM and pure QCD are very different at any given value of p_T so that a measurement of this ratio would clearly indicate if a single type of subprocess (CIM vs. QCD) was controlling both cross sections.

As a final note we give in Table 7 the energy dependence of the various cross sections as characterized by the ratio $E\frac{d\sigma}{d^3p}(\sqrt{s}=63)/E\frac{d\sigma}{d^3p}(\sqrt{s}=27)$. As expected $\bar{p}$ production exhibits the strongest increase with energy--the high ε power causes it to increase rapidly as $\varepsilon \to 1$ in a CIM realm and the switchover to QCD causes a swift rise with energy. QCD p_T^{-4} terms alone would not lead to such strong variations with energy.

C. Jet Cross Sections

We may use the quark and gluon cross sections of Table 5 to compute the p_T^{-4} jet cross section contributions for pp scattering. The CIM jet contributions were summarized in I. With our more precise T/P values etc. a few modifications appear.

$$E\frac{d\sigma}{d^3p}^{CIM}\left(pp \to \text{jet (meson induced)}\right) \sim 2\,N(M^*)\,E\frac{d\sigma}{d^3p}\left(pp \to \pi(\text{prompt})\right)$$

$$\sim 40\,E\frac{d\sigma}{d^3p}\left(pp \to \pi(\text{total})\right) \qquad (48)$$

$$\sim 320\,\frac{\varepsilon^9}{p_T^8}$$

where we took a T/P value of 2 and chose $N(M^*)=40$ corresponding to the number of meson resonances, M^*, produced at high p_T (e.g. 36 for the spin 0 and spin 1 nonets with statistical weighting plus ...). The explicit 2 is for triggering on either the meson jet or the opposite quark jet (in the $qM \to qM$ subprocess case). Similarly for $N(B^*)=35$ baryon resonances and a T/P value of 1.2 for baryons.

$$
\begin{aligned}
& E \frac{d\sigma}{d^3p}^{CIM} \left(pp \to \text{jet (baryon induced)}\right) \\
& \sim 2\, N(B^*)\, E \frac{d\sigma}{d^3p} \left(pp \to p(\text{prompt})\right) \\
& \sim \frac{70}{1.2} E \frac{d\sigma}{d^3p} \left(pp \to p(\text{total})\right) \\
& \sim 2.92 \times 10^4\, \varepsilon^7/p_T^{12}
\end{aligned}
\tag{49}
$$

The total/prompt ratios, being smaller than originally proposed in I, increase the CIM jet cross sections somewhat over the values given there. Several features of the CIM and QCD results are noteworthy.

1. For the p_T^{-4} terms the probability of a quark jet versus a gluon jet changes with ε.

$$
\frac{E \frac{d\sigma}{d^3p} (pp \to q \text{ or } \bar{q} \text{ jet})}{E \frac{d\sigma}{d^3p} (pp \to g \text{ jet})} > \begin{cases} \frac{.455}{.635} & \varepsilon = 1 \\ \sim .5 \text{ moderate } \varepsilon & \\ \to \infty \text{ as } \varepsilon \to 0 & \end{cases} \tag{50}
$$

2. For the CIM p_T^{-12} and p_T^{-8} contributions, 50% of the jets arise from quarks and 50% from mesonic resonances.

3. For typical FNAL energies CIM contributions are smaller than p_T^{-4} contributions for $p_T > 4 \frac{GeV}{c}$. We may, of course, compare our predicted total jet cross section to experiment. The data depends on the experiment[27,28]; we compare to the University of Washington collaboration[27] (with data at p_{Lab} = 340 GeV/c and 100 GeV/c i.e. $\sqrt{s}$ = 25.3 and 13.8 GeV) which has the widest angle calorimeter and obtains the largest cross

sections. Figure 11 shows the comparison. A shift by 1.5 GeV/c in p_T^{jet} produces good agreement. In other words particles with a total transverse momentum of 1.5 GeV/c would have to be misidentified as belonging to the jet in order for experiment and theory to agree. The experimental group estimates misidentification amounts to no more than 600-700 MeV/c. Similar discrepancies may be present for all jet production models.

The CIM predicts that some fraction of the time the observed jet should consist of only one particle. This fraction is computed as

$$\frac{\text{Single Particle Jet}}{\text{All Jets}} = \frac{\text{CIM}}{p_T^{-4}} \times \frac{1}{2} \times \frac{1}{10}$$

fraction dominated by CIM.	probability of resonance vs. quark jet for CIM terms.	number of stable particles divided by the total number of stable particles + resonances

$$= \frac{1}{60} - \frac{1}{80} \text{ for } 4 < p_T^{jet} < 5 \text{ GeV/c}$$

This small fraction is consistent with the absence of such a single particle effect in the data of the Malamud et al.[29] at approximately the 2% level.

CONCLUSION

We have, of course, not discussed all aspects of either the CIM or the p_T^{-4} contributions in this paper. However, even at the simplest level, of single particle cross sections, clear and systematic signals mark the transition from the sub-asymptotic p_T domain, dominated by CIM p_T^{-12} and p_T^{-8} contributions, to asymptotic p_T^{-4} behavior. A complete set of higher p_T measurements of cross sections for all trigger particle types and beams should provide a good test of the subprocess expansion-dimensional counting approach. "Modified p_T^{-4}" models (based on elementary QCD subprocesses

only) use scaling violations and/or quark and gluon k_T fluctuations to mask the elementary QCD behavior. These effects, however, are largely intrinsic to the colliding particles and hence will effect all types of produced particle similarly. The dependence of cross section behavior (especially the location of any transition zone) on trigger particle type is thus likely to be minimal. Another contrast is that in the "modified p_T^{-4}" approach the opposite side jet, balancing the trigger particle, should be predominately of gluonic origin (for current experimental ε ranges); experimentally these opposite side jets look like e^+e^- and deep inelastic quark jets.

No model, it seems will be able to describe the very large jet cross sections obtained by the most recent FNAL collaboration unless an unacceptably large value of α_s is employed. However, the experimental definition of a jet may still be a source of difficulty in making comparisons to theory. Thus, we hope that the results presented here will encourage experimentalists to continue detailed <u>high</u> p_T studies of single particle cross sections. Though the role of asymptotic freedom corrections in inclusive high p_T measurements and their effect on dimensional counting is far from understood, the successes of exact dimensional counting in describing exclusive cross sections and form factors leads us to anticipate that these ASF corrections will be small and our calculated single particle cross sections reliable.

ACKNOWLEDGEMENTS

Portions of this work were begun in collaboration with S. J. Brodsky and R. Blankenbecler. We would also like to thank them for helpful conversations. One of us (JFG) would like to thank SLAC for its kind hospitality during the writing of this paper.

FIGURE CAPTIONS

1. The structure of a typical subprocess contribution to A+B→C+X. Secondary particles a and b are at low transverse momentum relative to A and B. C and c have low relative transverse momentum.

2. a) A Feynman diagram whose asymptotic expansion yields two p_T^{-4} subprocess configurations, $qq \to qq$ and $qg \to qg$.

   b) Another diagram with a $qq \to qq$, p_T^{-4} expansion term but with non-leading, p_T^{-6} contributions from $gM \to q\bar{q}$.

   In both cases we imagine the upper quark line to be the trigger particle.

3. a) Emission of a gluon which has become an integral part of the hadronic proton wave function.

   b) Point-like gluon emission from a quark in the proton.

4. a) Comparison of our simplified fragmentation distributions for mesons with data from DASP. The cross section is that for $e^+e^- \to \pi^+ + e^+e^- \to \pi^-$.

   b) Comparison of DASP data for $2(e^+e^- \to \bar{p})$ with the theoretical predictions expressed in terms of x_p.

5. a) Data for $E\frac{d\sigma}{d^3p}$ $(pp \to \pi^+, \pi^-, K^+, p)$ at $\sqrt{s} = 27.4$ from Antreasyen et. al. is compared to theory. p_T^{-4} terms are not important in these plots.

   b) Corresponding plot for $pp \to K^-$. CIM and p_T^{-4} contributions and their sum are indicated separately.

   c) $pp \to \bar{p}$ as in b).

6. a) Data for $E\frac{d\sigma}{d^3p}$ $(pp \to \pi^o)$ at $\sqrt{s} = 62.4$ is compared to the theoretical prediction over a wide range of p_T. CIM and p_T^{-4} contributions are again indicated separately. Note that the overlap between the Eggert et al. data[22] and the CCOR data[23] at $p_T \sim 6$ GeV/c increases the reliability of the determination $\alpha_s = .15$ (for the p_T^{-4} terms).

b) Comparison of moderate p_T data at $\sqrt{s} = 52.7$ GeV from Eggert et al.[22] and CCRS[23] to the model. Over this region CIM terms dominate.

c) Comparison of high p_T data at $\sqrt{s} = 52.7$ GeV from Clark et al.[22] and CCOR[23] to the CIM terms alone and to CIM + p_T^{-4}.

7. a) Plot of theoretical predictions for $R = \frac{p_T^{-4} + \text{CIM}}{\text{CIM}}$ at $\sqrt{s} = 27$ GeV. R=2 marks the transition from CIM to p_T^{-4} behavior.

b) Same at $\sqrt{s} = 63$ GeV.

8. a) Plot of R (defined in 7a)) for $pp \to \pi^+$, $\pi^+p \to \pi^+$, and $\pi^-p \to \pi^+$ at two energies, $\sqrt{s} = 27$ GeV and $\sqrt{s} = 63$ GeV. The $\sqrt{s} = 27$ GeV curves are those which terminate at $p_T^{\text{Max}}(27)$ etc. Higher energy curves follow the obvious extrapolation—one rescales as the p_T^{Max} range is increased with increasing energy.

b) Corresponding plots of R for K^- production.

c) Corresponding plots of R for $\pi^-p \to p$ and $\pi^+p \to p$. The $pp \to p$ curves can be seen in Fig. 7a) and b).

9. a) Contributions to π^+ production from the important p_T^{-4} subprocesses relative to that from $gg \to gg \hookrightarrow \pi^+$ as a function of $\varepsilon = 1-x_T$.

b) As in a) for K^- production.

c) As in a) for p production.

d) As in a) for $\bar{p}$ production.

10. a) Plot of the ratio

$$\frac{E\frac{d\sigma}{d^3p}(\pi^- p \to \bar{p})}{E\frac{d\sigma}{d^3p}(pp \to \bar{p})}$$

as a function of p_T at $\sqrt{s}$ = 27 GeV and $\sqrt{s}$ = 63 GeV. Three curves at each energy are shown. That expected for CIM terms alone, for QCD p_T^{-4} terms alone and for the theoretically predicted mixture of QCD and CIM terms. (α_s = .15 is employed).

b) Corresponding plots for $\pi^- p \to p$ versus $pp \to p$.

c) Corresponding plots for $\pi^- p \to \pi^-$ versus $pp \to \pi^-$.

11. Wide angle calorimeter jet cross sections from Ref. 27 at $\sqrt{s}$ = 13.8 GeV and 25.3 GeV compared to prediction from combining CIM and p_T^{-4} contributions. α_s = .15 is used to normalize the p_T^{-4} yields. A shift of $\sim$1.5 GeV/c in p_T is required for agreement. The p_T^{-4} contribution alone is also indicated and shows that CIM terms are insignificant above p_T $\sim$4 GeV/c.

REFERENCES

1. S. Berman, J. Bjorken, J. Kogut, Phys. Rev. D4, 3388 (1971).

2. The first attempt to include these came in R. F. Cahalan et al. Phys. Rev. D11, 1199 (1975); See also J. F. Gunion 17th International Conference on High Energy Physics, London 1974. Later calculations include: R. Hwa et al., Phys. Rev. Lett. 36, 1418 (1977); E. Fischbach and G. Look, Phys. Rev. D16, 1369 and 1571, (1977); A. Contogouris and R. Gaskell and A. Nicolaidis, McGill preprints (1978).

3. More detailed p_T^{-4} calculations and ASF corrections appear in: D. Sivers and R. Cutler, Argonne preprint (1977) and Phys. Rev. D16, 679 (1977); B. Combridge, J. Kripfganz, and J. Ranft, Phys. Lett. 70B, 234 (1977) and J. F. Owens, E. Reya, and M. Glück, Florida State preprints (1977).

4. The effect of transverse, k_T, fluctuations of the quarks and gluons on scale-broken p_T^{-4} subprocesses has been considered by R. D. Field, Phys. Rev. Lett. 40, 997 (1978). Certain features of this treatment (namely the failure to include off shell effects) make it suspect to us. The exponentially damped fluctuations have an unrealistically large effect.

   For other fluctuation approaches see the proceedings of the workshop on High Transverse Momentum Phenomena, Bielefeld, Sept. 1977.

5. The most complete treatment of the constituent interchange model including normalization appears in R. Blankenbecler, S. J. Brodsky and J. F. Gunion "Normalization..." to be published in Phys. Rev. D. (SLAC-PUB-2057). This paper is hereafter referred to as I.

6. More details on p_T^{-6} processes appear in J. F. Gunion "The Interrelationship of the Constituent Interchange Model and Quantum Chromodynamics," UCD preprint. This review also summarizes the results of the present paper (though a few numbers have changed).

7. S. J. Brodsky and G. Farrar, Phys. Rev. Lett. 3, 1153 (1973). V. Matveev, R. Muradyn, and A. Tavkhelidze, Nuovo Cimento Lett. 7, 719 (1973).

8. R. Horgan, W. Caswell, and S. J. Brodsky, SLAC-PUB- in preparation. Certain types of momentum correlations are clearly harder to obtain by the subprocess method; they require developing subprocess series for 1,2,3.....particle cross sections and then combining results.

9. S. Ellis, M. Jacob, and P. Landshoff, Nucl. Phys. B108, 93 (1976) and P. V. Landshoff VIIth International Colloquium on Multiparticle Reactions, Tutzing (June 1976). See also J. D. Bjorken and G. R. Farrar, Phys. Rev. D9, 1449 (1974).

10. For recent reviews see S. J. Brodsky, SLAC-PUB-2009, J. F. Gunion, UCD preprint, and S. J. Brodsky and J. F. Gunion SLAC-PUB-1806. The first two papers outline the normalization procedure developed in Ref. 5.

11. The normalization of some CIM contributions has also been considered by M. K. Chase and W. J. Stirling DAMTP-77/15.

12. C. Sachrajda CERN-TH-2492, 2459 and Phys. Lett. 73B, 185 (1978); D. Politzer, Nucl. Physics B129, 30 (1977); G. Altarelli, G. Parisi and R. Petronzio CERN-TH-2450, 2413; and R. K. Ellis, H. Georgi, M. Machacek, D. Politzer and G. Ross, MIT-preprint; Y. L. Dokshitser, D. d'Yakonov, S. I. Troyan, 13th Winter School of the Leningrad Institute of Nuclear Physics.

13. See D. Sivers, S. J. Brodsky, and R. Blankenbecler, Phys. Reports 23 (1976) for a compilation. This report also includes references to many of the earlier high p_T works, in particular those by P. Landshoff and J. C. Polkinghorne.

14. These remarks are also applicable to the earlier approach of R. D. Field and R. P. Feynman, Phys. Rev. D15, 2390 (1977) and R. D. Field, R. P. Feynman and G. C. Fox, CALT-68-595 (1977), in which the $qq \to qq$ subprocess was given an ad hoc $1/p_T^8$ behavior which would underly all types of reactions.

15. The application of dimensional counting rules to distribution functions is considered in R. Blankenbecler and S. J. Brodsky, Phys. Rev. D10, 2973 (1974); J. F. Gunion, Phys. Rev. D10, 242 (1974); and G. Farrar, Nucl. Phys. B77, 429 (1974).

16. Consider a valence proton state. To reach a $2\bar{q}$ secondary we must add (at least) two $q\bar{q}$ pairs. Assume they occur with equal probability as $R\bar{R}$, $B\bar{B}$ or $G\bar{G}$ (R, B, G are the 3 colors). Now compute the overlap with an exotic meson (1 and 2 refer to the (non-valence) flavor types of the two $q\bar{q}$ pairs and C_1, C_2 their colors)

$$\sum_{C_1 C_2} \left| \left\langle \frac{1}{\sqrt{3}} (R_1\bar{R}_2 + B_1\bar{B}_2 + G_1\bar{G}_2) \middle| C_1\bar{C}_1 C_2\bar{C}_2 \right\rangle \right|^2$$

$$\alpha \frac{1}{3} \times 3 = 1$$

Compare this to the overlap with an anti-diquark of given color composition (e.g. $\bar{R}_1\bar{G}_2$)

$$\sum_{C_1 C_2} \left| \langle \bar{R}_1\bar{G}_2 | C_1\bar{C}_1 C_2\bar{C}_2 \rangle \right|^2 = 1$$

There are 9 such color combinations, three of which belong to a color triplet and thus (effectively) 1 of which corresponds to a color triplet state of given color. Thus both net factors are 1. Note we have treated different $C_1\bar{C}_1$ $C_2\bar{C}_2$ pair possibilities as incoherent.

17. We use the π^+, π^- and $\bar{p}$ data published in R. Brandelik et al. (DASP Collaboration), Phys. Lett. 67B,358 (1977).

18. S. J. Brodsky and J. F. Gunion, Phys. Rev. Lett. 37, 402 (1976).

19. This is just a crossed version of the Weizacker Williams distributions, $D_{\gamma/e}$ or $D_{g/q} \alpha \frac{1}{x}\left(1 + (1-x)^2\right)$.

20. We did not bother to keep these two terms in the crossed situation $p \to g$ $(G_{g/p})$ and $M \to g$ $(G_{g/M})$; for these distributions we are not as sensitive to the precise $x \to 1$ behavior but merely require a fairly reasonable overall description. One finds fairly small alterations for a form like $G_{g/p} \alpha \frac{1}{x}\left[(1-x)^4 + (1-x)^6\right]$ provided the overall momentum fraction carried by the gluons is 50% Eq. (7). In final fragmentation the exact z very near 1 behavior and normalization is much more critical.

21. D. Antreasyen et al., Phys. Rev. Lett. 38, 112 (1977); J. W. Cronin et al., Phys. Rev. D11, 3105 (1975).

22. K. Eggert et al., Nucl. Phys. B98, 49 (1975); A. G. Clark et al., CERN-EXP-78-0635) (1978). This latter experiment is also referred to as R702.

23. Two sets of data are referred to here:

    a) $\sqrt{s}$ = 52.7 GeV and 62.4 GeV π^o data from the CCRS collaboration, Nucl. Phys. B106, 1 (1976), $p_T \lesssim 8$ GeV/c.

b) $\sqrt{s}$ = 52.7 GeV and 62.4 GeV π^o data from the CERN-Columbia-Rockefeller R108 collaboration at high p_T. The $\sqrt{s}$ = 62.4 GeV graph is taken from the Sept. '77 "Large p_T Phenomena" ISR Workshop. The $\sqrt{s}$ = 52.7 GeV data was taken from a graph presented at a March 3 ('78) seminar at SLAC. These data are still very preliminary.

24. G. Donaldson et al., Phys. Rev. Lett. 36, 1110 (1976).

25. See H. Bogglid, VIII International Symposium on Multiparticle Dynamics, Kaysersburg, France (1977).

26. See for instance the summary presented by M. Della Negra in the proceedings of VII International Colloquium on Multiparticle Reactions Tutzing, June (1976).

27. Preliminary University of Washington E236 collaboration jet data presented by P. Mochet at SLAC.

28. The Cal-Tech E260 collaboration also has jet cross section data; their calorimeter acceptance is smaller and their cross sections lower. See C. Bromberg et al., Phys. Rev. Lett. 38, 1447 (1977) and Ref. 20. Other jet data was recently presented at the San Francisco APS Meeting.

29. E. Malamud, VIII International Symposium on Multiparticle Dynamics, Kayersberg (1977), presents a nice summary of the Cal. Tech. jet experiment.

30. See proceedings of 13th Rencontre de Moriond, Flaine, France (1977).

APPENDIX A: Charge Constraint Compatibility

In our calculations we have used simplified fragmentation function forms which do not appear to satisfy charge constraints. In this appendix we explicitly demonstrate the modifications to our fragmentation function forms which are required so that the charge constraint is satisfied. These modifications will be unimportant in the large x region where we work. For definiteness we consider only the u and $\bar{u}$ from π^+ case, but the generalization to other cases is obvious.

The momentum fraction and charge constraints to be satisfied are:

$$f\,\frac{u}{\pi^+} = .08 = \int_0^1 x\,G\,\frac{u}{\pi^+}\,(x)dx \tag{A1}$$

$$f\,\frac{\bar{u}}{\pi^+} = .01 = \int_0^1 x\,G\,\frac{\bar{u}}{\pi^+}\,(x)dx \tag{A2}$$

$$1 = \sum_{\text{colors}} \int_0^1 \left(G\,\frac{u}{\pi^+}\,(x) - G\,\frac{\bar{u}}{\pi^+}\,(x)\right)dx \quad . \tag{A3}$$

We further adopt the parameterization

$$x\,G\,\frac{u}{\pi^+}\,(x) = x\,G\,\frac{\bar{u}}{\pi^+} + V(x) \tag{A4}$$

where V(x) is a function representative of the difference between the valence and non-valence or 'sea' quark distributions per color, yet to be determined.

Experimental evidence suggests[30] that the non-valence or 'sea' quark distributions follow the dimensional counting form for all x (even $x \to 0$); so we take the standard form

$$x\,G\,\frac{\bar{u}}{\pi^+}\,(x) = \left(1+g\,\frac{\bar{u}}{\pi^+}\right)f\,\frac{\bar{u}}{\pi^+}\,(1-x)^{g_{\bar{a}}^{\pi^+}} = .06\,(1-x)^5 \quad . \tag{A5}$$

In addition, dimensional counting for $G\,\frac{u}{\pi^+}$ as $x \to 1$ requires $V(x) \sim 1-x$; $x \to 1$. We expect that as $x \to 0$, $V(x) \to 0$ like x so that the Pomeron theoreum will hold. Consequently we parameterize V(x) by

$$V(x) = \begin{cases} V_1\ (1-x) & x>\hat{x} \\ V_1\ (1-\hat{x}) & \hat{\hat{x}}<x<\hat{x} \\ V_2\ x & x<\hat{\hat{x}} \end{cases} \quad . \tag{A6}$$

Continuity of $V(x)$ requires that $V_2 = V_1 \frac{1-\hat{x}}{\hat{\hat{x}}}$ and we establish contact with our standard form for $G \frac{u}{\pi^+}$ by requiring

$$V_1 = \left(1+g \frac{u}{\pi^+}\right) N\left(\frac{u}{\pi^+}\right) f \frac{u}{\pi^+} = .18 \text{ (See Table 3)}$$

At this point we have two equations in the two unknowns $\hat{x}$ and $\hat{\hat{x}}$. More explicitly we must solve for $\hat{x}$ and $\hat{\hat{x}}$ from:

$$1 = 3\int_0^1 \frac{V(x)}{x}\, dx \tag{A7}$$

$$.07 = \int_0^1 V(x)\, dx \tag{A8}$$

where

$$V(x) = \begin{cases} .18\ (1-x) & x>\hat{x} \\ .18\ (1-\hat{x}) & \hat{\hat{x}}<x<\hat{x} \\ .18\ \frac{(1-\hat{x})}{\hat{\hat{x}}}\ x & x<\hat{\hat{x}} \end{cases} \quad . \tag{A9}$$

The solution of Equations (A7) and (A8) gives $\hat{x} \approx .42$ and $\hat{\hat{x}} \approx 7.9 \times 10^{-2}$ which leads to

$$x\ G \frac{u}{\pi^+}(x) = \begin{cases} .18\ (1-x) + .06\ (1-x)^5 & x>.42 \\ .18\ (1-.42) + .06\ (1-x)^5 & 7.9\times10^{-2}<x<.42 \\ 1.2\times10^4 x + .06(1-x)^5 & x<7.9\times10^{-2} \end{cases} \tag{A10}$$

as our modified fragmentation function consistent with the charge constraint. Since the $(1-x)^5$ part of (A10) is severly suppressed both numerically and by a higher $(1-x_T)$ power in the cross section, the effective fragmentation function agrees identically with our standard form in the large x region where we work. Thus we see that our simplified quark fragmentation functions can be made to be consistent with charge constraints without modifying the large x behavior.

TABLE 1*

Class I $\left(p_T^{-12}\right)$

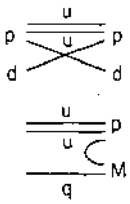

$$\frac{d\sigma}{dt} = \pi\alpha_B^2 \frac{s^2+t^2}{s^2 t^2 u^4}$$

$$\frac{d\sigma}{dt} = \frac{\pi\alpha_B \alpha_M M_{eff}^2}{2} \frac{u}{s^2 t^5}$$

Class II $\left(p_T^{-8}\right)$

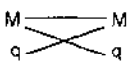

$$\frac{d\sigma}{dt} = \pi\alpha_M^2 \frac{1}{su^3}$$

Class III $\left(p_T^{-4}\right)$

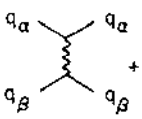

$$\frac{d\sigma}{dt} = \frac{\pi\alpha_s^2}{s^2}\left[\frac{4}{9}\left(\frac{s^2+u^2}{t^2} + \delta_{\alpha\beta}\frac{s^2+t^2}{u^2}\right) - \frac{8}{27}\frac{s^2}{ut}\delta_{\alpha\beta}\right]$$

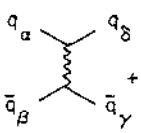

$$\frac{d\sigma}{dt} = \frac{\pi\alpha_s^2}{s^2}\left[\frac{4}{9}\left(\frac{s^2+u^2}{t^2}\delta_{\alpha\delta}\delta_{\beta\gamma} + \frac{u^2+t^2}{s^2}\delta_{\alpha\beta}\delta_{\gamma\delta}\right) - \frac{8}{27}\frac{u^2}{st}\delta_{all}\right]$$

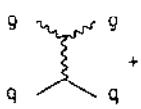

$$\frac{d\sigma}{dt} = \frac{\pi\alpha_s^2}{s^2}\left[\frac{4}{9}\left(\frac{u^2+s^2}{-us}\right) + \frac{u^2+s^2}{t^2}\right]$$

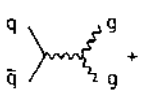

$$\frac{d\sigma}{dt} = \frac{\pi\alpha_s^2}{s^2}\left[\frac{32}{27}\left(\frac{u^2+t^2}{ut}\right) - \frac{8}{3}\left(\frac{u^2+t^2}{s^2}\right)\right]$$

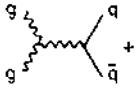

$$\frac{d\sigma}{dt} = \frac{\pi\alpha_s^2}{s^2}\left[\frac{1}{6}\left(\frac{u^2+t^2}{ut}\right) - \frac{3}{8}\left(\frac{u^2+t^2}{s^2}\right)\right]$$

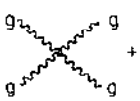

$$\frac{d\sigma}{dt} = \frac{\pi\alpha_s^2}{s^2}\left[\frac{9}{2}\left(3 - \frac{us}{t^2} - \frac{ut}{s^2} - \frac{st}{u^2}\right)\right]$$

* All cross sections equally applicable under particle ⟷ antiparticle replacement.

TABLE 2

Class I ($N_{coh} = 1$)

$\pi \alpha_B^2 / \hat{s}^6$ •

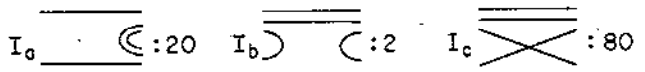

$\pi \alpha_B \alpha_M M_{eff}^2 / \hat{s}^6$ •

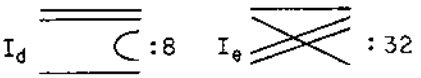

Class II

$\pi \alpha_M^2 / \hat{s}^4$ •

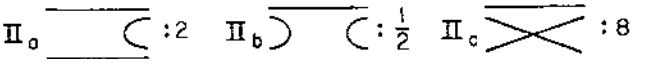

Class III

$\frac{1}{9} \pi \alpha_s^2 / \hat{s}^2$ •

III_{a1} $(q_\alpha q_\beta - q_\alpha q_\beta)$: $20 + \frac{28}{3} \delta_{\alpha\beta}$

III_{a2} $(\bar{q}_\alpha \bar{q}_\beta - \bar{q}_\alpha \bar{q}_\beta)$: $20 + \frac{28}{3} \delta_{\alpha\beta}$

III_b $(q_\alpha \bar{q}_\beta - q_\delta \bar{q}_\gamma)$: $20\, \delta_{\alpha\delta}\delta_{\beta\gamma} + 28_{\alpha\beta}\delta_{\gamma\delta} + \frac{4}{3} \delta_{all}$

III_{c1} $(gq - gq)$: 55

III_{c2} $(g\bar{q} - g\bar{q})$: 55

III_d $(q\bar{q} - gg)$: $\frac{28}{3}$

III_e $(gg - q\bar{q})$: $\frac{21}{16}$

III_f $(gg - gg)$: $\frac{2187}{8}$

TABLE 3

Distribution Function Parameters

a/A	$g_{a/A}$	$\hat{x}_a$	$f_{a/A}$	$N_{a/A}$	$f_{a/A}\ N_{a/A}$
		proton primary			
u/p	3	.2	.1	1.22	.122
d/p	3	.2	.067	1.22	.082
$s,\bar{s},\bar{u},\bar{d}/p$	7	0	.01	1	.01
g/p	4	0	.0625	1	.0625
$2q/p$	1	.6	.1	1.6	.16
$2\bar{q}/p$	9	.2	.036	2.66	.095
M/p	5	.3	.1	2.4	.24
B/p	3	.315	.12	1.6	.192
$\bar{B}/p$	11	.2	.06	3.64	.221
		pion primary			
$q/\pi=\bar{q}/\pi$ (valence)	1	.3	.083	1.1	.0913
$q/\pi=\bar{q}/\pi$ (non-valence)	5	0	.01	1	.01
g/π	2	0	.0625	1	.0625
$2q/\pi=2\bar{q}/\pi$	3	.4	.1	2.1	.21
M/π	3	.4	.1	2.1	.21
$B/\pi=\bar{B}/\pi$	5	.33	.08	2.8	.22

TABLE 4

Fragmentation Function Parameters

C/c	$g_{C/c}$	$d_{C/c}$
	c=quark	
π^+/u	1	.5
π^-/u	5	.5
p/u	3	1.0
n/u	3	.5
$\bar{p}/u=\bar{n}/u$	7	1.0
	c=gluon	
p/g	4	.9
π^+/g	2	.5

TABLE 5

Contributions to $p_T^4 \; E \frac{d\sigma}{d^3p}$ $(pp \to aX)$

a \ sub process	a1	a2	b	c1	c2	d	e	f
u	$.034\epsilon^7$ + $.0068\epsilon^{11}$	0	$.022\epsilon^{11}$ + $4.6\times10^{-5}\epsilon^{15}$	$.12\epsilon^8$	0	0	$.0021\epsilon^{11}$	0
d	$.025\epsilon^7$ + $.0046\epsilon^{11}$	0	$.015\epsilon^{11}$ + $4.6\times10^{-5}\epsilon^{15}$	$.077\epsilon^8$	0	0	$.0021\epsilon^{11}$	0
s	$.011\epsilon^{11}$ + $3.4\times10^{-4}\epsilon^{15}$	0	$.0011\epsilon^{11}$ + $.0015\epsilon^{15}$	$.021\epsilon^{12}$	0	0	$.0021\epsilon^{11}$	0
$\bar{u}$	0	.0013	$.013\epsilon^{11}$ + $5.1\times10^{-4}\epsilon^{15}$	0	$.021\epsilon^{12}$	0	$.0021\epsilon^{11}$	0
$\bar{d}$	0	.0013	$.013\epsilon^{11}$ + $5.1\times10^{-4}\epsilon^{15}$	0	$.021\epsilon^{12}$	0	$.0021\epsilon^{11}$	0
$\bar{s}$ (=s)	0	.0013	$.012\epsilon^{11}$ + $5.4\times10^{-4}\epsilon^{15}$	0	$.021\epsilon^{12}$	0	$.0021\epsilon^{11}$	0
g	0	0	0	$.197\epsilon^8$ + $.021\epsilon^{12}$	$.063\epsilon^{12}$	$.0053\epsilon^{11}$ + $2.1\times10^{-4}\epsilon^{15}$	0	$.434\epsilon^9$

TABLE 6

Contributions to $p_T^4 \, E \frac{d\sigma}{d^3p}$ $\left(\begin{matrix}\pi^+\\ \pi^-\end{matrix} p \to aX\right)$

a \ sub process	a1	a2	b	c1	c2	d	e	f
u	$\begin{pmatrix}.017\\.008\end{pmatrix}\varepsilon^5$	0	$\begin{pmatrix}.0086\\.0094\end{pmatrix}\varepsilon^5$	$\begin{pmatrix}.091\\.04\end{pmatrix}\varepsilon^6$	0	0	$\begin{pmatrix}.0019\\.0019\end{pmatrix}\varepsilon^7$	0
	$\begin{pmatrix}.0092\\.0053\end{pmatrix}\varepsilon^9$		$\begin{pmatrix}.022\\.004\end{pmatrix}\varepsilon^9$	$\begin{pmatrix}0\\.0063\end{pmatrix}\varepsilon^{10}$				
	$\begin{pmatrix}0\\2.2\ 10^{-4}\end{pmatrix}\varepsilon^{13}$		$\begin{pmatrix}6.5\ 10^{-5}\\7.2\ 10^{-4}\end{pmatrix}\varepsilon^{13}$					
d	$\begin{pmatrix}.0054\\.016\end{pmatrix}\varepsilon^5$	0	$\begin{pmatrix}.0063\\.0062\end{pmatrix}\varepsilon^5$	$\begin{pmatrix}.027\\.077\end{pmatrix}\varepsilon^6$	0	0	$\begin{pmatrix}.0019\\.0019\end{pmatrix}\varepsilon^7$	0
	$\begin{pmatrix}.0045\\.0081\end{pmatrix}\varepsilon^9$		$\begin{pmatrix}.003\\.021\end{pmatrix}\varepsilon^9$	$\begin{pmatrix}.0063\\0\end{pmatrix}\varepsilon^{10}$				
	$\begin{pmatrix}2.2\ 10^{-4}\\0\end{pmatrix}\varepsilon^{13}$		$\begin{pmatrix}7.2\ 10^{-4}\\6.5\ 10^{-5}\end{pmatrix}\varepsilon^{13}$					
s	$\begin{pmatrix}8.6\ 10^{-3}\\8.6\ 10^{-3}\end{pmatrix}\varepsilon^9$	0	$\begin{pmatrix}5.44\ 10^{-4}\\8.1\ 10^{-4}\end{pmatrix}\varepsilon^5$	$\begin{pmatrix}.024\\.024\end{pmatrix}\varepsilon^{10}$	0	0	$\begin{pmatrix}.0019\\.0019\end{pmatrix}\varepsilon^7$	0
	$\begin{pmatrix}5.3\ 10^{-4}\\5.3\ 10^{-4}\end{pmatrix}\varepsilon^{13}$		$\begin{pmatrix}6.6\ 10^{-3}\\6.6\ 10^{-3}\end{pmatrix}\varepsilon^9$					
			$\begin{pmatrix}1.2\ 10^{-3}\\1.2\ 10^{-3}\end{pmatrix}\varepsilon^{13}$					
$\bar{u}$	0	$\begin{pmatrix}5.8\ 10^{-3}\\1.3\ 10^{-2}\end{pmatrix}\varepsilon^9$	$\begin{pmatrix}5.4\ 10^{-4}\\1.5\ 10^{-2}\end{pmatrix}\varepsilon^5$	0	$\begin{pmatrix}0\\.05\end{pmatrix}\varepsilon^6$	0	$\begin{pmatrix}.0019\\.0019\end{pmatrix}\varepsilon^7$	0
		$\begin{pmatrix}9.8\ 10^{-4}\\4.3\ 10^{-4}\end{pmatrix}\varepsilon^{13}$	$\begin{pmatrix}9.9\ 10^{-3}\\1.2\ 10^{-2}\end{pmatrix}\varepsilon^9$		$\begin{pmatrix}.024\\.018\end{pmatrix}\varepsilon^{10}$			
			$\begin{pmatrix}7.1\ 10^{-4}\\5.1\ 10^{-4}\end{pmatrix}\varepsilon^{13}$					

(cont'd)

TABLE 6 (cont'd)

a \ sub process	a1	a2	b	c1	c2	d	e	f
$\bar{d}$	0	$\begin{pmatrix}.002\\.0058\end{pmatrix}\varepsilon^9$	$\begin{pmatrix}1.4\ 10^{-2}\\8.1\ 10^{-4}\end{pmatrix}\varepsilon^5$	0	$\begin{pmatrix}.05\\0\end{pmatrix}\varepsilon^6$	0	$\begin{pmatrix}.0019\\.0019\end{pmatrix}\varepsilon^7$	0
		$\begin{pmatrix}4.4\ 10^{-4}\\9.6\ 10^{-4}\end{pmatrix}\varepsilon^{13}$	$\begin{pmatrix}1.25\ 10^{-2}\\9.8\ 10^{-3}\end{pmatrix}\varepsilon^9$		$\begin{pmatrix}.018\\.024\end{pmatrix}\varepsilon^{10}$			
			$\begin{pmatrix}5.1\ 10^{-4}\\7.1\ 10^{-4}\end{pmatrix}\varepsilon^{13}$					
$\bar{s}$	0	$\begin{pmatrix}.0058\\.0058\end{pmatrix}\varepsilon^9$	$\begin{pmatrix}5.4\ 10^{-4}\\8.1\ 10^{-4}\end{pmatrix}\varepsilon^5$	0	$\begin{pmatrix}.024\\.024\end{pmatrix}\varepsilon^{10}$	0	$\begin{pmatrix}.0019\\.0019\end{pmatrix}\varepsilon^7$	0
		$\begin{pmatrix}9.8\ 10^{-4}\\9.8\ 10^{-4}\end{pmatrix}\varepsilon^{13}$	$\begin{pmatrix}9.4\ 10^{-3}\\9.4\ 10^{-3}\end{pmatrix}\varepsilon^9$					
			$\begin{pmatrix}7.4\ 10^{-4}\\7.4\ 10^{-4}\end{pmatrix}\varepsilon^{13}$					
g	0	0	0	$\begin{pmatrix}.17\\.17\end{pmatrix}\varepsilon^6$	$\begin{pmatrix}.17\\.17\end{pmatrix}\varepsilon^6$	$\begin{pmatrix}.0025\\.0037\end{pmatrix}\varepsilon^5$	0	$\begin{pmatrix}.394\\.394\end{pmatrix}\varepsilon^7$
				$\begin{pmatrix}.096\\.096\end{pmatrix}\varepsilon^{10}$	$\begin{pmatrix}.096\\.096\end{pmatrix}\varepsilon^{10}$	$\begin{pmatrix}.0035\\.0033\end{pmatrix}\varepsilon^9$		
						$\begin{pmatrix}.0003\\.0003\end{pmatrix}\varepsilon^{13}$		

TABLE 7

Ratio of Production Cross Sections

$(\sqrt{s} = 63\ \text{GeV})/(\sqrt{s} = 27\ \text{GeV})$

Beam and Trigger Type	$p_T\left(\frac{\text{GeV}}{c}\right)$ 4	8	12
$pp \to \pi^+$	7.8	351	1.3×10^{7}
$pp \to K^-$	15.5	1897	6.3×10^{8}
$pp \to p$	3.4	33.3	1.5×10^{3}
$pp \to \bar{p}$	25.9	9368	3.2×10^{10}
$\pi^+p \to \pi^+$	3.7	18.1	4.4×10^{2}
$\pi^-p \to \pi^+$	5.8	141	2.1×10^{5}
$\pi^+p \to K^-$	8.9	435	4.2×10^{6}
$\pi^-p \to K^-$	5.2	101	1.2×10^{5}
$\pi^+p \to p$	4.6	117	1.3×10^{3}
$\pi^-p \to p$	6.1	275	3.9×10^{3}
$\pi^+p \to \bar{p}$	15.1	1207	1.4×10^{7}
$\pi^-p \to \bar{p}$	15.4	1026	1.0×10^{7}

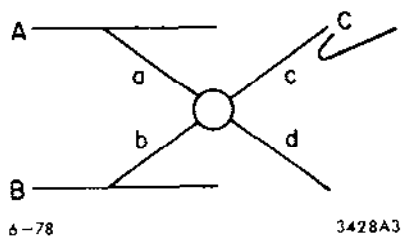

Fig. 1

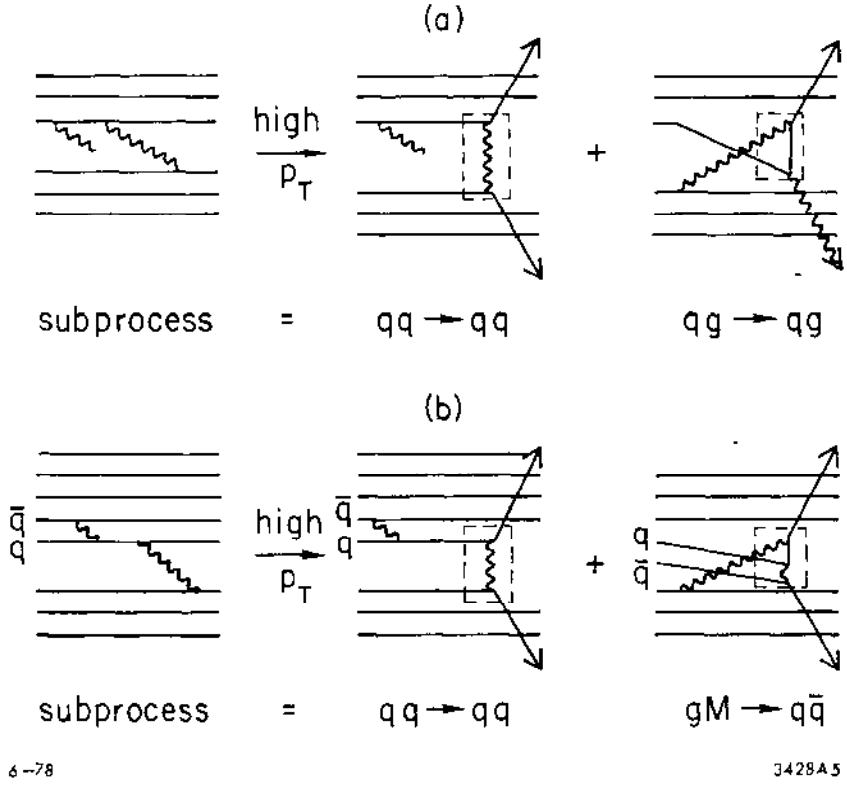
(a)
high
p_T
+
subprocess = qq → qq
qg → qg
(b)
$\bar{q}$
q
high
$\bar{q}$
q
p_T
+
q
$\bar{q}$
subprocess = qq → qq
gM → q$\bar{q}$
6-78
3428A5

Fig. 2

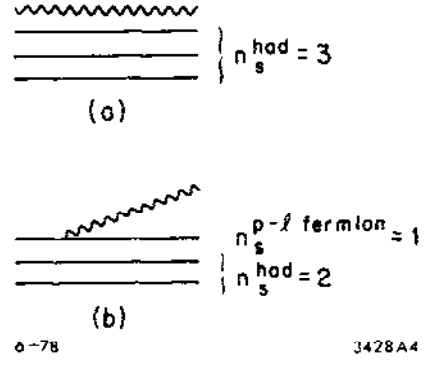

Fig. 3

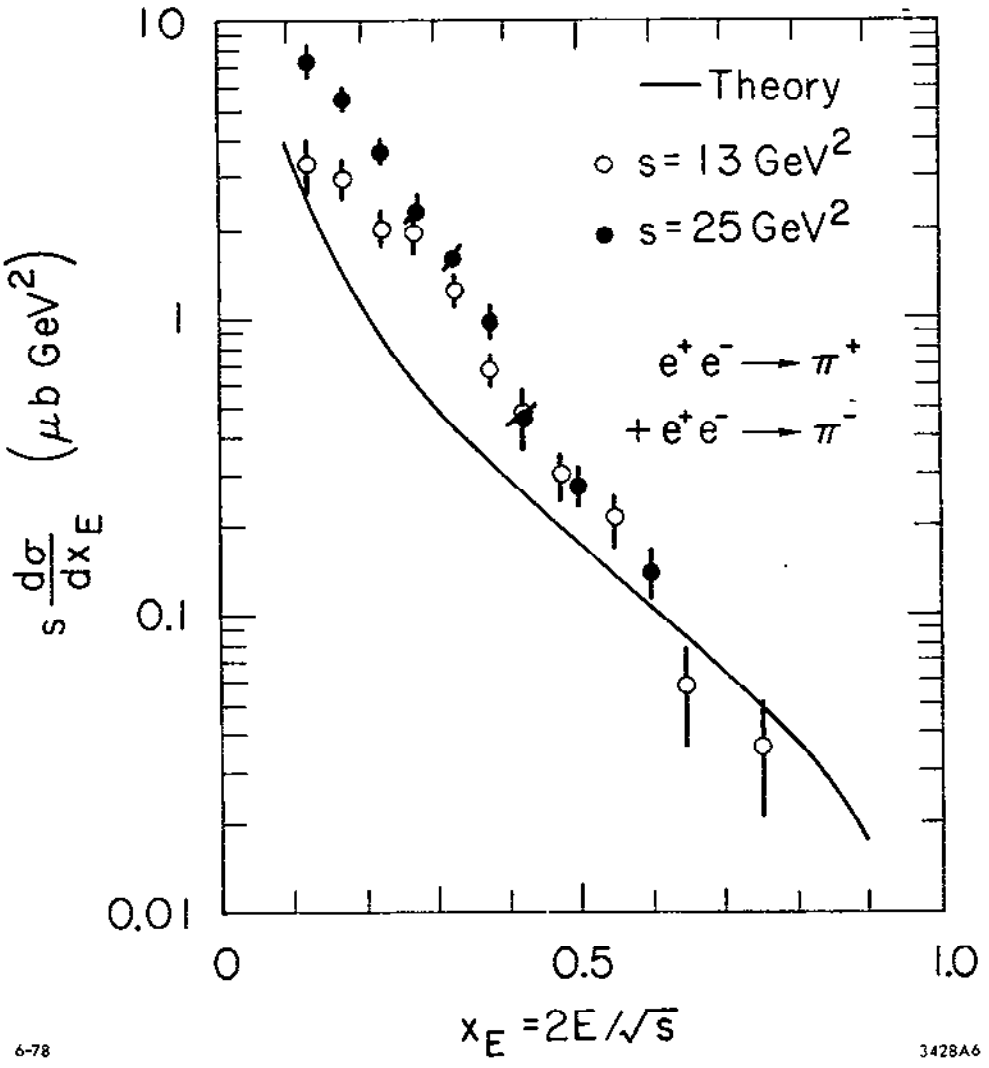
10
1
0.1
0.01
0
0.5
1.0
$s\frac{d\sigma}{dx_E}$ $(\mu b\ GeV^2)$
$x_E = 2E/\sqrt{s}$
Theory
$s = 13\ GeV^2$
$s = 25\ GeV^2$
$e^+e^- \rightarrow \pi^+ + e^+e^- \rightarrow \pi^-$
6-78
3428A6

Fig. 4a

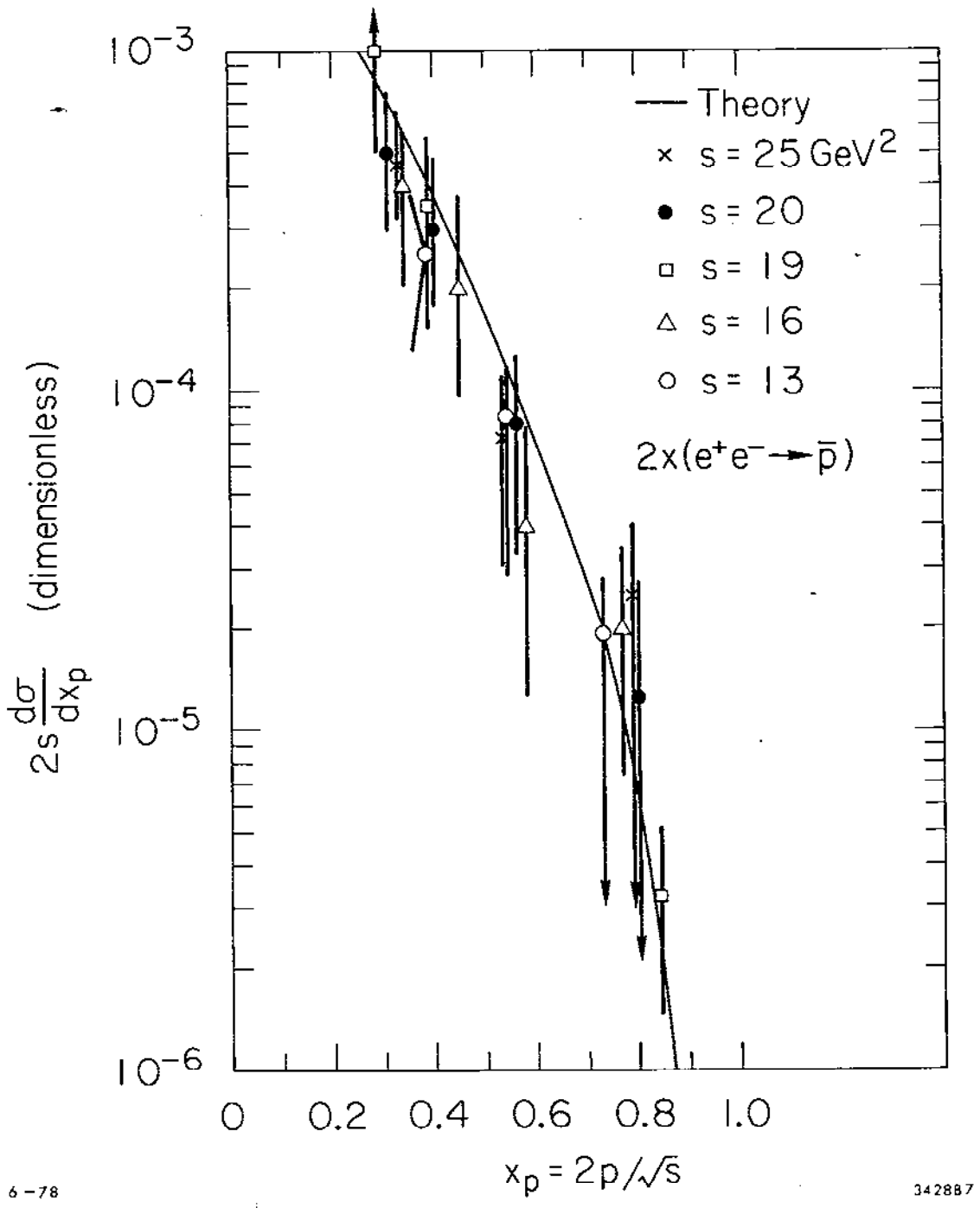
Theory
s = 25 GeV²
s = 20
s = 19
s = 16
s = 13
2x(e⁺e⁻ → p̄)
$2s\frac{d\sigma}{dx_p}$ (dimensionless)
10^{-3}
10^{-4}
10^{-5}
10^{-6}
0
0.2
0.4
0.6
0.8
1.0
$x_p = 2p/\sqrt{s}$
6-78
342887

Fig. 4b

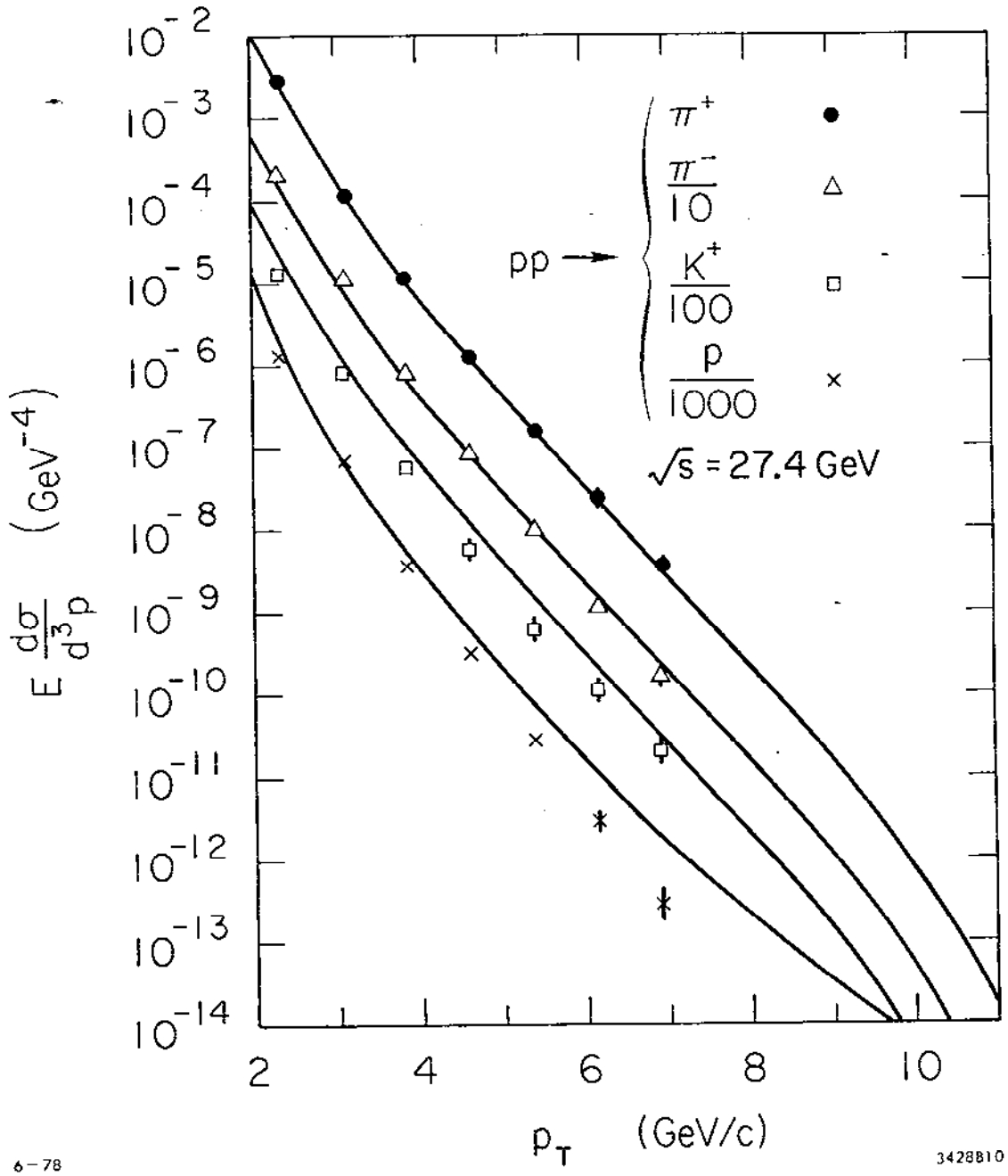
10^{-2}
10^{-3}
10^{-4}
10^{-5}
10^{-6}
10^{-7}
10^{-8}
10^{-9}
10^{-10}
10^{-11}
10^{-12}
10^{-13}
10^{-14}
$E\frac{d\sigma}{d^3p}$ (GeV^{-4})
2
4
6
8
10
p_T (GeV/c)
pp →
π^+
$\frac{\pi^-}{10}$
$\frac{K^+}{100}$
$\frac{p}{1000}$
$\sqrt{s}$ = 27.4 GeV
6-78
3428810

Fig. 5a

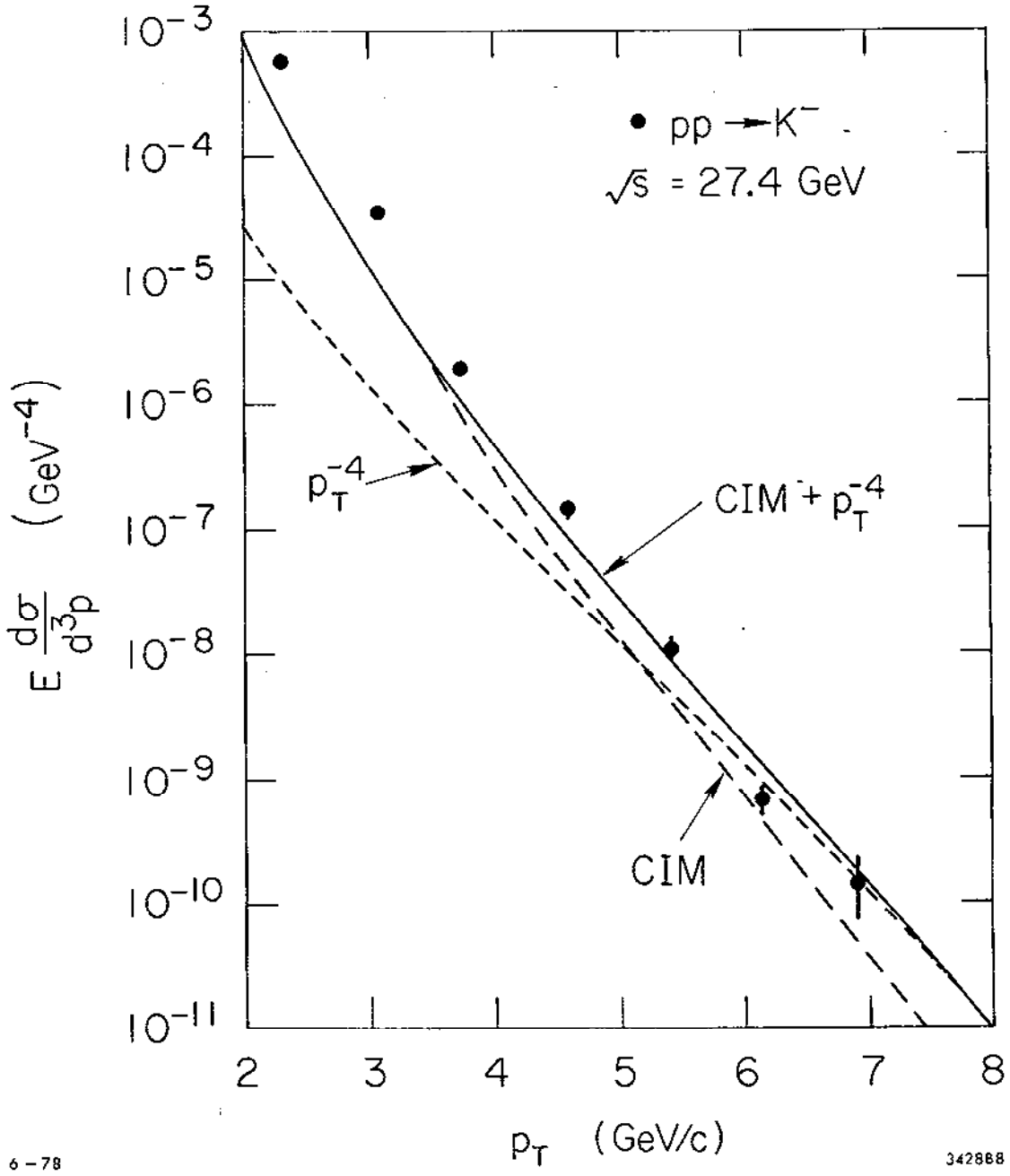
10^{-3}
10^{-4}
10^{-5}
10^{-6}
10^{-7}
10^{-8}
10^{-9}
10^{-10}
10^{-11}
$E\frac{d\sigma}{d^3p}$ (GeV^{-4})
pp → K$^-$
$\sqrt{s}$ = 27.4 GeV
p_T^{-4}
CIM + p_T^{-4}
CIM
2
3
4
5
6
7
8
p_T (GeV/c)
6 – 78
342888

Fig. 5b

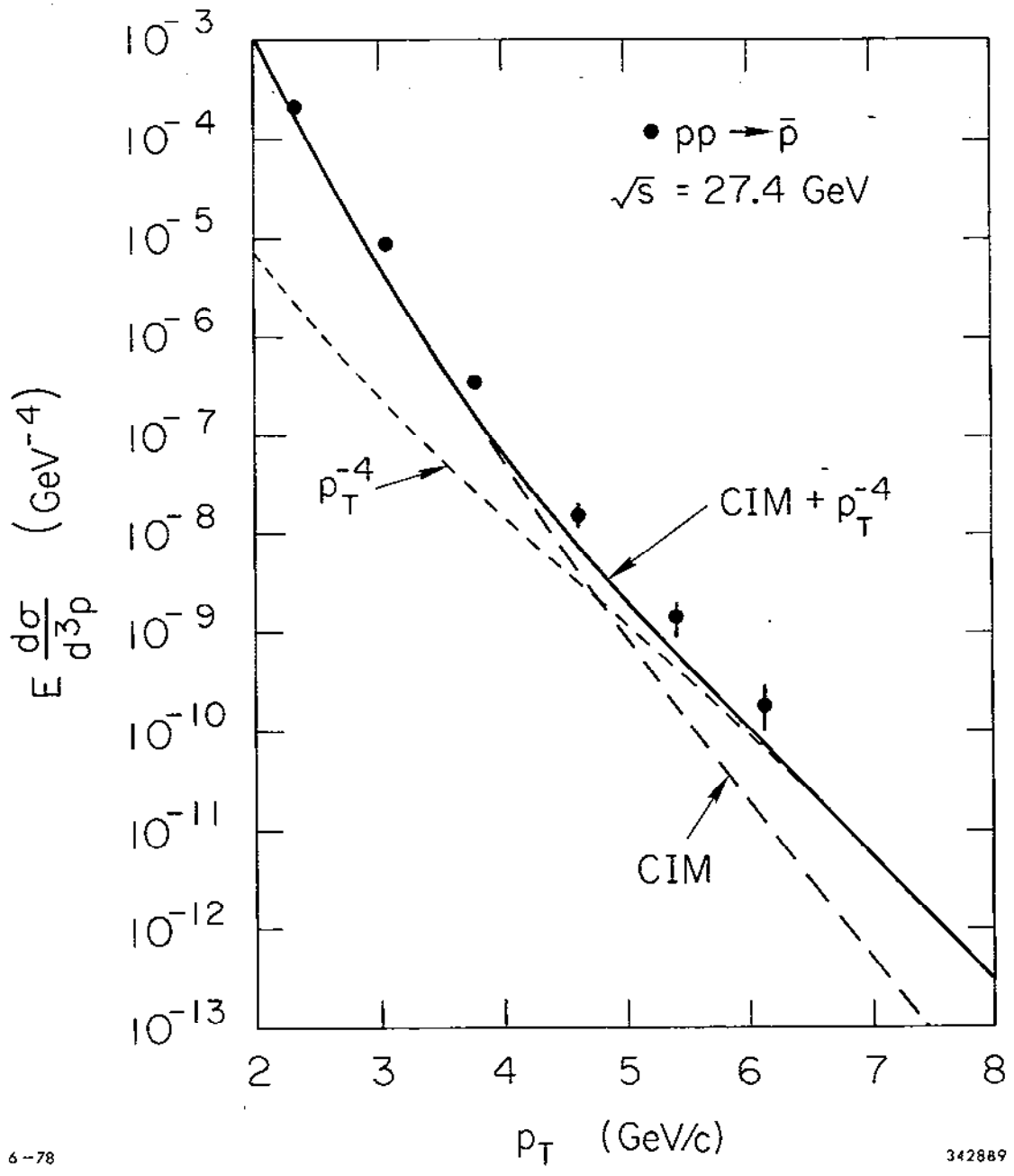
10^{-3}
10^{-4}
10^{-5}
10^{-6}
10^{-7}
10^{-8}
10^{-9}
10^{-10}
10^{-11}
10^{-12}
10^{-13}
$E\frac{d\sigma}{d^3p}$ (GeV^{-4})
• $pp \rightarrow \bar{p}$
$\sqrt{s}$ = 27.4 GeV
p_T^{-4}
CIM + p_T^{-4}
CIM
2
3
4
5
6
7
8
p_T (GeV/c)
6-78
342889

Fig. 5c

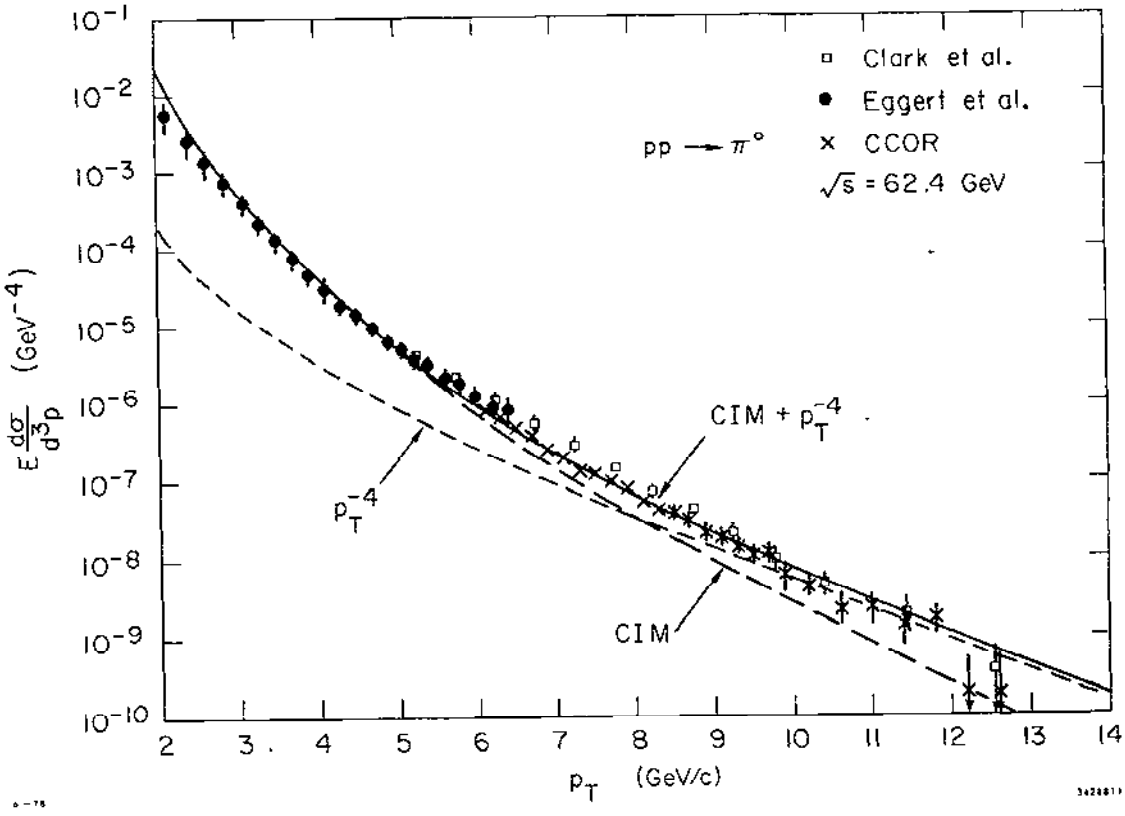
Clark et al.
Eggert et al.
CCOR
pp → π°
√s = 62.4 GeV
CIM + p_T^-4
p_T^-4
CIM
E d³σ/dp³ (GeV^-4)
p_T (GeV/c)

Fig. 6a

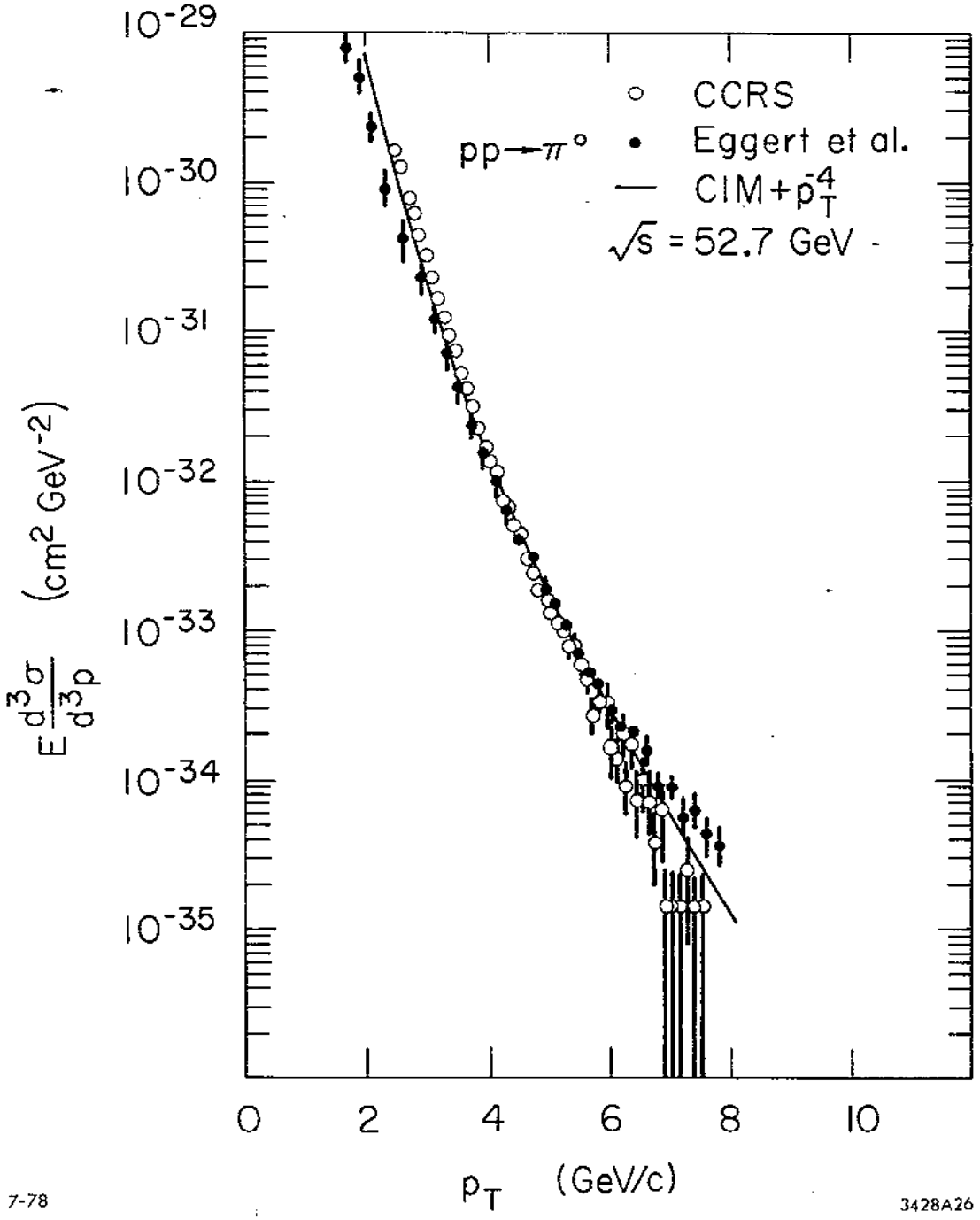
10^{-29}
10^{-30}
10^{-31}
10^{-32}
10^{-33}
10^{-34}
10^{-35}
$E\frac{d^3\sigma}{d^3p}$ (cm^2 GeV^{-2})
pp→π°
CCRS
Eggert et al.
CIM+p_T^{-4}
$\sqrt{s}$ = 52.7 GeV
0
2
4
6
8
10
p_T (GeV/c)
7-78
3428A26

Fig 6b

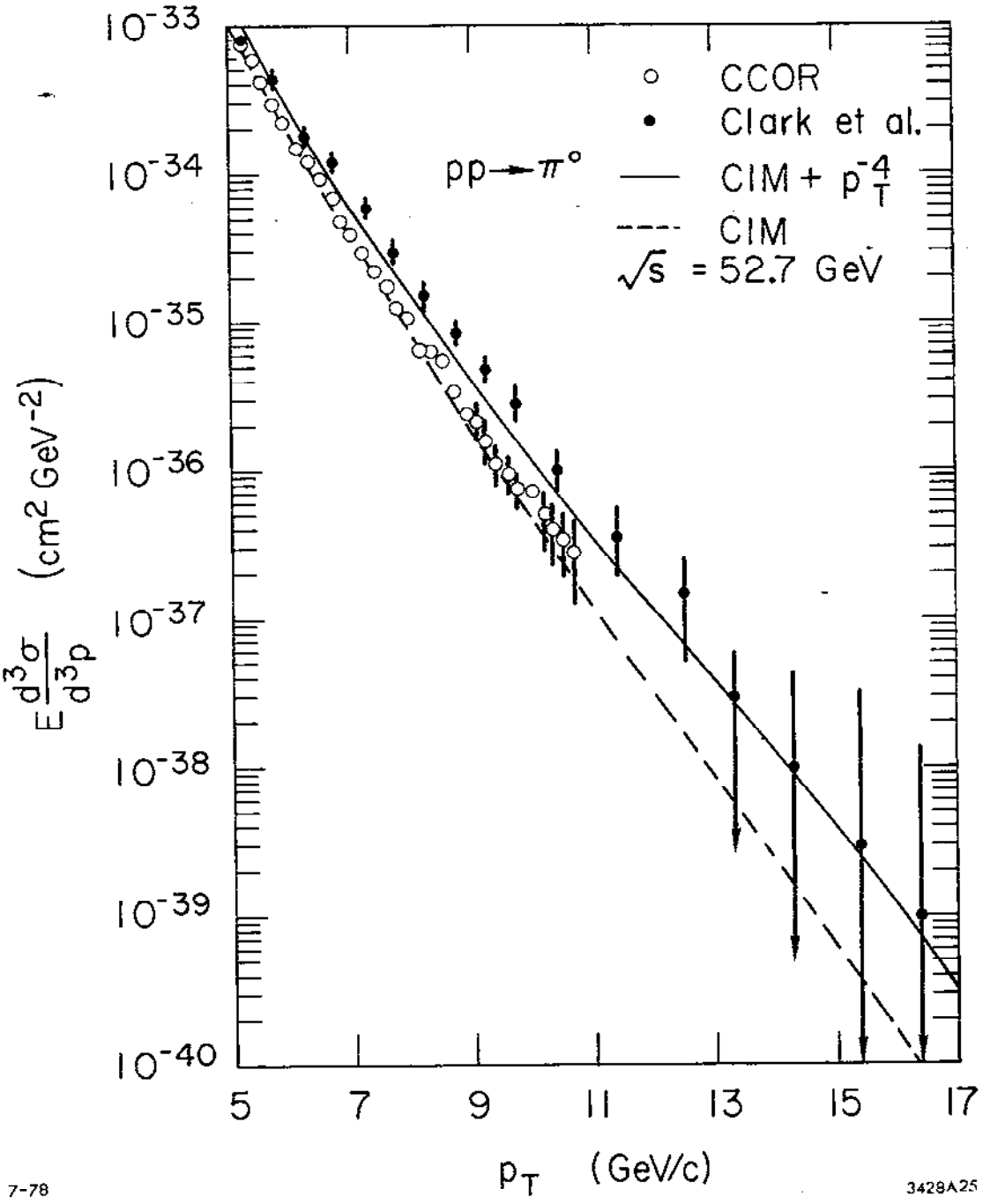
CCOR
Clark et al.
pp→π°
CIM + p_T^-4
CIM
√s = 52.7 GeV
E d³σ/d³p (cm² GeV⁻²)
10⁻³³
10⁻³⁴
10⁻³⁵
10⁻³⁶
10⁻³⁷
10⁻³⁸
10⁻³⁹
10⁻⁴⁰
5
7
9
11
13
15
17
p_T (GeV/c)
7-78
3428A25

Fig. 6c

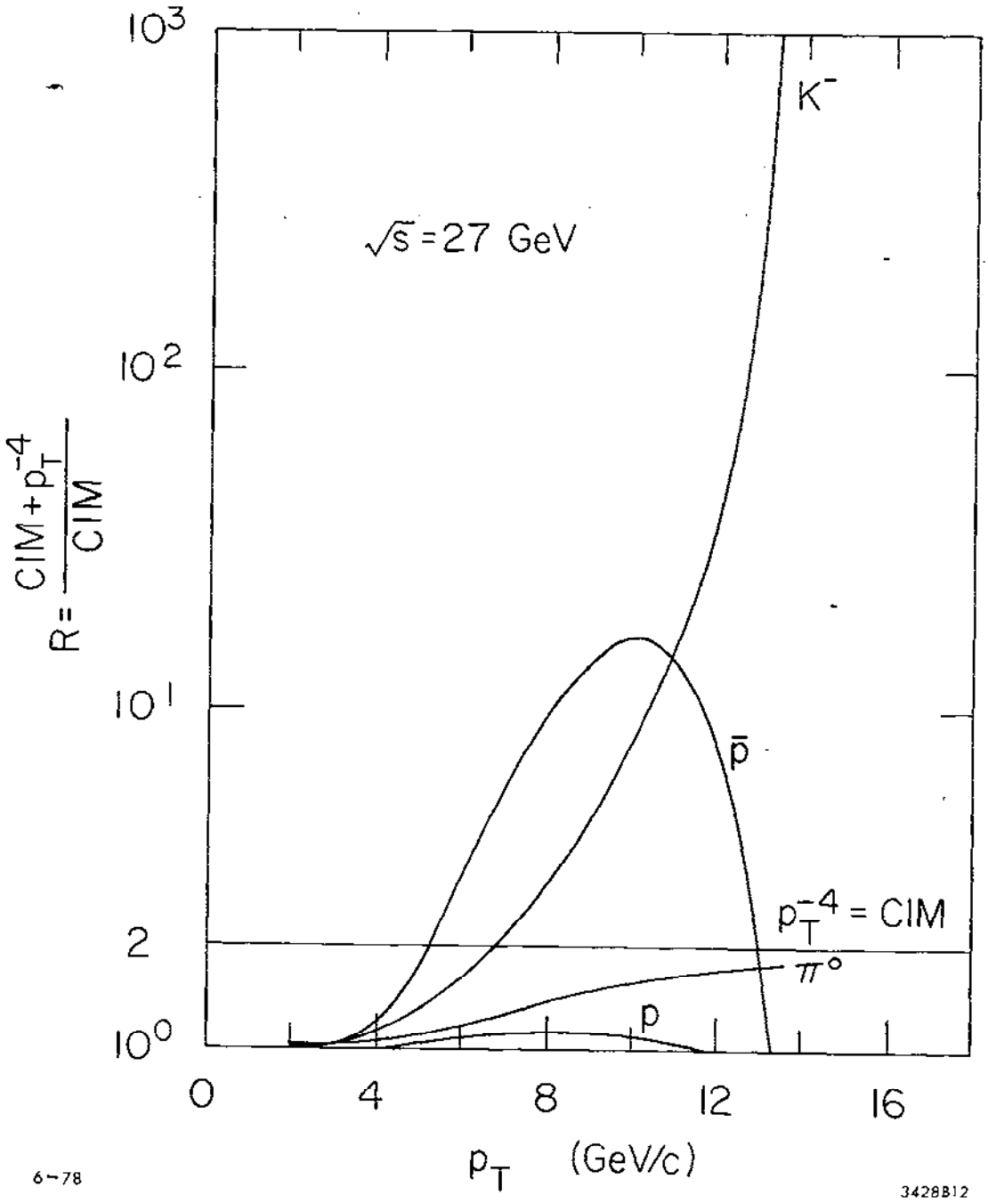
10^3
10^2
10^1
2
10^0
$R = \frac{CIM + p_T^{-4}}{CIM}$
$\sqrt{s}$ = 27 GeV
K^-
$\bar{p}$
p_T^{-4} = CIM
π°
p
0
4
8
12
16
p_T (GeV/c)
6-78
3428B12

Fig. 7a

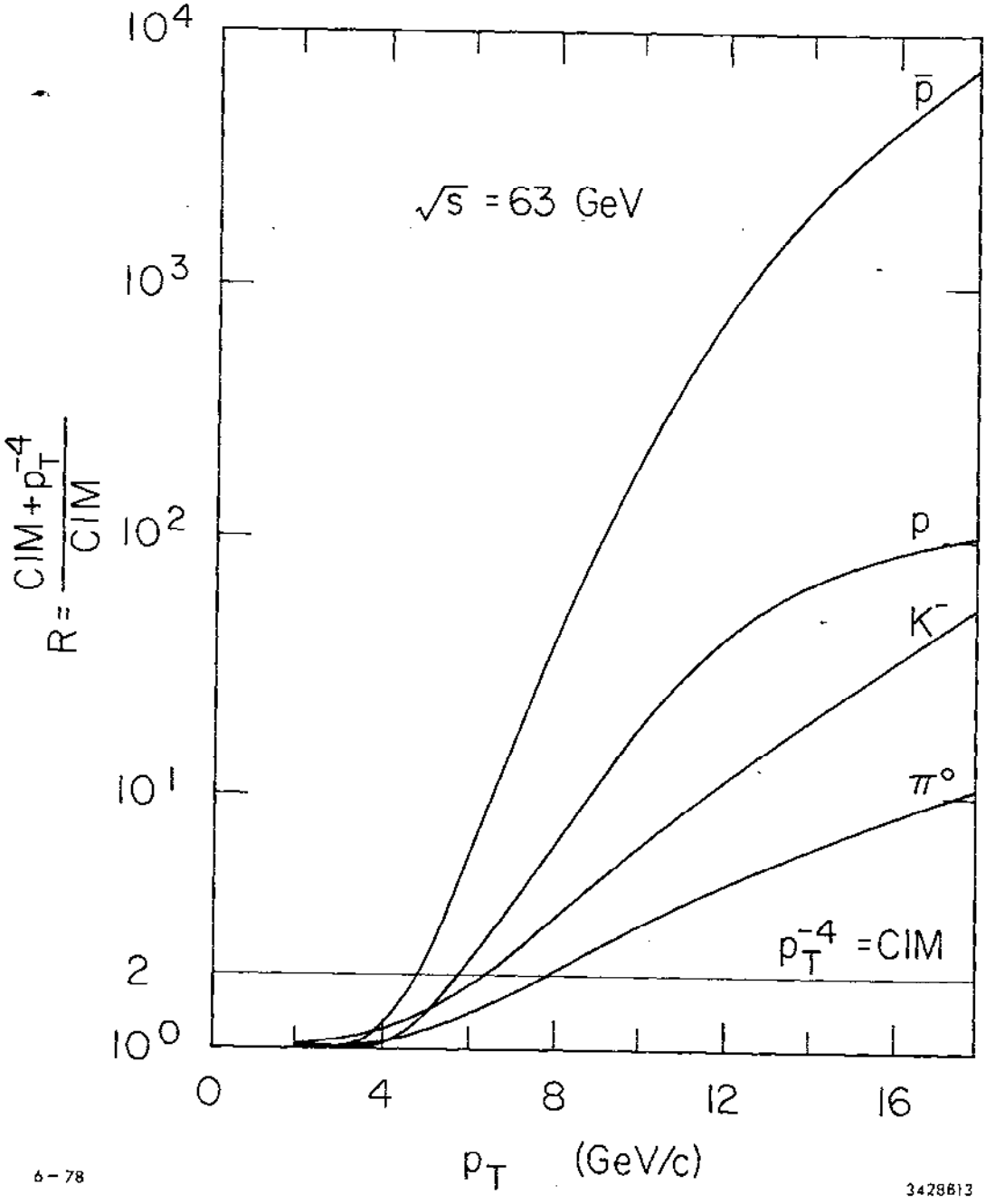
10^4
10^3
10^2
10^1
2
10^0
$R = \frac{CIM + p_T^{-4}}{CIM}$
$\sqrt{s}$ = 63 GeV
$\bar{p}$
p
K^-
π°
p_T^{-4} = CIM
0
4
8
12
16
p_T (GeV/c)
6-78
3428B13

Fig. 7b

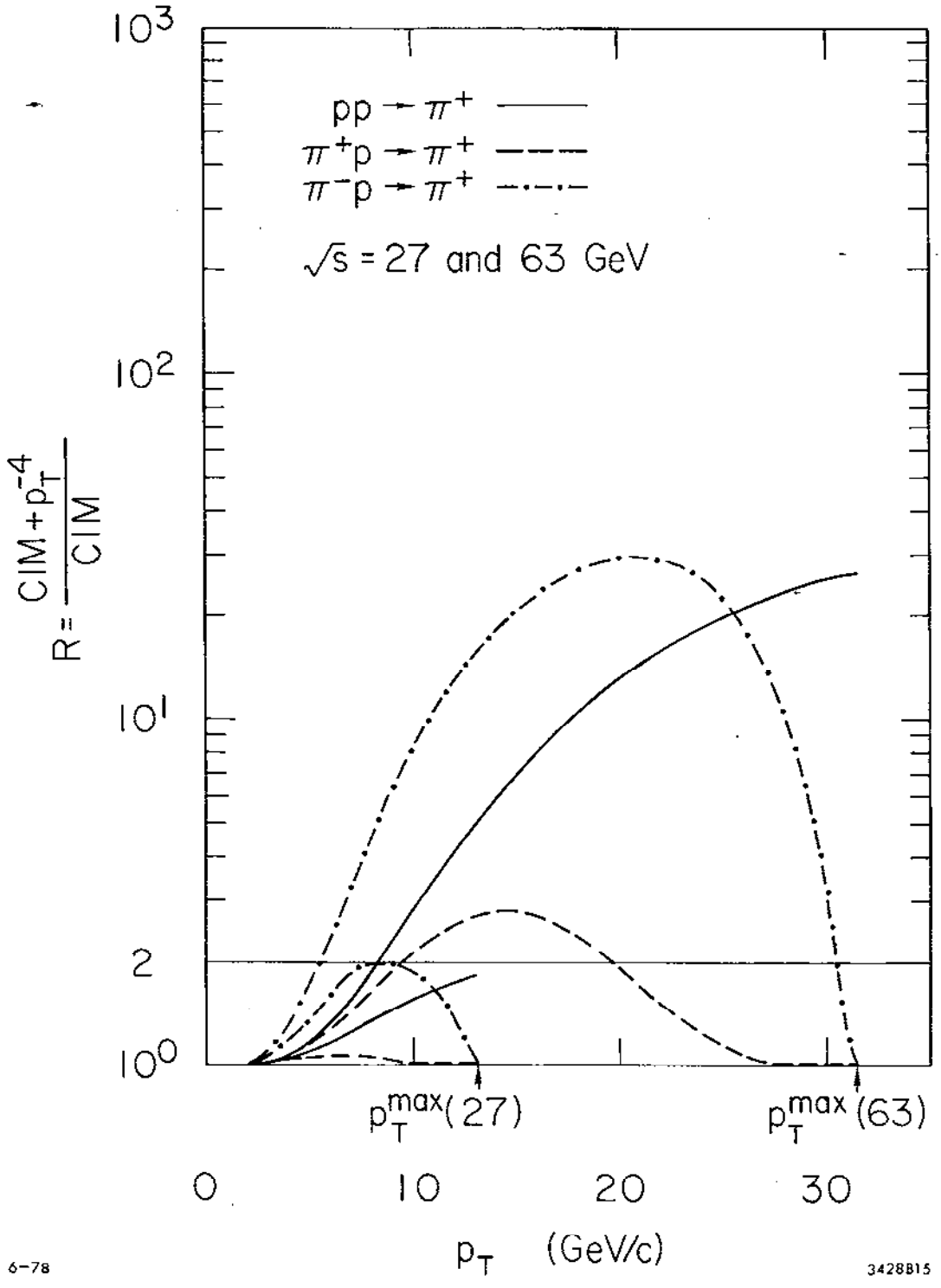
10^3
10^2
10^1
2
10^0
$pp \to \pi^+$
$\pi^+p \to \pi^+$
$\pi^-p \to \pi^+$
$\sqrt{s}$ = 27 and 63 GeV
$R = \frac{CIM + p_T^{-4}}{CIM}$
$p_T^{max}(27)$
$p_T^{max}(63)$
0
10
20
30
p_T (GeV/c)
6-78
3428B15

Fig 8a

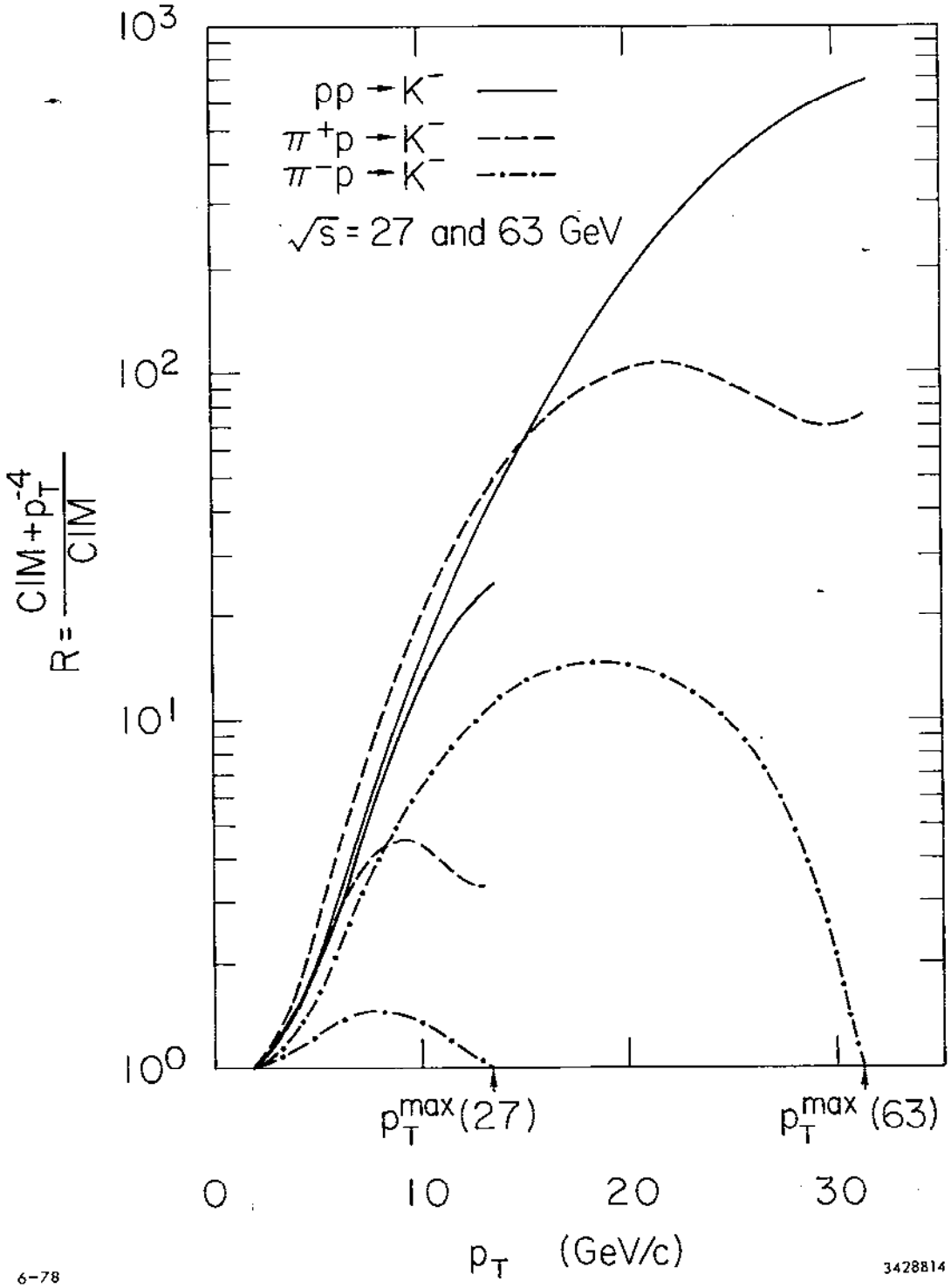
10^3
10^2
10^1
10^0
$pp \to K^-$
$\pi^+ p \to K^-$
$\pi^- p \to K^-$
$\sqrt{s} = 27$ and 63 GeV
$R = \frac{CIM + p_T^{-4}}{CIM}$
$p_T^{max}(27)$
$p_T^{max}(63)$
0
10
20
30
p_T (GeV/c)
6-78
3428814

Fig. 8b

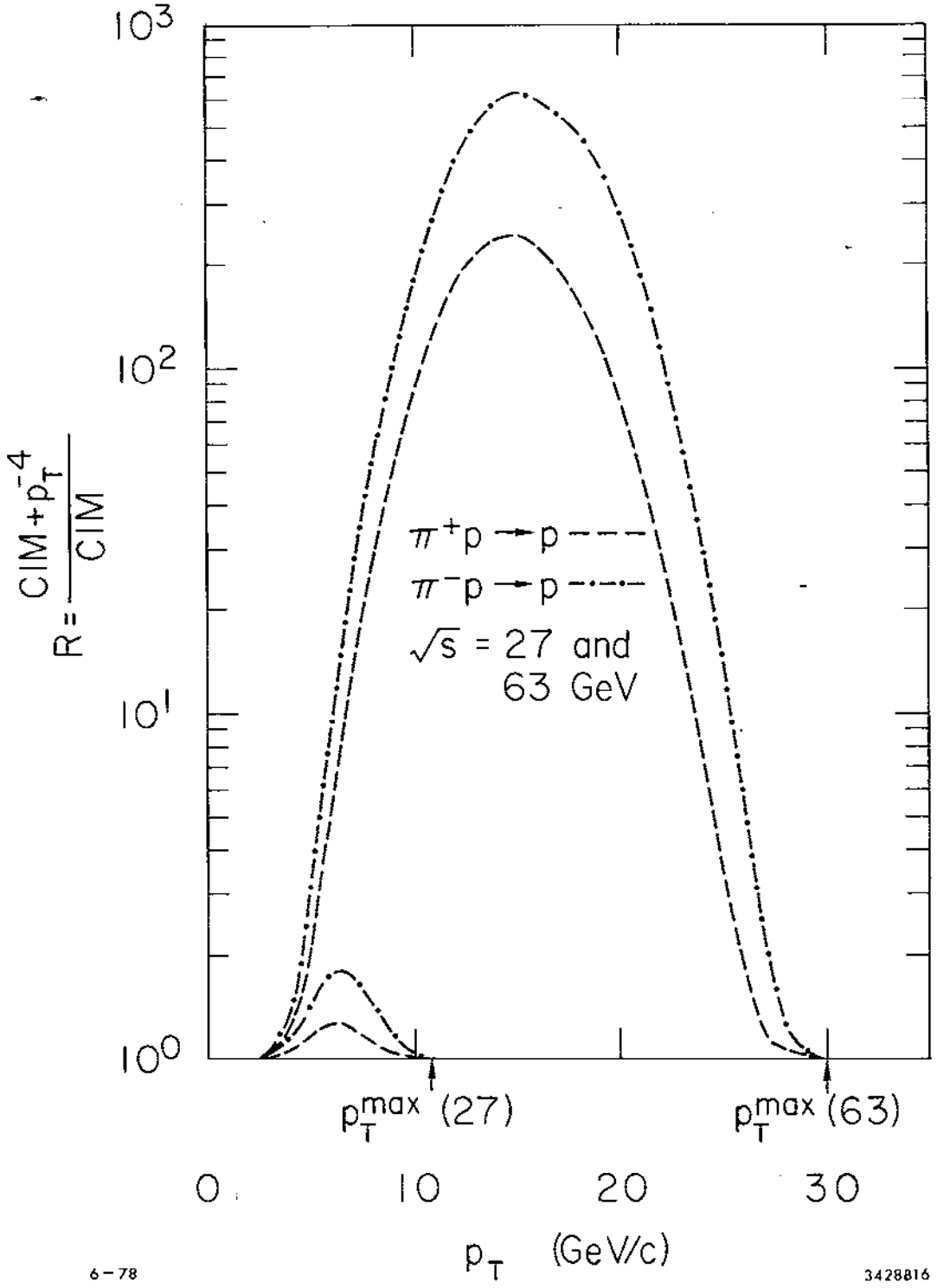
10^3
10^2
10^1
10^0
$R = \frac{CIM + p_T^{-4}}{CIM}$
$\pi^+ p \rightarrow p$ - - -
$\pi^- p \rightarrow p$ -·-·-
$\sqrt{s}$ = 27 and 63 GeV
p_T^{max} (27)
p_T^{max} (63)
0
10
20
30
p_T (GeV/c)
6-78
3428816

Fig. 8c

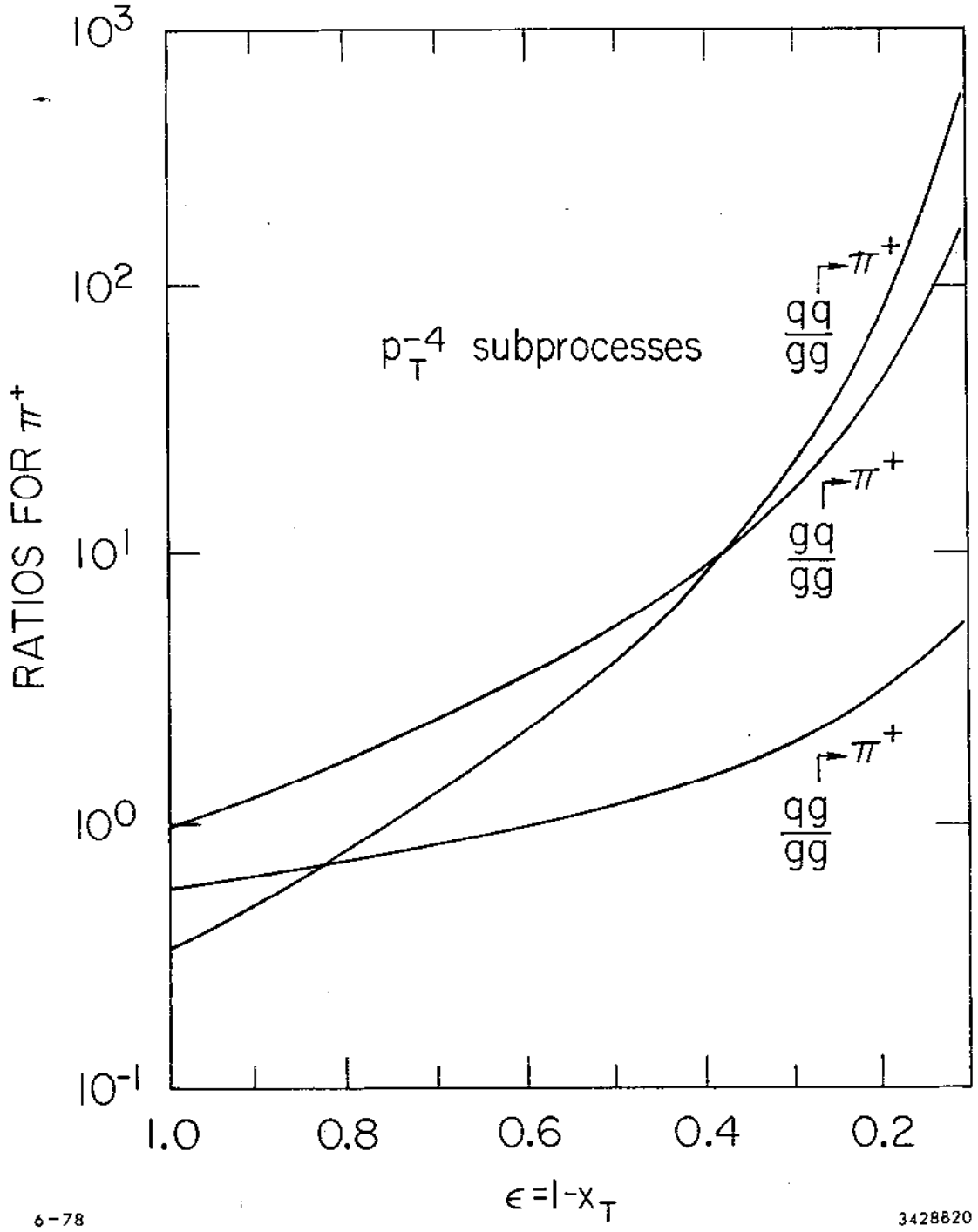
10^3
10^2
10^1
10^0
10^{-1}
RATIOS FOR π^+
p_T^{-4} subprocesses
π^+
$\frac{qq}{gg}$
π^+
$\frac{gq}{gg}$
π^+
$\frac{qg}{gg}$
1.0
0.8
0.6
0.4
0.2
$\epsilon = 1 - x_T$
6-78
3428820

Fig. 9a

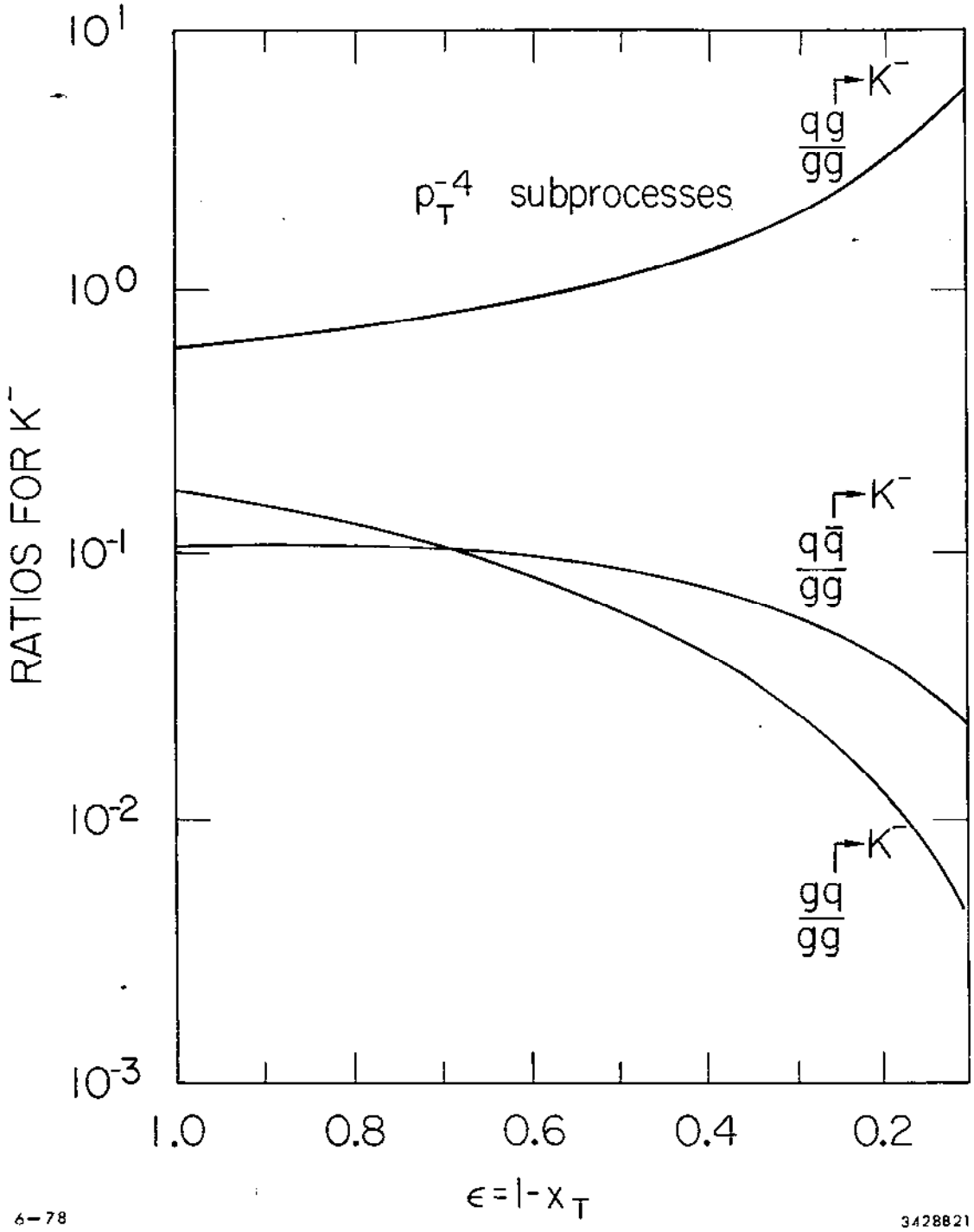
10^1
10^0
10^{-1}
10^{-2}
10^{-3}
RATIOS FOR K^-
p_T^{-4} subprocesses
$\frac{qg}{gg} \to K^-$
$\frac{q\bar{q}}{gg} \to K^-$
$\frac{gq}{gg} \to K^-$
1.0
0.8
0.6
0.4
0.2
$\epsilon = 1 - x_T$
6-78
3428821

Fig 9b

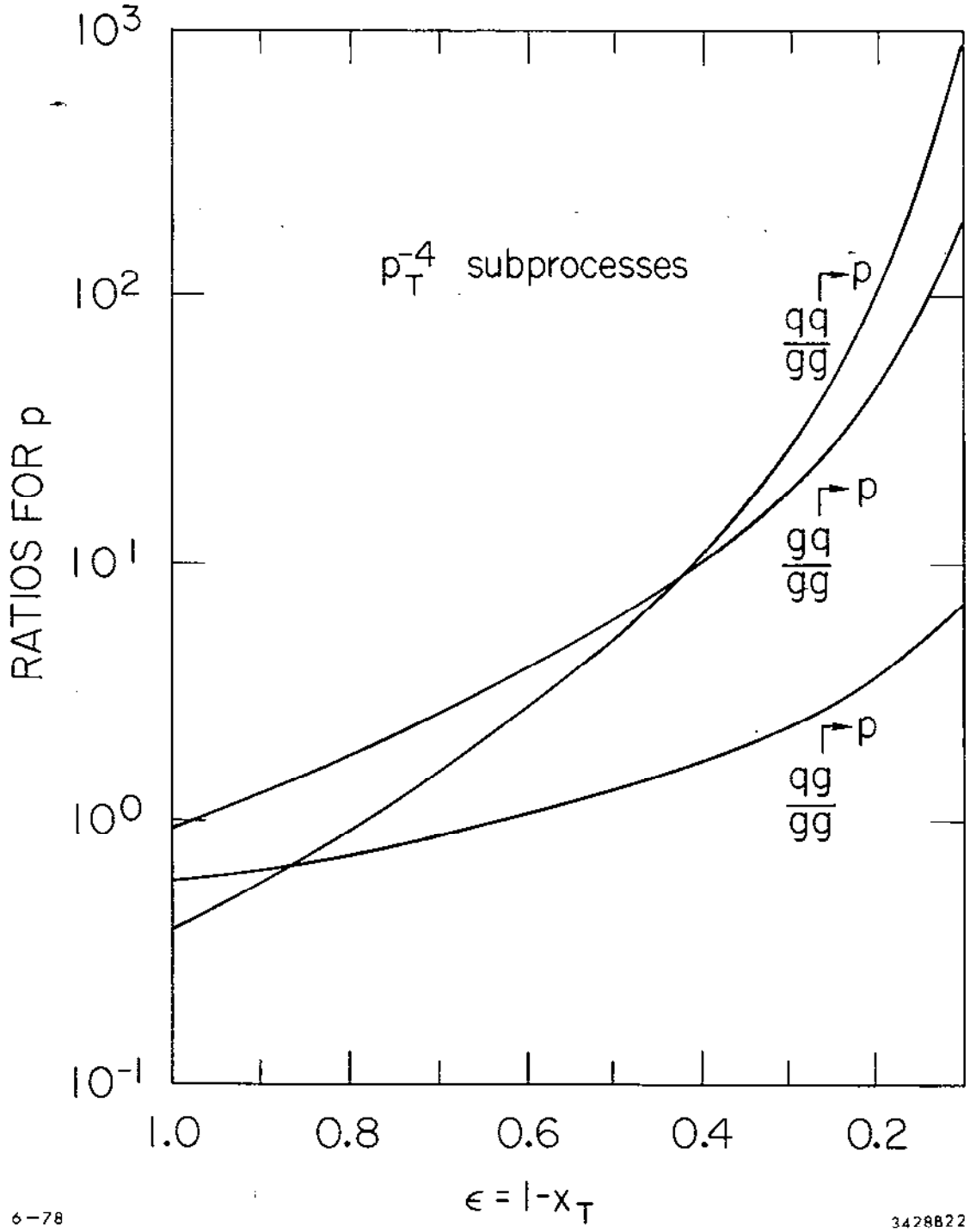
10^3
10^2
10^1
10^0
10^{-1}
RATIOS FOR p
p_T^{-4} subprocesses
p
qq/gg
p
gq/gg
p
qg/gg
1.0
0.8
0.6
0.4
0.2
$\epsilon = 1 - x_T$
6-78
3428B22

Fig. 9c

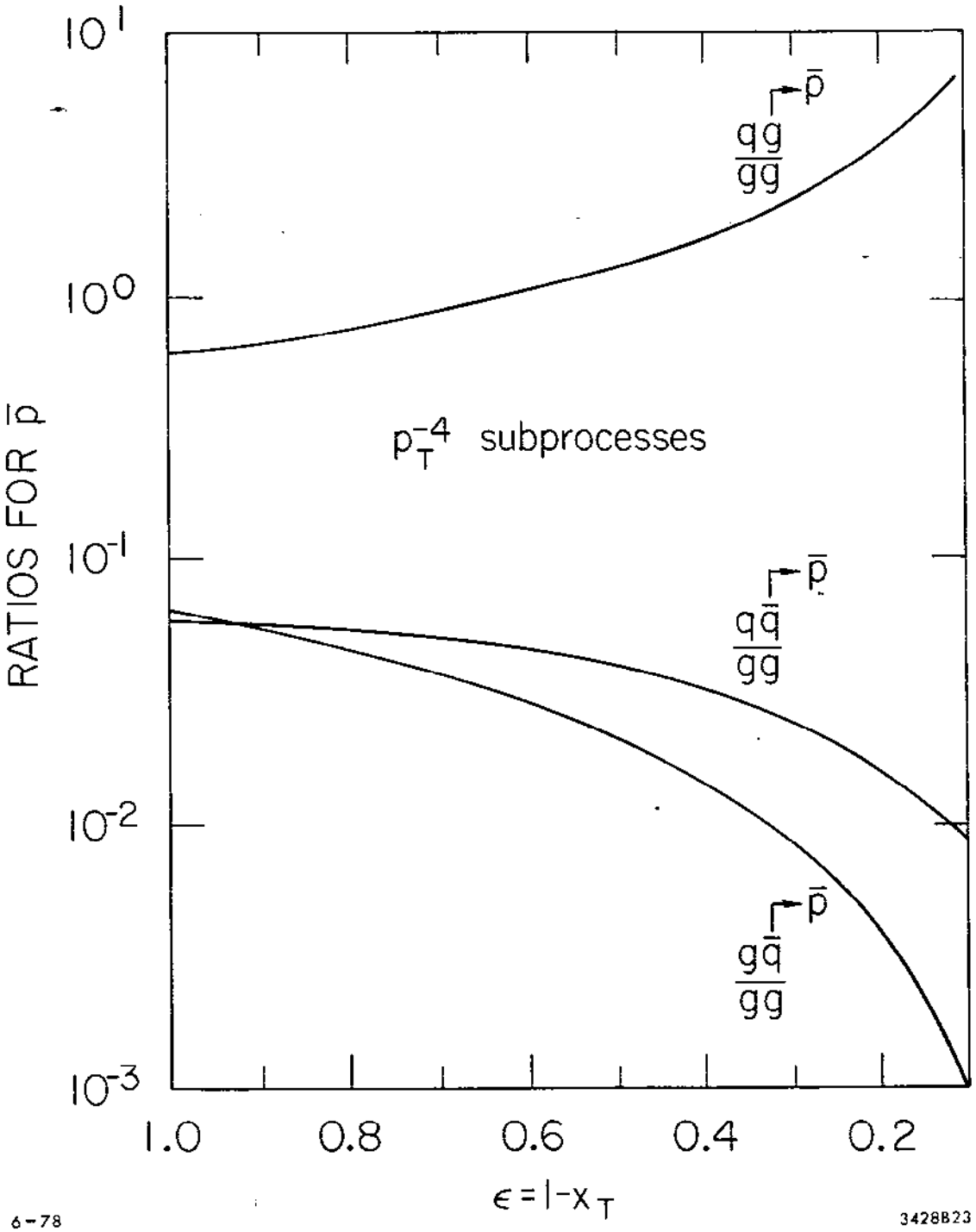
RATIOS FOR $\bar{p}$
10^{1}
10^{0}
10^{-1}
10^{-2}
10^{-3}
p_T^{-4} subprocesses
$\frac{qg}{gg} \to \bar{p}$
$\frac{q\bar{q}}{gg} \to \bar{p}$
$\frac{g\bar{q}}{gg} \to \bar{p}$
1.0
0.8
0.6
0.4
0.2
$\epsilon = 1 - x_T$
6-78
3428B23

Fig. 9d

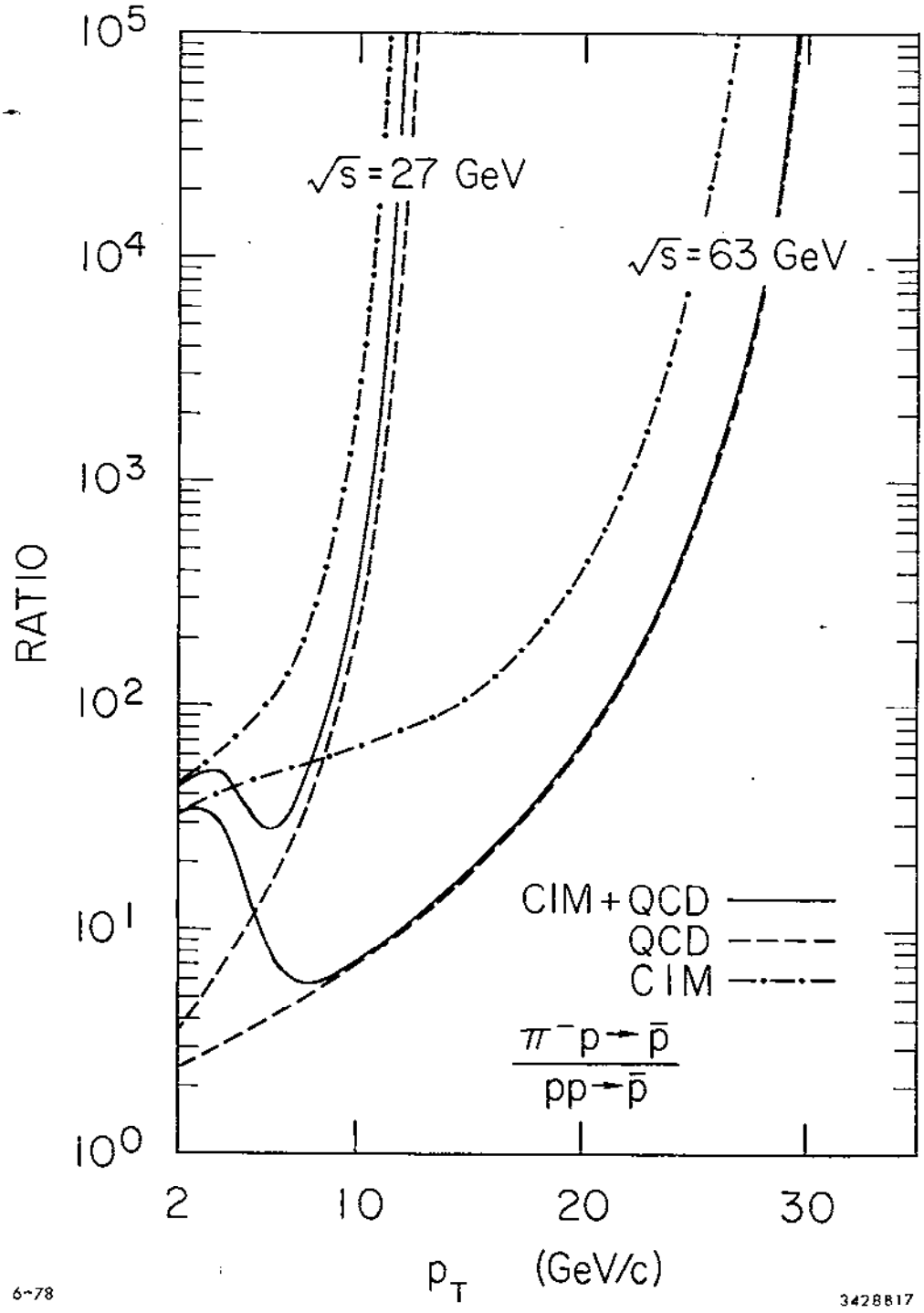
10^5
10^4
10^3
10^2
10^1
10^0
RATIO
$\sqrt{s}$ = 27 GeV
$\sqrt{s}$ = 63 GeV
CIM + QCD
QCD
CIM
$\frac{\pi^- p \to \bar{p}}{pp \to \bar{p}}$
2
10
20
30
p_T (GeV/c)
6-78
3428817

Fig. 10a

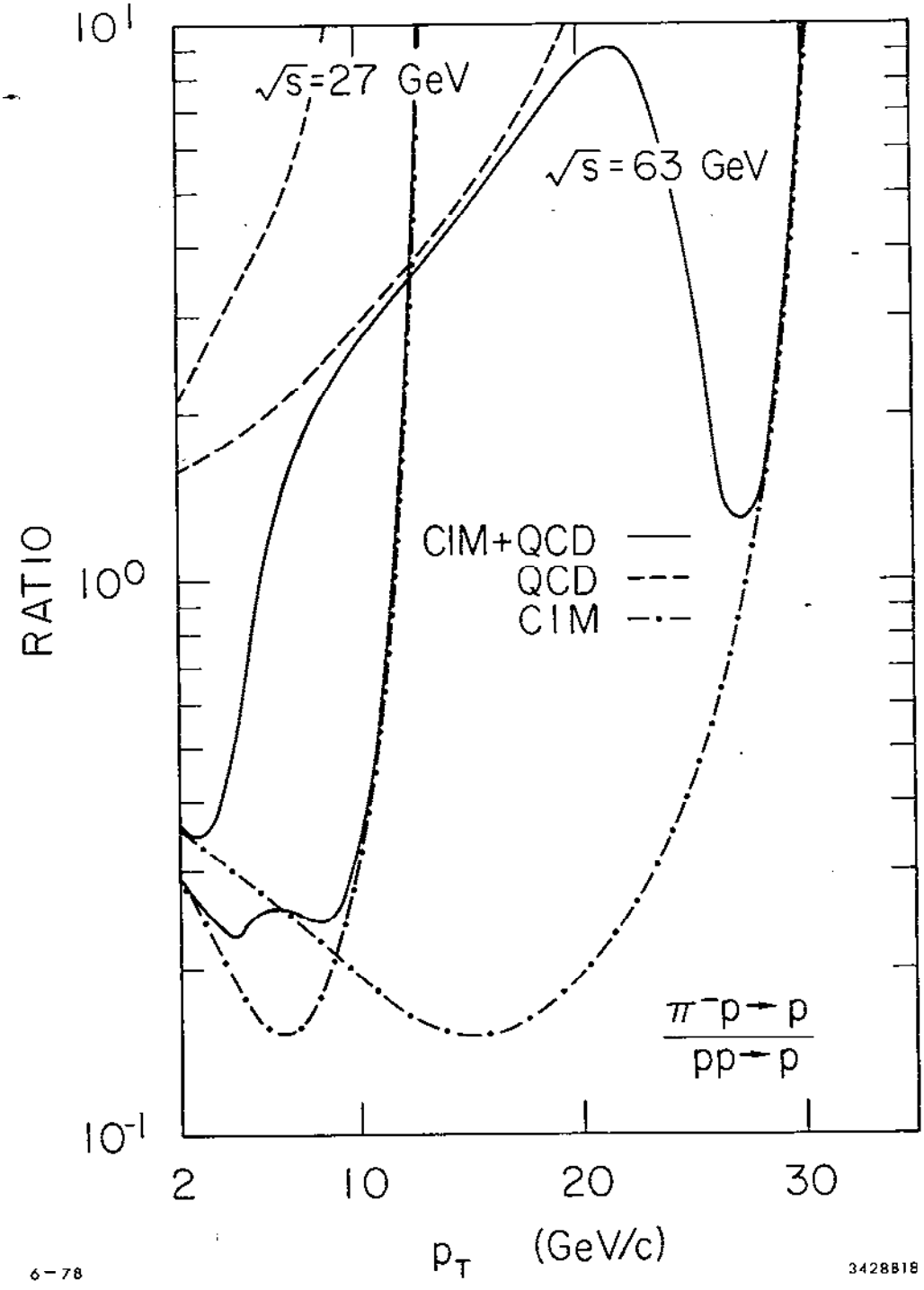
10^1
10^0
10^{-1}
RATIO
$\sqrt{s}$=27 GeV
$\sqrt{s}$ = 63 GeV
CIM+QCD
QCD
CIM
$\frac{\pi^- p \to p}{pp \to p}$
2
10
20
30
p_T (GeV/c)
6-78
3428B18

Fig. 10b

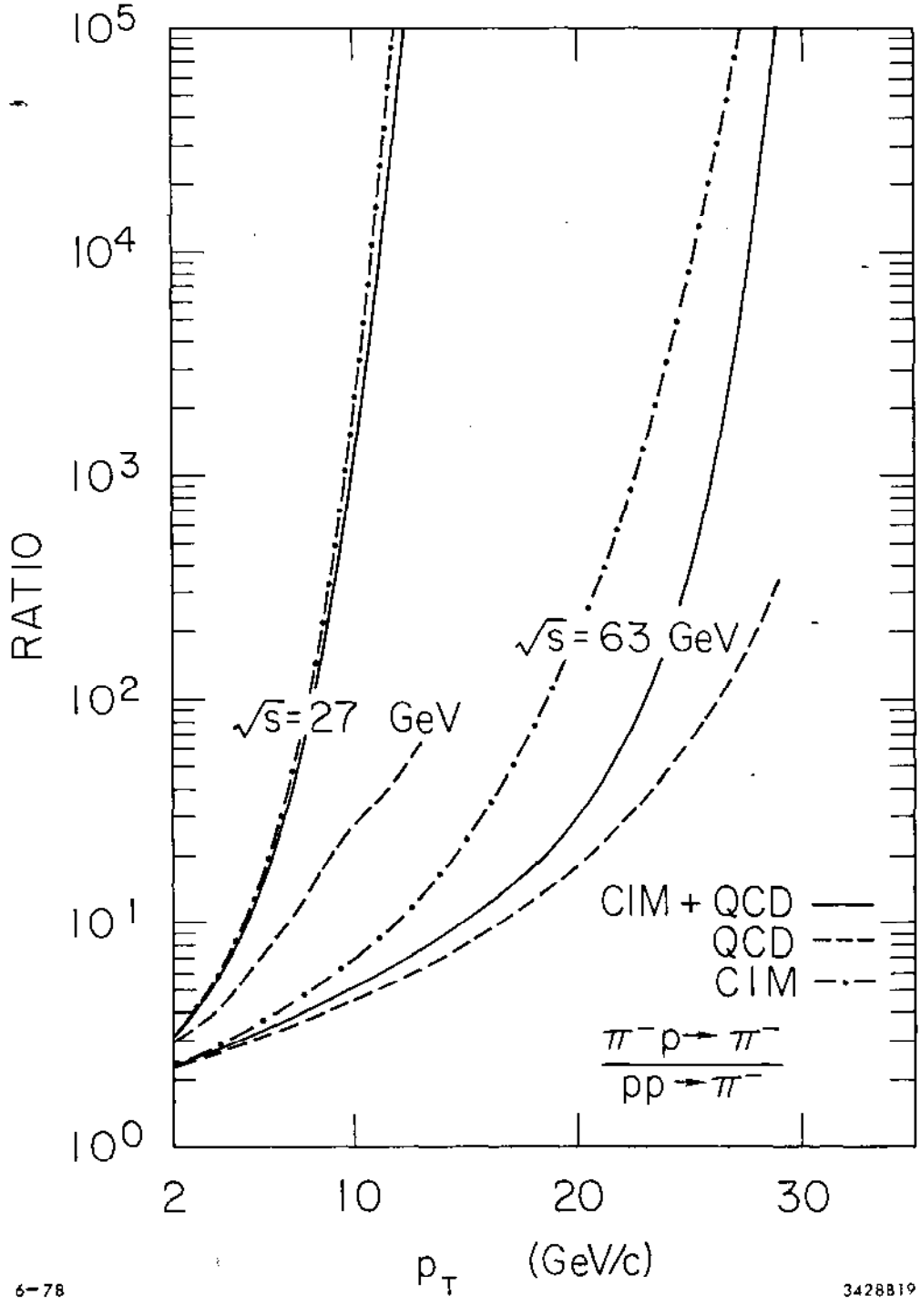
RATIO
10^5
10^4
10^3
10^2
10^1
10^0
$\sqrt{s}$ = 27 GeV
$\sqrt{s}$ = 63 GeV
CIM + QCD
QCD
CIM
$\frac{\pi^- p \to \pi^-}{pp \to \pi^-}$
2
10
20
30
p_T (GeV/c)
6-78
3428B19

Fig. 10c

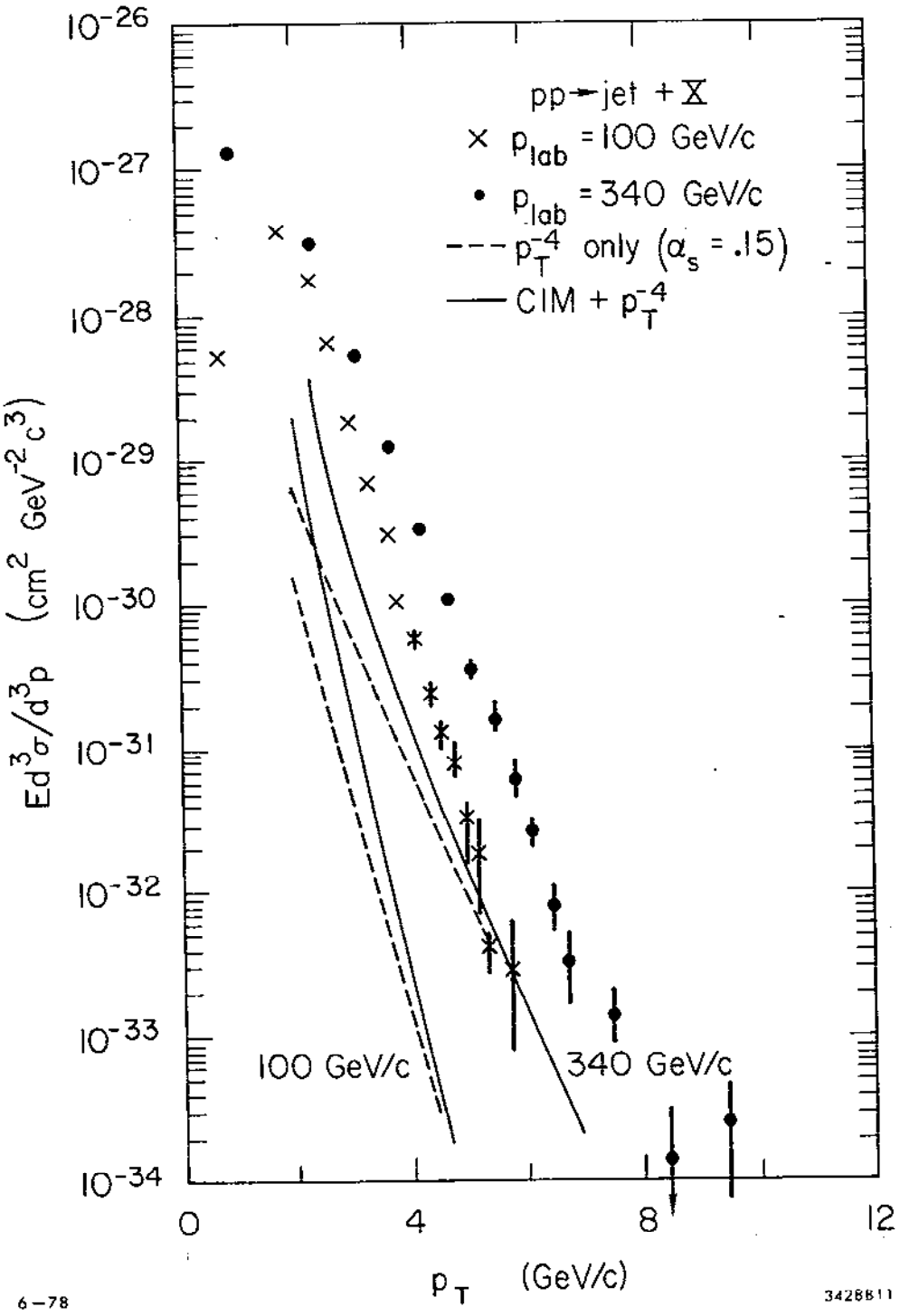
pp→jet + X
× p_{lab} = 100 GeV/c
• p_{lab} = 340 GeV/c
--- p_T^{-4} only (α_s = .15)
— CIM + p_T^{-4}
100 GeV/c
340 GeV/c
$Ed^3\sigma/d^3p$ (cm^2 GeV^{-2}c^3)
p_T (GeV/c)
10^{-26}
10^{-27}
10^{-28}
10^{-29}
10^{-30}
10^{-31}
10^{-32}
10^{-33}
10^{-34}
0
4
8
12
6-78
3428B11

Fig. 11